

# Investigating the effect of compression on the permeability of fibrous porous media

by

Martha Catharina van Heyningen

Thesis presented in fulfilment of the requirements for the degree of Master of Science in Applied Mathematics in the Faculty of Science at Stellenbosch University



Supervisor: Dr. Sonia Woudberg

April 2014

# Declaration

By submitting this thesis/dissertation electronically, I declare that the entirety of the work contained therein is my own, original work, that I am the sole author thereof (save to the extent explicitly otherwise stated), that reproduction and publication thereof by Stellenbosch University will not infringe any third party rights and that I have not previously in its entirety or in part submitted it for obtaining any qualification.

Date: April 2014

Copyright ©2014 Stellenbosch University

All rights reserved

## Abstract

Fluid flow through porous media plays an important role in a variety of contexts of which filtration is one. Filtration efficiency of fibrous filters depends on the micro-structural characterization of these porous materials and is reflected in the permeability thereof. Compression of fibrous porous media has a significant effect on the permeability. Experimental data indicate that the permeability varies generally with more than an order of magnitude over the narrow porosity range in which the compression takes place. Relative to the amount of experimental studies regarding this phenomenon, there is a scarcity of geometric models in the literature that can account for the effect of compression on the permeability of a fibrous porous medium. Within the context of existing geometric pore-scale models based on rectangular geometry, a new model is presented and an existing model improved to predict the effect of one-dimensional compression in the streamwise direction. In addition, without compromising on a commitment to mathematical simplicity, empirical data of a non-woven fibrous porous medium was used to highlight the effect of model geometry on its predictive capability. Different mathematical expressions for the relationship between compression and porosity were considered. The permeability is expressed explicitly in terms of the fibre diameter and the compression fraction and implicitly in terms of the porosity. The porosity is incorporated through the relationship between the linear dimensions of the geometric model. The general applicability of the model(s) was validated by making use of data on airflow through a soft fibrous porous material as well as through glass and nylon fibres. The permeability predictions fall within the same order of magnitude as the experimental data. Given the mathematical simplicity of the model(s), the prediction capability is satisfactory. Attention is drawn to assumptions made and model restrictions within the analytical modelling procedure. A general predictive equation is presented for the permeability prediction in which a solid distribution factor is introduced. The proposed models serve as basis for further adaptation and refinement towards prediction capability.

## Opsomming

Vloei van vloeistowwe deur poreuse media speel 'n belangrike rol in 'n verskeidenheid kontekste waarvan filtrasie een is. Die filtrasie doeltreffendheid van vesel filters hang af van die mikro-strukturele karakterisering van hierdie poreuse materiale en word gereflekteer in die permeabiliteit. Kompresie van veselagtige poreuse media het 'n beduidende effek op die permeabiliteit. Eksperimentele data dui aan dat die verandering in permeabiliteit gewoonlik oor meer as 'n orde grootte strek oor die klein porositeitsinterval waarin die kompresie plaasvind. Relatief tot die aantal eksperimentele studies rakende hierdie verskynsel, is daar 'n tekort aan geometriese modelle in die literatuur wat die effek van kompresie op die permeabiliteit van veselagtige poreuse media in ag kan neem. Binne die konteks van bestaande geometriese kanaal-skaal modelle gebaseer op reghoekige geometrie, is 'n nuwe model voorgestel en 'n bestaande model verbeter om die effek van een-dimensionele kompresie in die stroomsgewyse rigting te voorspel. Sonder om die verbintenis tot wiskundige eenvoud prys te gee, is empiriese data van 'n nie-geweefde veselagtige poreuse medium gebruik om die effek van die geometrie van 'n model op sy voorspellingsvermoë uit te lig. Verskillende wiskundige uitdrukkings is oorweeg vir die verband tussen kompresie en porositeit. Die permeabiliteit is eksplisiet uitgedruk in terme van die veseldiameter en die kompresie breukdeel en implisiet in terme van die porositeit. Die porositeit is ge-inkorporeer deur die verhouding tussen die lineêre dimensies van die geometriese model. Die algemene toepaslikheid van die model(le) is gestaaf deur gebruik te maak van data oor lugvloei deur 'n sagte veselagtige poreuse materiaal sowel as deur glas en nylon vesels. Die voorspellings van die permeabiliteit val binne dieselfde grootte orde as die eksperimentele data. Gegee die wiskundige eenvoud van die model(le), is die voorspellingsvermoë bevredigend. Aandag is gevestig op aannames wat gemaak is en modelbeperkings binne die analitiese modellerings prosedure. 'n Algemene voorspellingsvergelyking is voorgestel vir die voorspelling van die permeabiliteit waarin 'n vaste stof distribusie faktor ge-inkorporeer is. Die voorgestelde modelle dien as basis vir verdere aanpassing en verfyning van voorspellingsvermoë.

## Acknowledgements

The journey into unknown territory would not have been such a memorable experience were it not for:

- Ingrid Mostert and Willie Brink who brought me to the starting line.
- Sonia Woudberg who took on the challenge of a road less traveled by.
- My Mom, Rina van Heyningen, who prayed us through the journey and who shares my passion for trying to understand God's works of art.
- Hardus Diedericks and his open door policy.
- Milton Maritz who helped me decode my ideas.
- Adrian, Daniek, Francois, Graaf Grobler, Hanno, Mapundi, Maretha, Marèt and Marianne.
- Family and friends, you know who you are ... how boring any journey will be without you...

Financial assistance from the National Research Foundation (NRF) towards this research is hereby acknowledged. Opinions expressed and conclusions arrived at, are those of the author and are not necessarily to be attributed to the NRF.

# Contents

<b>1</b>	<b>Introduction</b>	<b>1</b>
<b>2</b>	<b>Theoretical background</b>	<b>6</b>
2.1	Assumptions . . . . .	6
2.2	Flow through porous media . . . . .	8
2.2.1	Fundamental porous media concepts . . . . .	9
2.2.2	Volume averaging . . . . .	11
2.2.3	Permeability . . . . .	15
<b>3</b>	<b>Literature study</b>	<b>18</b>
3.1	Studies from the literature . . . . .	19
3.1.1	Discussion . . . . .	26
3.2	Literature regarding RRUCs . . . . .	27
3.2.1	Foam RRUC model . . . . .	27
3.2.2	Granular RRUC model . . . . .	28
3.2.3	Fibre RRUC model . . . . .	29
3.3	Experiments pertaining to the present study . . . . .	36
3.3.1	Influence of structural parameters on permeability (Le Coq (2008))	36
3.3.2	Permeability of soft porous media (Akaydin et al. (2011)) . . . . .	39
<b>4</b>	<b>Two-strut fibre RRUC model</b>	<b>42</b>
4.1	Relationship between porosity and compression fraction . . . . .	43

4.2	Geometric model . . . . .	48
4.3	Modelling steps . . . . .	51
4.4	Permeability prediction based on different compression fraction - porosity relationships . . . . .	54
4.4.1	Linear (regression) relationship between compression fraction and porosity (equation (4.2)) . . . . .	55
4.4.2	General non-linear relationship between compression fraction and porosity (equation (4.6)) . . . . .	62
4.4.3	Specific non-linear relationship between compression fraction and porosity (equation (4.8)) . . . . .	66
4.4.4	Summary . . . . .	69
<b>5</b>	<b>Modified two-strut fibre RRUC model</b>	<b>72</b>
5.1	Solid-change in the two-strut fibre RRUC . . . . .	72
5.1.1	Solid with side lengths $d_{\perp}$ , $\frac{1}{\sqrt{2}} d_s$ and $\sqrt{2} d_s$ . . . . .	73
5.1.2	Solid with side lengths $d_{\perp}$ , $\frac{1}{\sqrt{2e}} d_s$ and $\sqrt{2e} d_s$ . . . . .	78
5.2	The choice of hydraulic diameter revisited . . . . .	81
5.3	Alternative method for determining $d_{\parallel 0}$ . . . . .	83
<b>6</b>	<b>Model validation</b>	<b>88</b>
6.1	Soft fibrous porous medium . . . . .	88
6.2	Data sets from Jackson & James (1986) . . . . .	91
<b>7</b>	<b>Conclusions and future work</b>	<b>95</b>
7.1	Conclusions . . . . .	95
7.2	Future work . . . . .	101
<b>A</b>	<b>General fluid flow concepts</b>	<b>102</b>

# Nomenclature

## Standard characters

$d$	$[m]$	linear dimension
$d_s$	$[m]$	linear dimension of solid in RRUC
$d_{\parallel}$	$[m]$	linear dimension of solid in RRUC parallel to streamwise direction
$d_{\parallel 0}$	$[m]$	linear dimension of solid in RRUC parallel to streamwise direction in uncompressed state
$d_{\perp}$	$[m]$	linear dimension of solid in RRUC perpendicular to streamwise direction
$D_h$	$[m]$	hydraulic diameter
$e$	$[\ ]$	compression fraction
$e_{\text{exp}}$	$[\ ]$	experimental compression fraction values
$f_b$	$[N.kg^{-1}]$	external body forces per unit mass
$h$	$[m]$	height of sample porous medium after compression
$h_0$	$[m]$	initial uncompressed height of sample porous medium
$k$	$[m^2]$	Darcy permeability
$k_{\text{exp}}$	$[m^2]$	experimental permeability values
$L$	$[m]$	linear dimension
$\underline{n}$	$[\ ]$	outwardly directed unit normal vector for the fluid-phase on the solid surface
$p$	$[Pa]$	interstitial pressure
$\underline{q}$	$[m.s^{-1}]$	superficial velocity, Darcy velocity or specific discharge
$Q$	$[m^3.s^{-1}]$	volumetric flow rate
$R_h$	$[m]$	hydraulic radius
$Re$	$[\ ]$	Reynolds number



$S_{fs}$	$[m^2]$	fluid-solid interface in RRUC
$\mathcal{S}_{fs}$	$[m^2]$	fluid-solid interface in REV
$S_{  }$	$[m^2]$	surface area in RRUC adjacent to streamwise fluid volume
$S_{\perp}$	$[m^2]$	surface area in RRUC adjacent to transverse fluid volume
$U_f$	$[m^3]$	total fluid volume in RRUC
$\mathcal{U}_f$	$[m^3]$	total fluid volume in REV
$U_0$	$[m^3]$	total (fluid and solid) volume of RRUC
$\mathcal{U}_0$	$[m^3]$	total (fluid and solid) volume of REV
$U_s$	$[m^3]$	total solid volume in RRUC
$U_t$	$[m^3]$	total transfer volume in RRUC
$U_{  }$	$[m^3]$	total streamwise volume in RRUC
$U_{\perp}$	$[m^3]$	total transverse volume in RRUC
$\underline{u}$	$[m.s^{-1}]$	drift velocity
$\underline{v}$	$[m.s^{-1}]$	interstitial fluid velocity
$\underline{w}_{  }$	$[m.s^{-1}]$	streamwise average pore velocity
$\underline{w}_{\perp}$	$[m.s^{-1}]$	transverse average pore velocity
$x, y, z$	$[m]$	distance along Cartesian coordinate

## Greek symbols

$\alpha$	$[ ]$	solid distribution parameter
$\Delta$	$[ ]$	change in streamwise property
$\epsilon$	$[ ]$	porosity
$\epsilon_0$	$[ ]$	porosity of the uncompressed state
$\mu$	$[N.s.m^{-2}]$	fluid dynamic viscosity
$\rho$	$[kg.m^{-3}]$	fluid density
$\tau$	$[N.m^{-2}]$	local shear stress
$\tau_w$	$[N.m^{-2}]$	local wall shear stress
$\phi$	$[ ]$	solid volume fraction
$\chi$	$[ ]$	tortuosity factor
$\psi$	$[ ]$	property defined in fluid phase

## Miscellaneous

$\nabla$	del operator
$\langle \rangle$	phase average operator
$\langle \rangle_f$	intrinsic phase average operator
$\{ \}$	deviation operator
$\underline{\quad}$	vector (underlined)
$\underline{\underline{\quad}}$	diadic (doubly underlined)

## Acronyms

REV	<u>R</u> epresentative <u>E</u> lementary <u>V</u> olume
RRUC	<u>R</u> ectangular <u>R</u> epresentative <u>U</u> nit <u>C</u> ell

## Subscripts

$f$	fluid matter
$fs$	fluid-solid interface
$h$	hydraulic
$s$	solid matter
$w$	wall
$\parallel$	parallel to streamwise direction
$\perp$	perpendicular to streamwise direction

# List of Figures

3.1	Unit cell used by Tamayol & Bahrami (2009). [Source: Tamayol & Bahrami (2009)] . . . . .	22
3.2	Original RRUC model proposed for flow through a rigid, isotropic and consolidated porous medium. [Source: Du Plessis & Masliyah (1988)] . . . . .	28
3.3	Original RRUC model proposed for flow through rigid, isotropic granular porous media. [Source: Du Plessis & Masliyah (1991)] . . . . .	29
3.4	Fibre RRUC model for predicting the permeability of a fibrous porous medium. . . . .	30
3.5	Three-strut fibre RRUC model (a) before and (b) after compression. [Source: Woudberg (2012a)] . . . . .	34
3.6	Glass fibre non-wovens. [Source: Le Coq (2008)] . . . . .	37
4.1	Different relationships between the compression fraction (filter thickness relative to its uncompressed state) and the compression induced porosity. . . . .	47
4.2	Two-strut fibre RRUC model (a) before and (b) after compression. . . . .	49
4.3	Permeabilities predicted by the two-strut- and three-strut fibre RRUC models, based on a linear relationship between $e$ and $\epsilon$ (equation (4.2)). . . . .	57
4.4	RRUC side lengths parallel (top) and perpendicular (bottom) to the stream-wise direction, as a function of compression induced porosity. (Linear relationship between $e$ and $\epsilon$ .) . . . . .	58
4.5	RRUC side lengths parallel (top) and perpendicular (bottom) to the stream-wise direction, as a function of compression induced porosity, for the porosity domain $[0.75; 0.95]$ . (Linear relationship between $e$ and $\epsilon$ .) . . . . .	60
4.6	RRUC volumes as a function of compression induced porosity for the porosity domain $[0.75; 0.95]$ . (Linear relationship between $e$ and $\epsilon$ .) . . . . .	61

4.7	Permeabilities predicted by the two-strut- and three-strut fibre RRUC models for the porosity domain [0.75; 0.95]. (Linear relationship between $e$ and $\epsilon$ .) . . . . .	61
4.8	Permeabilities predicted by the two-strut- and three-strut fibre RRUC models, based on the general non-linear relationship between $e$ and $\epsilon$ (equation (4.6)). . . . .	63
4.9	RRUC side lengths parallel (top) and perpendicular (bottom) to the streamwise direction as a function of compression induced porosity. (General non-linear relationship between $e$ and $\epsilon$ .) . . . . .	64
4.10	RRUC side length perpendicular to the streamwise direction as a function of compression induced porosity for the porosity domain [0.75; 0.95]. (General non-linear relationship between $e$ and $\epsilon$ .) . . . . .	65
4.11	Permeabilities predicted by the two-strut- and three-strut fibre RRUC models for the porosity domain [0.75; 0.95]. (General non-linear relationship between $e$ and $\epsilon$ .) . . . . .	65
4.12	Permeabilities predicted by the two-strut- and three-strut fibre RRUC models based on a specific non-linear relationship between $e$ and $\epsilon$ (equation (4.8)). . . . .	67
4.13	RRUC side lengths parallel (top) and perpendicular (bottom) to the streamwise direction as a function of compression induced porosity. (Specific non-linear relationship between $e$ and $\epsilon$ .) . . . . .	68
4.14	Influence of the relationship between $e$ and $\epsilon$ on the permeability-prediction of the two-strut fibre RRUC model. . . . .	69
4.15	Influence of the relationship between $e$ and $\epsilon$ on the permeability prediction of the three-strut fibre RRUC model. . . . .	70
5.1	Solid with dimensions $d_{\perp}$ , $\frac{1}{\sqrt{2}} d_s$ and $\sqrt{2} d_s$ for two-strut fibre RRUC model.	74
5.2	Permeabilities predicted by the two-strut- and two-strut sqrt(2) fibre RRUC models. (Specific non-linear relationship between $e$ and $\epsilon$ .) . . . . .	77
5.3	Solid with dimensions $d_{\perp}$ , $\frac{1}{\sqrt{2e}} d_s$ and $\sqrt{2e} d_s$ for two-strut fibre RRUC model.	78
5.4	Permeabilities predicted by the two-strut-, the two-strut sqrt(2)- and the two-strut sqrt(2e) fibre RRUC models. (Specific non-linear relationship between $e$ and $\epsilon$ .) . . . . .	80
5.5	Two-strut fibre RRUC model (a) before and (b) after compression. . . . .	84
5.6	Top view (left) and side view (right) of the two-strut fibre RRUC for the uncompressed state ( $e=1$ ). . . . .	85

5.7	Permeabilities predicted by the two-strut- and two-strut alternative $d_{\parallel 0}$ fibre RRUC models. (General non-linear relationship between $e$ and $\epsilon$ .) . . .	87
6.1	Top view (left) and side view (right) of the two-strut $\sqrt{2e}$ fibre RRUC for the uncompressed state ( $e=1$ ). . . . .	89
6.2	Permeabilities predicted by the two-strut alternative $d_{\parallel 0}$ - and the two-strut $\sqrt{2e}$ alternative $d_{\parallel 0}$ fibre RRUC models for a soft porous medium. (General non-linear relationship between $e$ and $\epsilon$ .) . . . . .	90
6.3	Top view (left) and side view (right) of the two-strut general alternative $d_{\parallel 0}$ fibre RRUC. . . . .	92
6.4	Permeability predictions of the three-strut- and two-strut general alternative $d_{\parallel 0}$ fibre RRUC models for glass fibres with radius 0.082 mm. . . . .	93
6.5	Permeability predictions of the three-strut- and two-strut general alternative $d_{\parallel 0}$ fibre RRUC models for nylon fibres with radius 0.0965 mm. . . . .	93
7.1	Overview of the investigation into the effect of compression of a fibrous porous medium on the permeability there-of. . . . .	97
7.2	Overview of the relative percentage difference between the permeability predictions of the proposed models and the experimental values obtained by Le Coq (2008). . . . .	98
7.3	Solid with dimensions $d_{\perp}$ , $\frac{1}{\sqrt{\alpha e}} d_s$ and $\sqrt{\alpha e} d_s$ for the general two-strut fibre RRUC model. . . . .	99
7.4	Top view (left) and side view (right) of the general two-strut fibre RRUC for the uncompressed state ( $e=1$ ). . . . .	100

# List of Tables

3.1	Volume and surface partitioning referring to the original fibre RRUC model.	31
3.2	Selection of data from Le Coq (2008) regarding glass fibre non-wovens (average diameter 2.7 $\mu\text{m}$ ; average length 0.9 mm).	39
3.3	Selection of data from Akaydin et al. (2011) regarding regular polyester pillow material (average diameter 10 $\mu\text{m}$ ).	41
4.1	Verification of the use of the non-linear relationship between $e$ and $\epsilon$ .	45
4.2	Values for the hydraulic diameter corresponding to the four stages of compression (experiment), based on a linear relationship between $e$ and $\epsilon$ .	55
4.3	Relative percentage error in the permeability prediction of the two-strut- and three-strut fibre RRUC models. (Linear relationship between $e$ and $\epsilon$ .)	56
4.4	Relative percentage error in the permeability prediction of the two-strut and three-strut fibre RRUC models. (General non-linear relationship between $e$ and $\epsilon$ .)	62
4.5	Relative percentage error in the permeability prediction of the two-strut and three-strut fibre RRUC models. (Specific non-linear relationship between $e$ and $\epsilon$ .)	66
5.1	Relative percentage error in the permeability prediction of the two-strut- and two-strut $\sqrt{2}$ fibre RRUC models. (Specific non-linear relationship between $e$ and $\epsilon$ .)	76
5.2	Relative percentage error in the permeability predictions of the two-strut- and two-strut $\sqrt{2e}$ fibre RRUC models. (Specific non-linear relationship between $e$ and $\epsilon$ .)	79
5.3	Relative percentage error in the permeability prediction of the two-strut- and two-strut alternative $d_{\parallel 0}$ fibre RRUC models. (General non-linear relationship between $e$ and $\epsilon$ .)	86

6.1	Relative percentage error in the permeability prediction of the two-strut alternative $d_{\parallel 0}$ - and the two-strut $\sqrt{2e}$ alternative $d_{\parallel 0}$ fibre RRUC models for a soft porous medium. (General non-linear relationship between $e$ and $\epsilon$ .)	91
6.2	Relative percentage errors in the permeability prediction of the two-strut general alternative $d_{\parallel 0}$ fibre RRUC model for anisotropic fibrous porous media of different radii. . . . .	94

# Chapter 1

## Introduction

Fluid flow through porous media plays an important role in a variety of contexts of which construction engineering, petroleum engineering, geosciences, soil and rock mechanics, biology, biophysics and material science are examples. Non-woven fibrous porous media possess the ability to form a stable structure even at very high porosities, and are used in numerous applications such as filters, wipes, heat insulators, as well as automotive-, incontinence- and medical products. According to Jaganathan et al. (2009), understanding the morphological changes of a fibrous porous medium due to a compressive stress is critically important in product development. The bulk behaviour of permeability under compressive stress depends on the structure of the material as well as on the application in which it is used. This behaviour of permeability is very different in different contexts such as biological tissues (e.g. articular cartilage), rock mechanics, and structural engineering (Akaydin et al. (2011)).

According to Nabovati et al. (2009) permeability prediction, and more generally, the investigation of the effect of pore structure on macroscopic properties of porous media, have posed a major challenge to researchers and engineers in industrial and academic disciplines. Fluid flow simulation in porous media, on a macroscopic level, requires the permeability as input while the analysis of the effect of pore-scale parameters on the macroscopic properties is a challenging task. Due to the complex structure (in general) of porous media, the flow patterns within the pores are complicated. Since permeability is highly medium-specific, the development of an accurate generic geometric model for permeability, as a function of the bulk properties of the medium, is an ongoing process.

The determination of permeability for a specific material usually requires experimental work. As alternative approaches, analytical and numerical methods aim to predict the permeability by solving equations representing fluid flow inside the pores of the porous medium. Rapid increase in available computing power and the ongoing development of advanced numerical algorithms imply that detailed numerical simulations of flow in/through porous media are now feasible. Removing the constraints of the analytical approaches, more complex pore geometries, which resemble real porous media structures more closely, can be used in fluid flow simulations (Nabovati et al. (2009)).

Advances in nuclear magnetic resonance imaging and localized flow and velocity measure-



ments, make it possible to study flow processes in detail, either directly e.g. in bore cores, or, for example, in phantom systems comprising glass beads. Mansfield & Bencsik (2001), made use of these advanced techniques to measure the fluid velocity distribution and fluid flow of water passing through a porous material (phantom system of glass beads) in order to determine the degree of causality between one steady-state flow condition and another. According to Mansfield & Bencsik (2001) there appears to be a randomness associated with the establishment and subsequent re-establishment of water flow through the bead pack. It was concluded that the use of a causal theory to predict the details of the flow velocity distribution at different flow rates in porous media is not optimal. The current study is based on causality between physical properties while acknowledging the fact that inclusion of stochastic effects in further modelling processes is an option.

The importance of (pure) analytical models is not annihilated by the fact that available (and evolving) computing power makes simulations ever more effective and accurate in solving problems (although computationally expensive), but it does change the role that analytical investigation plays. This study will present a model that balances mathematical simplicity with a predictive capacity which is adequately accurate to serve as a verification indicator for imaging, experiments and/or simulations.

The main aim of this study is to present a first order analytical mathematical model for *predicting the effect of compression on the permeability* of an unconsolidated fibrous porous medium. Parallel to this, there will be a focus on the *effect of parameter change on the prediction capability of a model*. This will form a basis for conclusions regarding the effectiveness of the model.

The premise underlying the aim of this study is that given the porosity of a fibrous porous medium in an uncompressed state, within the Darcy flow regime, the permeability can be predicted by solely attributing pressure losses to shear stresses. A prerequisite is that the geometry of the model represents the structure of the porous medium (before and after compression) sufficiently accurate. If the effect of compression on porosity can accurately be expressed mathematically, the prediction capability will be enhanced. It is expected that the permeability predictions obtained in this manner could provide first order predictions suitable for the exploratory phases of new applications.

The development of the model will be guided by the following questions:

- What should the geometric representation be for the prediction of the effect of compression on a **fibrous** porous medium?
- How can mathematical simplicity be balanced with prediction capability?
- Apart from the porosity in the uncompressed state, what other information regarding the porous medium can be employed to enhance the prediction capability of the model?
- Which mathematical function should represent the relationship between porosity and compression to enhance the model?

The combination of the above mentioned aspects will also play a role and therefore the investigation will focus on the effect of parameter change whilst keeping other parameters

constant in order to find the combination of parameters which leads to a usable prediction capability.

Often the underlying assumptions of experimental, analytical modelling and simulation results are not explicit but represented with margins of errors. Discrepancies between sets of results that are compared may be due to (subtle) differences in assumptions made (which includes the choice of formulas used). For instance, in a literature review, Steinke & Kandlikar (2006) found a common thread through articles that have reported some form of discrepancy between the experimental data and the predicted theoretical values. Implicitly assuming that entrance and exit losses and/or developing flow are negligible, the results of these studies seemed to question the conventional theory in micro-channel flows. Throughout the present study an explicit awareness of assumptions will be evident in order to make sense of possible discrepancies with results of other studies and/or with conventional theory.

A single set of empirical data regarding glass fibre non-wovens will be employed to highlight the influence of model-parameter change on the predictive capability of the model. The rationale behind this is to improve the prediction power of a model within a chosen context, in the same way as determining the influence of one variable on a system by keeping the other variables constant. Based on conclusions regarding the analytical model developed as described, another set of empirical data (regarding soft fibrous porous media) will be employed for verification purposes, based on the available empirically determined parameters. A relevant summary of information regarding the two experiments, of which the data will be used in this study, will be given in Chapter 3. The prediction capability of the model will also be evaluated through data regarding glass- and nylon fibres.

Through comparison of the modelling results for the different fibrous porous media, conclusions will be drawn regarding the causality between parameter change and the permeability prediction capability of the model. Also, conclusions will refer to assumptions made in the analytical and experimental contexts in order to determine whether the applicability of the analytical model can be generalized to other fibrous porous media. Changing a model-parameter or a combination there-of also provides information on how the difference in the output of the analytical mathematical model can be assigned to different sources of uncertainty in its input values. A sensitivity analysis will therefore be implicitly done in an unconventional manner and not through employing the estimates for experimental error ranges.

Without violating the essential characteristics of the system under investigation, the author's understanding and approximation of the actual system will be expressed through a set of assumptions. This will be done knowing that because any model is a subjective, simplified and idealized version of the actual system, no unique model exists for a given 'flow through (fibrous) porous medium' system (Bear & Bachmat (1990)).

The mathematical modelling will be based on the continuum approach. In this approach the actual multi-phase porous medium is replaced by a fictitious continuum and the interstitial flow conditions are related to the measurable macroscopic flow behaviour using volume averaging of the transport equations over a Representative Elementary Volume (REV). According to Fung (1977), a material continuum is a material for which the

momentum, energy and mass densities exist in a mathematical sense and therefore this concept is in essence a mathematical idealization.

A pore-scale modelling procedure which aims to approximate a porous material by imbedding the average geometric characteristics of a REV within the smallest possible hypothetical Rectangular Representative Unit Cell (RRUC) was originally introduced by Du Plessis and Masliyah for isotropic foam-like media (Du Plessis & Masliyah (1988)). The new representative geometric model introduced in this study is based on selected RRUC concepts. The link between the new model (to be proposed in this study) and volume averaging with closure modelling, will become evident in Sections 3.2 and 4.2. The rationale behind the choice of the geometric model is to represent the average geometry of the porous medium in such a way that the dimensions there-of can be used to scale the relevant velocities and shear stresses.

The underlying question of whether the effect of compression on fibrous porous media can be predicted using rectangular geometry, has its origin in the point of view that the simplicity of a model does not necessary imply un-usability. Keeping track of the (explicit and implicit) implications that follow from this reasoning will accentuate critical aspects of a modelling process focused on simplicity.

Since all reasoning is based on, and expressed through, concepts and ideas, a theoretical background, as well as assumptions regarding concepts pertaining to this study, will be presented in Chapter 2. Although these concepts are often perceived as ‘general knowledge’ for academics in this field, the underlying assumptions of these modelling ‘building blocks’ are not always explicit. Giving a background of the scientific field in which this study will take place, will highlight the combination of assumptions made in modelling processes in general and, more specific, in this study.

Compression changes the shape of the voids available for flow in a specific manner which in effect creates a ‘different’ porous medium of which the structural properties can usually be related to the original porous medium. The modelling of flow through a fibrous porous medium with the aim of predicting the permeability there-of still forms the core of an attempt to predict the effect of compression on the medium.

An in-depth literature study was performed regarding different modelling procedures and a selection there-of will be summarized in Chapter 3, thus providing a sufficient (although not comprehensive) overview of the differences and similarities in modelling processes. Highlighting ‘what others have done’ based on different assumption frameworks, also emphasizes the fact that the analytical model development in this study has an overt focus on balancing mathematical simplicity with accuracy.

Employing the concepts discussed in Chapter 2, an attempt will be made to develop a model with reasonable predictive capability regarding the effect of compression on permeability. Informed by different modelling procedures (Chapter 3) without compromising the author’s commitment to mathematical simplicity, a new model will be introduced in Chapter 4. Throughout the development the results will be compared with those of a model presented in Woudberg (2012a), and in the process enhancing not only the prediction capability of the new model, but also the existing model.

In Chapter 5 parameters of the newly introduced model will be changed and the influence there-of on the permeability prediction investigated. This will be done based on a single set of data regarding glass fibre non-wovens. In Chapter 6 the model will furthermore be validated by comparing the permeability prediction to experimental permeability data on soft fibrous porous media as well as data on glass- and nylon fibres provided by Jackson & James (1986). Chapter 7 comprises of (summarizing) conclusions and consequently concepts that may form part of future enhancements of the model.

# Chapter 2

## Theoretical background

### 2.1 Assumptions

In this study, the Eulerian description will be used in the modelling procedure. The Lagrangian description is ill suited for flowing and deforming matter since the boundary of the material volume is itself a function of time. Reynolds' transport theorem facilitates the use of a control volume fixed in space.

Under the assumption that the *fluid density* ( $\rho$ ) is constant everywhere (homogeneous, incompressible *fluid*), the continuity equation (equation (A.1)) reduces to

$$\nabla \cdot \underline{v} = 0. \quad (2.1)$$

This implies that isochoric *flow* (the material derivative of the density is zero i.e. incompressible *flow*) is assumed. This assumption results in considerable simplification and very little error (Bird et al. (2007)).

The assumption of incompressible flow for experiments where air, a compressible fluid, is used, can be justified as follows: For the modelling processes in this study, flow velocities significantly less than the speed of sound is assumed. Since the maximum pressure change associated with motion is of the order  $(\rho v^2)/2$ , the Mach number is significantly less than unity and this change in pressure is negligible (Fung (1977)) relative to the undisturbed pressure.

The modelling procedure in this study is based on the assumption that the fluid resembles a *Newtonian fluid* (Appendix A). The Navier-Stokes (momentum) equations (equations (A.2), (A.3) and (A.4)), will therefore be employed with the shear stresses as functions of (only) velocity gradients and viscosity. As will become clear in Chapter 4, the fact that the shear stresses can be expressed in terms of velocity gradients (equation (A.5)) is essential in the modelling process of this study.

In the present study the pressure is determined solely by the equations of motion and the accompanying boundary conditions (Fung (1977)). (Thermodynamically, the pressure of a fluid is a function of its density and temperature and in some applications it is also

necessary to solve an equation of state relating these thermodynamic variables.)

Although in most applications with homogeneous fluids the hydrostatic pressure plays no role in fluid motions and can be subtracted from the total pressure (Worster (2009)), it will not be done in this investigation. The only body force that will be taken into account in the modelling process is the one due to gravitation and it will be included (implicitly) in the pressure term.

When modelling flow through porous media the viscosity of the fluid and the permeability of the porous medium are important variables in the mathematical description of the exact relationship between the pressure gradient and the fluid velocity gradient. Since the focus of this study is on the permeability of a porous medium, only a short general reference to viscosity ( $\mu$ ) is given in Appendix A. (Shear stress is an essential concept in the modelling of pressure losses in this study, therefore it is important to highlight core aspects of this parameter.) The present study is based on the assumption that the properties of laminar flow may be employed, keeping in mind that this restricts the application of the model. This assumption implies that viscosity is an (implicit) intrinsic part of the modelling process.

The (Newtonian) fluid is assumed to be homogeneous and isotropic (no concentration gradients) with uniform (constant) viscosity. The results of this analytical investigation are therefore only applicable in contexts where the temperature, pressure and composition of the fluid justify the assumption of constant viscosity. When the word ‘viscosity’ is used in this study, dynamic viscosity is implied.

In an incompressible viscous fluid the internal friction causes mechanical dissipation which may increase the internal energy and temperature of the fluid or may result in heat conduction. This flow of heat is usually uncoupled from momentum transfer if the variation in viscosity with temperature is *not* considered or negligible (Hughes (1979)). In this study, the analytical modelling of flow through fibrous porous media will be based on the assumption that the system is isothermal and consequently the energy equation will not be employed.

Although assuming a no-slip condition at the fluid-solid interface generally implies that a development region will be present in the micro-channels of the porous medium, the modelling process will be based on the assumption that fully developed flow is applicable in the geometric model. The friction factor will not be employed in the present study although in the models that will be discussed in Chapter 3 (including previous RRUC models) the friction factor (equation (A.7)) forms an essential part of the different modelling procedures.

In summary, the modelling process will incorporate the properties associated with a homogeneous, isotropic Newtonian fluid (constant density and viscosity). No body forces except gravitational forces (implicitly included in the pressure term) will be considered. Underlying the assumptions mentioned above is the assumption that conditions of isothermal, isochoric, single phase, laminar and fully developed flow, with a no-slip condition at the fluid-solid interfaces are *justified* for a *first order* modelling process.

## 2.2 Flow through porous media

In general a **porous medium** can be described as a continuous multiphase material where the persistent solid phase and the connected void space are both represented throughout the whole domain occupied by the medium. The **porosity** ( $\epsilon$ ) of a porous medium is in general defined as the fraction of void volume with respect to total volume of porous medium (Bear (1988)) and can therefore also be expressed as a percentage. According to Montillet & Le Coq (2003) porosity is one of the most determining parameters of flow through porous media and the bulk porosity is generally used in equations related to flow and mass transfer phenomena. The porosity variation along a given direction is generally not used in analytical flow models because of the mathematical complexity it introduces. It may happen that there are voids in the material that are not available for fluid flow and therefore the effective porosity refers to the fraction of the total volume in which fluid flow is effectively taking place. The effective pore space includes catenary (inter-connected) and dead-end (cul-de-sac) pores and excludes closed (non-connected) pores. In the model of Woudberg (2012a) the dead-end pores are not included as part of the effective pore space, based on experimental data in literature showing a very low percentage contribution to effective pore volume by dead-end pores. For highly porous media the **Solid Volume Fraction** (SVF), defined as

$$\phi \equiv 1 - \epsilon, \quad (2.2)$$

is mostly used to indicate the percentage solid in a porous matrix relative to the total volume of the matrix. For the purpose of this study the porosity of the porous medium will consistently be used in predictive equations obtained through the analytical investigation.

Measurements of the pore volume and pore size distributions of a porous medium sample can be performed using methods of which mercury porosimetry, liquid displacement and image analysis are examples. Image analysis can eliminate the risk of destruction of the porous medium and for this Scanning Electron Microscopy, Light microscopy, X-ray computed tomography (CT scan), computed axial tomography (CAT scan) or Magnetic Resonance Imaging (MRI) can be used. Information regarding the method(s) used to measure the pore volume (including the underlying assumptions) is important since the margin of error in the calculation of e.g. porosity, is experiment-dependent.

The Reynolds number (equation (A.6)) for flow *through porous media* is defined as

$$Re \equiv \frac{\rho q d}{\mu}, \quad (2.3)$$

with  $q$  the magnitude of the superficial velocity and  $d$  some length dimension of the porous matrix which should, in analogy to pipe flow, represent the average diameter of the elementary channels of the porous medium. For unconsolidated porous media it is customary to use a representative dimension of the grains or the fibres, due to the relative ease of determining it (Bear (1988)). This custom will be honored in this study.

For a porous medium, the hydraulic diameter is defined as four times the volume available for flow in the porous medium, divided by the area of the fluid-solid interface associated with the volume available for flow (Whitaker (1999)).

In the next section general fundamental porous media concepts and equations will be presented which will be referred to in Chapter 3 when different modelling procedures (from the literature) are summarized.

### 2.2.1 Fundamental porous media concepts

Three different categories of porous media considered by Woudberg (2012a) are granular media, foamlike media and fibre beds. Although foamlike media are generally categorized as consolidated fibrous porous media, these porous structures are not the focus of this study. **Foamlike** media are classified as consolidated (or non-dispersed) porous media since the solid matrix is connected. Foams are used in practical applications e.g. for heat transfer enhancement (Woudberg (2012a)). The analytical model to be developed in this study will be based on an existing analytical model for foamlike media (Woudberg (2012a)) which was used to predict the effect of compression on the permeability of a fibrous porous medium.

The term ‘**fibrous** porous medium’ will be used for a porous medium that is composed of unconsolidated rod-like particles or a complicated mesh of curving, intertwining fibres. Manufactured and natural fibrous media are essential in many processes of which filtration, biological transport and adsorption are examples (Thompson et al. (2002)). According to Pradhan et al. (2012) fibrous porous media require much less material to form a stable structure than granular porous media. This is mainly attributed to the relatively complex organization as well as the characteristics of the basic fibres. The internal structure of the fibrous porous media is generally characterized by the fibre orientation and the fibre packing density. When the assemblages consist of long, *straight* relatively closely spaced fibres it is referred to as a fibre bed (Woudberg (2012a)).

For the purpose of modelling, fibrous porous media can, according to Tamayol & Bahrami (2009), be categorized according to the orientation of the fibres relative to one another:

- One-dimensional: The fibres are all parallel to each other, independent of the plane.
- Two-dimensional: The fibres are located in parallel planes with random orientation within the plane.
- Three-dimensional: The fibres have random orientations in space.

The analytical model(s) developed in this study will be based only on three-dimensional fibrous porous media (not foams) which, due to compression, resembles some two-dimensional properties. A detailed description of the applicable properties of the two types of porous media which are incorporated in the modelling process of this study, will be described in a subsequent chapter.

For the sake of completeness, and since the definition of permeability relates back to the modelling of fluid flow through **granular** porous media, a few important aspects in the historical development thereof are highlighted:



Granular porous media refer to relatively closely spaced granules (not necessary spherical and/or uniform) in contact with each other and usually held immobile by a tube or other vessel of which it forms the packing material. These packed beds are also classified as unconsolidated (or dispersed) porous media since the solid matrix is not connected (Woudberg (2012a)). A packed column is a type of packed bed which is of interest in chemical engineering and is widely used to perform separation processes and heterogeneous catalytic reactions.

The first significant attempt at addressing fluid discharge through porous media was postulated by Darcy after conducting experiments to examine the factors that govern the rate of water flow through vertical homogeneous sand filters. **Darcy's** phenomenologically derived constitutive relation states that the volumetric flow rate ( $Q$ ) is proportional to the constant cross-sectional area of the column, inversely proportional to the length of the filter and proportional to the difference in piezometric head across the length of the filter.

The **superficial velocity** (specific discharge, Darcy velocity or filter velocity),  $q$ , defined as the volumetric flow rate divided by the cross-sectional area normal to the direction of flow, is therefore (linearly) proportional to the hydraulic gradient (Bear (1988)). This experimentally derived form of Darcy's law (for a homogeneous, incompressible fluid) was limited to one-dimensional flow but has been generalized to three-dimensional flow where  $q$  and the hydraulic gradient are three-dimensional vectors. According to Nabovati et al. (2009) this relationship is valid in the creeping flow regime where (for porous media) the Reynolds number is significantly less than unity, i.e. at low Reynolds numbers where fluid inertial effects are negligible (e.g. Du Plessis & Van der Westhuizen (1993)). Deviations from Darcy's law at Reynolds numbers larger than 10 are attributed to inertial forces (Skartsis et al. (1992)).

According to Du Plessis & Van der Westhuizen (1993), initial experimental observations indicated that the pressure gradient is related to the square of the superficial velocity at higher Reynolds number flow ( $Re > 10^2$ ). In 1901 **Forchheimer** postulated an improved empirical relationship (first proposed by Dupoit in 1863) which consists of the Darcy equation with an additional term which is quadratic in superficial velocity.

The **Blake-Kozeny** equation for porous media consisting of solid particles through which fluid flows, is based on the assumption that this fluid flow resembles flow through a bundle of entangled tubes and that the hydraulic diameter of these tubes is linked to the effective particle diameter of the solid particles. Experimental data was used to account for the non-cylindrical surfaces of the solid matrix and the tortuous flow paths in typical packed-columns. The assumption is implicitly made that the packing of solid particles is statistically uniform so that there is no channeling.

According to Bear (1988), **Carman** described the effect of the tortuous nature of porous media on the velocity as well as on the driving force in a porous medium and this led to the introduction of the **tortuosity** concept. This characteristic that fluid particles follow tortuous flow paths through a porous medium has been defined in different ways, depending on the assumptions made. The tortuosity ( $\chi$ ) reflects the effect of the geometry of the porous structure on the length of the flow paths and was defined as the dimensionless

number (Du Plessis (1991))

$$\chi \equiv \frac{\text{linear displacement}}{\text{total tortuous pathlength}}, \quad (2.4)$$

or (later) as (Du Plessis & Van der Westhuizen (1993)),

$$\chi \equiv \frac{\text{total tortuous pathlength}}{\text{characteristic length}}. \quad (2.5)$$

According to (for instance) Tamayol & Bahrami (2011) the tortuosity factor is defined as the ratio of the average distance that a particle should travel in a porous medium to the direct distance covered. Several theoretical and empirical relationships for the determination of tortuosity have been proposed in the literature and according to Tamayol & Bahrami (2011) one of the most popular empirical models for the determination of tortuosity is Archie's law, i.e.

$$\chi = \left(\frac{1}{\epsilon}\right)^a, \quad (2.6)$$

where  $a$  is a tuning parameter that is determined through comparison of Archie's empirical correlation with experimental data for a specific porous medium. (A concise discussion on tortuosity is given by Woudberg (2012a).)

The above mentioned concepts will be referred to again when discussing information selected during the literature study and/or in the modelling process of the present study. Underlying many models of fluid flow (including the present one) is the continuum approach. Since the geometric model(s) employed in this study are based on existing models developed through closure modelling for volume averaged transport equations, important aspects of volume averaging will be highlighted in a concise manner in the next section.

## 2.2.2 Volume averaging

Due to the complexity of actual pore structures and the length scales involved, fluid transport in porous media is, (according to Thompson et al. (2002)), usually modelled using the continuum approach. These methods are very effective when the necessary averaged parameters are known or predicted with a high degree of certainty. However, these parameters must often be determined through experiments, especially in cases where the macroscopic parameters of interest depend strongly on pore-scale behaviour. This can limit the explicit incorporation of aspects such as pore structure, wettability variations or interface behaviour into a model (Thompson et al. (2002)).

According to Whitaker (1999), the method of volume averaging can be used to rigorously derive continuum equations for porous media. Equations which are valid within a particular phase of a multi-phase system, can be spatially smoothed to produce equations that are valid everywhere in the continuum. In effect a change of scale can be accomplished by the method of volume averaging which bridges the 'gap' between the velocity field in the pore space and Darcy's law which is valid everywhere in the porous medium.

Averaged parameters contain implicitly assumed length scales and therefore the proper choice of scales are of great importance. If the mean free path of a fluid molecule is comparable to a length scale of its confinement the continuum assumption of fluid mechanics is no longer a good approximation (Bear (1988)).

According to Bird et al. (2007), whenever the mean free path of gas molecules approaches the dimensions of the flow conduit, the velocity of the individual gas molecules at the solid-fluid interface has a finite value (not necessarily zero) and therefore contribute an additional flux. This is called the slip phenomenon, Klinkenberg effect, free molecular flow or Knudsen flow. This effect is evident in flow of a gas at low pressure through a porous medium. The slip-flow effect in micro-fluidic devices, where the no-slip assumption at the walls breaks down, is a case where the Knudsen number (defined as the ratio of molecular mean-free-path to the characteristic length scale of the problem) can be used to estimate the applicability of the continuum equations and whether free-molecular models should rather be employed (Zade et al. (2011)).

In this study it will be assumed that continuum equations are applicable, although, for a high level of compression, the slip phenomenon may play a role in the micro-channels.

According to the **volume averaging theory**, macroscopic balance equations for various transport phenomena may be obtained by averaging interstitial transport equations and fluid properties volumetrically over a **Representative Elementary Volume** (REV). In the case of single phase flow in porous media the velocity field in the *pore space* is determined by the Navier-Stokes equation, the continuity equation and the no-slip boundary condition. The change of scale from the microscopic pore space equations to the macroscopic equations (e.g. Darcy's law), is performed in three steps, namely obtaining the local volume average of the equations, developing a closure problem for the spatial deviations in the pressure and velocity (which are contained in the averaged equations), and then solving the closure problem in order to make predictions (Whitaker (1999)).

A REV is defined as a volume  $\mathcal{U}_0$  consisting of both fluid and solid parts which is statistically representative of the properties of the porous medium. According to Bear & Bachmat (1990), the condition under which a porous medium can be treated as a continuum is the existence of a range of volumes for a REV that satisfy certain size constraints. It is important to note that the size of the REV is not a single constant value. A REV is a volume that may vary in size within a certain range, the limits of which are determined on one end by the point where extreme fluctuations occur in the ratio of mass to volume, and on the other hand by some characteristic (macroscopic) length, such as the distance between two measuring points. According to Bear (1988), the REV volume should be much smaller than the size of the entire flow domain in order to represent what happens at a point inside this volume. The REV should *also* be significantly larger than the size of a single pore to ensure that it includes a sufficient number of pores to permit a meaningful statistical average required for the continuum concept.

According to Whitaker (1986), the traditional restriction on length scales, i.e.

$$l_s \ll r_0 \ll L_s, \quad (2.7)$$

where  $l_s$  is a characteristic length of the pore scale,  $r_0$  is the radius of the averaging volume and  $L_s$  is a length scale of the macroscopic boundaries, is not an inherent restriction in the

averaging method itself. It is nothing more than a convenient restriction that is satisfied by many systems of practical importance.

For a detailed description on how REV's are chosen and used to produce a continuum model of a porous medium, the reader is referred to Bear & Bachmat (1990).

Conceptually a REV is defined for each and every point of the averaging domain and according to Du Plessis & Diedericks (1997) it is assumed to have a constant size, shape and orientation at all times under consideration. Taking the volumetric centroid of the REV as the spatial point for which the (volumetric) average of a property  $\psi$  defined in the fluid filled part,  $\mathcal{U}_f$ , is determined, the **phase average**,  $\langle \psi \rangle$ , is defined as

$$\langle \psi \rangle \equiv \frac{1}{\mathcal{U}_0} \iiint_{\mathcal{U}_f} \psi \, d\mathcal{U}. \quad (2.8)$$

According to Whitaker (1986),  $\langle \psi \rangle$  is in general not the preferred average since it is not equal to  $\psi$ , when  $\psi$  is constant. The **intrinsic phase average**,

$$\langle \psi \rangle_f \equiv \frac{1}{\mathcal{U}_f} \iiint_{\mathcal{U}_f} \psi \, d\mathcal{U}, \quad (2.9)$$

is more representative of the conditions in the fluid phase. (Note that the definitions express averages for single-phase flow.) The **local (spatial) deviation** is defined as

$$\{\psi\} \equiv \psi - \langle \psi \rangle_f. \quad (2.10)$$

The porosity at any point of the porous medium is defined as the fluid phase average of 1 for the REV with centroid at that particular point:

$$\epsilon \equiv \frac{\mathcal{U}_f}{\mathcal{U}_0}, \quad (2.11)$$

and therefore the relationship between the phase and intrinsic phase averages is:

$$\langle \psi \rangle = \epsilon \langle \psi \rangle_f. \quad (2.12)$$

According to Whitaker (1999), for a property  $\psi$  defined in the fluid phase, the spatial averaging theorem for the fluid-solid system can be expressed as:

$$\langle \nabla \psi \rangle = \nabla \langle \psi \rangle + \frac{1}{\mathcal{U}_0} \iint_{\mathcal{S}_{fs}} \underline{n} \psi \, d\mathcal{S}, \quad (2.13)$$

with  $\underline{n}$  the outwardly directed unit normal vector for the fluid-phase on the differential area  $d\mathcal{S}$  and  $\mathcal{S}_{fs}$  the fluid-solid interface area contained within the averaging volume (Du Plessis & Diedericks (1997)).

For a viscous fluid (the velocity of the fluid-solid interface is equal to that of the fluid adjacent to it) the averaging of the time derivative of a property  $\psi$  leads to

$$\left\langle \frac{\partial \psi}{\partial t} \right\rangle = \frac{\partial \langle \psi \rangle}{\partial t} - \frac{1}{\mathcal{U}_0} \iint_{\mathcal{S}_{fs}} \underline{n} \cdot \underline{v} \psi \, d\mathcal{S}, \quad (2.14)$$

with  $\underline{v}$  the interstitial fluid velocity.

The concepts of a REV and volume averaging lead to the introduction of various measurable macroscopic quantities. The **superficial velocity**,  $\underline{q}$  will be used as velocity variable in averaged equations (Du Plessis (1991)). Its relationship with the phase averaged velocities and the porosity  $\epsilon$  is given by

$$\underline{q} = \langle \underline{v} \rangle = \epsilon \langle \underline{v} \rangle_f . \quad (2.15)$$

The superficial velocity determines the streamwise direction which is therefore, at any point in the porous domain, the direction of the average of the interstitial velocity in the REV with centroid at that point. The **drift velocity**,  $\underline{u}$  is defined as the *intrinsic* phase average of the interstitial velocity  $\underline{v}$ , which leads to

$$\underline{q} = \epsilon \underline{u} , \quad (2.16)$$

known as the Dupuit-Forchheimer relation. According to Nabovati et al. (2009) the complex structure of the pore-level geometry, especially in media of low porosity, produces narrow flow passages in which, as a rule of thumb, the local flow velocity is *proportional* to the volume-averaged flow velocity divided by the porosity.

The volumetric phase averaging of the continuity equation (2.1) under the assumptions of incompressible flow as well as a no-slip condition on the fluid-solid interface, yields

$$\nabla \cdot \underline{q} = 0 , \quad (2.17)$$

which governs conservation of fluid mass in the presence of solid matter (Du Plessis (1991)).

The volumetric phase averaged Navier-Stokes equation for an incompressible Newtonian fluid (under a no-slip assumption) may be expressed as

$$\begin{aligned} -\epsilon \nabla \langle p \rangle_f &= \rho \frac{\partial \underline{q}}{\partial t} + \rho \nabla \cdot (\underline{q} \underline{q} / \epsilon) + \rho \nabla \cdot \langle \{ \underline{v} \} \{ \underline{v} \} \rangle - \mu \nabla^2 \underline{q} \\ &+ \frac{1}{\mathcal{U}_0} \iint_{\mathcal{S}_{fs}} (\underline{n} \{ p \} - \underline{n} \cdot \underline{\tau}) d\mathcal{S}, \end{aligned} \quad (2.18)$$

where  $\underline{n}$  is the outwardly (relative to the fluid) directed unit vector normal to the fluid-solid interface. The local shear stress tensor,  $\underline{\tau}$ , has components given by equation (A.5) with  $\nabla \cdot \underline{v} = 0$ . As already mentioned, the gravitational (body) force is included in the pressure as a pressure head in equation (2.18).

Equation (2.18) is the governing equation for transport of momentum in porous media and the surface integral term contains all the information on the fluid-solid interaction (Du Plessis & Van der Westhuizen (1993)).

Assuming isothermal, time-independent, single phase flow, with no chemical or electrical influences, through a fully saturated unbounded porous medium, as well as assuming uniform viscosity and superficial velocity, the expression for the (intrinsic) pressure gradient

simplifies to:

$$-\epsilon \nabla \langle p \rangle_f = \frac{1}{\mathcal{U}_0} \iint_{\mathcal{S}_{fs}} (\underline{n} \{p\} - \underline{n} \cdot \underline{\tau}) d\mathcal{S}. \quad (2.19)$$

In this investigation it is further assumed that  $\nabla \epsilon$  is negligible so that the following equation forms the core of the closure modelling on which the method used in this study, is based:

$$-\epsilon \nabla \langle p \rangle_f = \frac{1}{\mathcal{U}_0} \iint_{\mathcal{S}_{fs}} (\underline{n} p - \underline{n} \cdot \underline{\tau}) d\mathcal{S}. \quad (2.20)$$

Due to the fact that in actual porous media there are always gradients in the porosity and/or saturation and/or pressure on all scales, it is possible that the centroid of the fluid phase (pore space) and the centroid of the averaging volume (e.g. the manometer opening) do not coincide. This implies that the intrinsic phase average pressure and the average pressure over the opening of the manometer are not the same. Korteland et al. (2010) introduced and investigated other potentially plausible averaging operators. The underlying mathematics of these averaging operators is beyond the scope of this study.

The permeability concept will be concisely addressed in the next section in order to provide the context in which the effect of compression of the porous medium is reflected in the permeability there-of.

### 2.2.3 Permeability

According to Darcy's law for unidirectional creeping flow through a porous medium the superficial fluid velocity is proportional to the pressure gradient. Hydraulic conductivity is the proportionality constant in which the (intrinsic) permeability is incorporated, and which depends on the porosity as well as the micro-structural geometry e.g. fibre arrangement, void connectivity and inhomogeneity of the medium.

Different properties of a porous medium have an influence on the permeability of the medium. Based on fluid flow simulations (using the lattice Boltzmann method) Nabovati et al. (2009) concluded that for straight cylindrical fibres of finite length the permeability increases with increasing aspect ratio (length to diameter ratio) when this ratio is less than about 6. (At a certain porosity the fibre diameter was kept constant and the fibre length changed.) This effect is negligible for values of the aspect ratio larger than 6. It was also found that fibre curvature has a negligible effect on the permeability of the medium (Nabovati et al. (2009)).

Pradhan et al. (2012) generated a series of virtual fibrous structures to determine the influence of three-dimensional fibre orientation on permeability and found that a fibrous structure with higher preferential orientation of fibres along the flow direction display higher transverse (relative to the flow direction) permeability. The current investigation will focus on the relationship between compression and permeability. The change in porosity due to compression and the consequent change in the diameters of the micro-flow channels, will explicitly be accounted for in the permeability prediction. Furthermore,

since it is reasonable to accept that compression causes changes in different properties (e.g. fibre orientation) of a porous medium, the effect of solid (re)distribution will also be investigated.

In many cases the relationship between permeability and porosity is qualitative and is not quantitative in any way. As in the case of pumice stone, clays and shales, it is possible to have high porosity and little or no permeability. Permeability therefore depends implicitly on the inter-connectedness of the pore spaces, and not just on the porosity itself, although permeability is often expressed only as a function of porosity.

The SI unit for permeability is  $\text{m}^2$ , but a more practical unit is the millidarcy (mD) with  $1 \text{ darcy} \approx 9.87 \times 10^{-13} \text{ m}^2$  or  $0.987 \mu\text{m}^2$ . In general, the magnitude of the permeability ( $k$ ) of a porous medium depends on a direction. For instance in reservoir rocks the vertical permeability is often much less than the horizontal permeability because of shale layers or other sedimentary structures.

According to Nabovati et al. (2009) it was proven analytically that the permeability of a porous medium is in general (for anisotropic porous media) a symmetric second order tensor which has six distinct components. (Since in general the pressure gradient as well as the velocity are vectors and each component of the pressure gradient influences each component of the velocity, the permeability can be visualized as an operator turning the pressure gradient into velocity by linear modifications of components.) In the principal coordinate space (since a symmetric second order tensor can always be diagonalized), Darcy's law can be applied in three directions of which, for example, the one in the  $x$ -direction of a rectangular Cartesian coordinate system is given by

$$q_x = -\frac{k_{xx}}{\mu} \frac{\partial p}{\partial x}. \quad (2.21)$$

For isotropic materials the permeability can be represented as a single scalar value since the three principal diagonal elements are equal and non-zero and all off-diagonal components are zero (Akaydin et al. (2011)). Nabovati et al. (2009) report simulation results that support the fact that it is valid to give a scalar value for permeability of random porous media since the off-diagonal elements are significantly smaller than the diagonal elements which differ by about two orders of magnitude.

Kołodziej et al. (1998) investigated an unidirectional fibre arrangement choosing one axis ( $z$ ) of the coordinate system ( $x, y, z$ ), parallel to the fibres' axes. The permeability tensor then have three non-zero entries on the principal diagonal with the other entries all equal to zero. For a homogeneous bundle of fibres the permeability is characterized by two scalar quantities since it is usually assumed that the two components of the permeability tensor in the principal directions perpendicular to the fibres are equal. In their investigation regarding non-homogeneous (non-uniform fibre spacing) fibrous media, Kołodziej et al. (1998) also assumed the permeabilities in the directions perpendicular to the unidirectional fibres to be equal.

When modelling, in this study, the effect of compression on the permeability of three-dimensional fibrous porous media, the porous medium is not assumed to be isotropic (before or after compression). For the modelling process the coordinate system will be

chosen in such a way that the pressure gradient and average streamwise velocity coincides with a relevant principal direction (of the permeability tensor). The predicted permeability will in addition be expressed as a scalar.

Although permeability is regarded as dependent on the geometry of the porous medium, different permeabilities can become apparent when using different fluids, i.e. liquids versus gases. Difference in gas and water permeabilities for a specific porous medium can be analyzed in view of the Klinkenberg effect which is due to slip flow of gas at pore walls which enhances gas flow when pore sizes are very small. Physically it means that the significant molecular collisions are with the pore wall rather than with other gas molecules.

According to Shou et al. (2011), for superfine fibres ranging from 50 nm to 5  $\mu\text{m}$ , the continuum non-slip assumption is not strictly correct. After studying the effect of the Knudsen number on the dimensionless hydraulic permeability of fibrous porous media, Shou et al. (2011) concluded that the effect on the Darcy hydraulic permeability caused by the fibre radius is significantly larger than that of the accompanied slip influence. In the present study air is the fluid used in the two relevant experiments to measure permeability and the radius of the fibres in question are on average 2.7  $\mu\text{m}$  and 10  $\mu\text{m}$ , respectively. Nevertheless, for the modelling process to be employed in this study it will be assumed that the conditions of no-slip at the surfaces of the fibres as well as the application of the continuum equations are reasonable. Viscous flow is assumed in this study and the characteristic length (hydraulic diameter) is more than two orders of magnitude that of the molecular mean-free-path of air at atmospheric pressure. The effect of slip-flow on permeability will therefore not be incorporated in the present study.

It is important to note that in the mathematical description of the relationship between the superficial fluid velocity and the pressure gradient in a porous medium, inertial coefficients also play a role when flow in the Darcy regime is not assumed. Since this study will only be concerned with flow in the Darcy regime, inertial coefficients such as the passability (which relates the pressure drop to the square of the superficial velocity for Reynolds numbers significantly larger than unity (Woudberg (2012a))), will not be addressed. Adapting the model(s) developed in this study to incorporate the effect of developing flow may be considered as future work.

The bulk behaviour of permeability under compressive stress is different in different applications e.g. biological tissues and rocks. Dynamic compression of the solid and fluid phases of a soft porous medium (e.g. soft snow) causes mutual interaction between the two phases which changes the flow resistance through the pores and therefore also the permeability. It must therefore be kept in mind that techniques to measure permeability under compression have often been developed with a specific application in mind (Akaydin et al. (2011)). For the purposes of this study a stationary porous medium after uni-axial compression will be assumed. Thus, after each compression the porosity is measured or calculated.

Experiments, simplifying assumptions, verification, reflection and adaptation are important aspects in a modelling procedure. A selection of information from the literature study will highlight these and other aspects regarding the development of different models for fluid flow through fibrous porous media. Chapter 3 will be devoted to the different (and similar) ways in which modelling is done.



# Chapter 3

## Literature study

When developing a mathematical model, whether a financial, statistical, fluid flow or any other model, the assumptions made as well as the modelling procedure itself should be informed by what has been done by others regarding the chosen context.

This chapter is devoted to a concise (and subjective) summary of articles that were chosen to represent the relevant information acquired during the literature study. This summary will not reflect the effectiveness of different models but highlight the ‘ideas’ and ‘tools’ used. Modelling processes in general are influenced by the perceptions (insights) of the modeller and therefore, when filtering information from the different sources, the ‘historical development of ideas’ and the assumptions made, are the main focus.

Predicting the effect of compression on the permeability of a fibrous porous medium can be done by employing models developed for uncompressed media. Given the porosity of a porous medium in a compressed state, a permeability prediction can be made. For models based on an assumption of isotropy the prediction will most probably be an over-estimation of the permeability e.g. the isotropic foam model referred to by Woudberg (2012a). Nevertheless, information regarding modelling processes not directly focussed on compression of fibrous porous media was (and is) considered just as important for the aim of the literature study as processes focused on the effect of compression. Experimental work and/or simulations, with accompanying assumptions and methods of processing and interpretation of data, are also rich sources of information.

Since the literature study was also aimed at gathering (subtle) information regarding the modelling process itself with accompanying assumptions and reflections, the information selected in the next sections are not limited to the assumptions made in the present study.

The first section will refer to general literature regarding fibrous porous media, the second to literature regarding RRUCs and the last section will provide information regarding experiments of which the data was employed in the present study. A short general discussion regarding the information presented as well as its relevance to the present study will be given after the different articles from the literature were discussed.

## 3.1 Studies from the literature

Information selected from relevant articles regarding the prediction of the permeability of fibrous porous media is presented. The choice was made to do this presentation using the minimum amount of equations and rather to describe the modelling processes in words, since formulas do not always facilitate thinking about the principle behind it. The mathematics behind the modelling procedures will therefore be omitted. The main aim is to highlight the different approaches and assumptions in the different permeability investigations.

### **Jackson & James (1986)**

According to Jackson & James (1986), the permeability of a fibrous porous medium depends on the arrangement, concentration and size of the fibres. In this literature study, data and theories related to the dependency of the resistance of a fibrous medium on the structure of the medium were filtered and comparisons were made. This was done on the basis of the hydrodynamic permeability as defined by Darcy's law. The permeability was non-dimensionalized by dividing it by the square of the fibre diameter or radius. When necessary, the permeability values were converted from parameters such as the fibre drag, the drag coefficient or the friction factor. The filtering of data was done according to the following criteria: Reynolds numbers (based on fibre diameter and superficial velocity) less than 10, the Knudsen number (when applicable) less than 0.01 and known fibre diameters and solid volume fractions.

Based on the comparison of the chosen experimental data, it is concluded that the most important factors of fibre arrangement, that have an effect on permeability, are fibre alignment and homogeneity of the porous medium. They found that when fibres are normal to flow, the resistance could be double the resistance when fibres are aligned with the flow. When all the fibres are normal to the flow, the alignment of fibres relative to one another (for instance parallel or not) also has an effect on the permeability. A more uniform distribution of fibres in a medium leads to a lower permeability. Non-uniformities in the porous structure as well as channelling (due to an excessive pressure drop applied to loose fibres) can cause a significant increase in permeability.

Comparison of the selected theoretical work (up until 1986), shows that the general approach has been to idealize the porous medium as a matrix of rods and then to solve Stokes' equations for a particular problem. Three categories are apparent, namely flow parallel to an array of parallel rods, flow perpendicular to an array of parallel rods and flow through three-dimensional arrays of rods. The 'unit cell' approach (polygon with a rod at the center), where the rods are arranged in a periodic pattern e.g. square, triangular, hexagonal or rectangular arrays, reduces the problem to solving Stokes' equations in the unit cell. A no-slip condition at the rod surface is employed and usually a zero velocity gradient at the edge of the cell. For flow through three-dimensional arrays, the problem of a rod oblique to the superficial velocity was solved by allowing the permeability to have different values in the directions parallel and perpendicular to the flow. The permeability of the three-dimensional medium is then determined by averaging over the three principal rod directions. Power series techniques, Fourier series methods and other techniques were respectively employed for solving Stokes' equation in different models.

The conclusions of the literature study by Jackson & James (1986) are the following: (i) The scatter in the data for diverse fibrous materials is caused by inhomogeneity and by variations in fibre shape and arrangement. The data correlates reasonably well when the non-dimensional permeability and the solid volume fraction are used as parameters. (ii) The resistance of an array of fibres aligned to the flow can be predicted with some accuracy (as shown by the agreement of the predictions of the analytical techniques). Such predictions have limited usefulness since actual media rarely consist of fibres aligned in the direction of flow. (iii) For arrays normal to the flow, the collective curve produced by the data represents the minimum permeability for uniform arrays of parallel circular fibres. Lower permeabilities can be produced through modelling only by non-parallel arrangements of fibres or by fibres which are highly non-circular. (iv) The prediction by a three-dimensional model can be satisfactory if it realistically combines the flow resistances of rods parallel and perpendicular to the flow.

### **Skartsis et al. (1992)**

Skartsis et al. (1992) reviewed theoretical and experimental studies focused on the flow of Newtonian fluids through consolidated fibre beds within the context of the autoclave and other composite manufacturing processes, where the description of resin flow through a fibre bed is critical.

It is evident from the review that Darcy's law is the basic equation used for laminar flow through porous media which is fully saturated with a Newtonian fluid and that the Blake-Kozeny-Carman equation is applied for isotropic porous media with porosities between 0.4 and 0.7. At higher and lower porosities the correction due to 'increased path length' is not found to be sufficient and it is suggested that the additional pressure drops due to the converging-diverging character of the flow channels should be included.

Despite objections against e.g. the constant diameter capillary assumption, it is stated that when assuming slow Newtonian flow through porous media (as will be assumed in the present study) the proportionality between flow rate and pressure drop is retained within limited porosity ranges.

In general, non-uniformities in a random porous medium statistically eliminate one another. For aligned fibres, on the other hand, any non-uniformity will cause a biased flow which can not be accounted for only by tortuosity and therefore the Blake-Kozeny-Carman equation can not be used as an explicit (general) relationship between permeability and porosity. According to Skartsis et al. (1992), a more accurate approach is to find analytical and/or numerical solutions for each particular case by solving the complete equations of motion for the porous medium in question and then compare the solution to Darcy's law to find a relationship between porosity and permeability.

When modelling random fibres, the proper representation of randomness is a critical issue and one approach is to consider the resistance to flow as a weighted average of the resistance due to flow parallel and normal to cylinders. A key result for flow through actual fibre beds is (according to Skartsis et al. (1992)) that the resistance to transverse flow through *aligned* fibres was found to be twice that for axial flow in experiments conducted by Sullivan in the 1940's.

From experiments it became clear that the kind of fibres (e.g. stiffness) as well as the type of fluid passing through a fibre bed, influences the pressure drop. Non-uniformity in fibre arrangement in an actual aligned fibre bed is an important factor that influences permeability, especially as porosity increases. An increase in tortuosity from fibre bending (non-uniform fibre arrangement) could counter the ‘wide-path’ permeability increase due to the non-uniformity. For transverse flow, the non-uniform arrangement of fibres should produce a chain effect where the narrowest path(s) limit(s) the flow.

Stiffness and diameter of fibres were found to be determining factors in the distribution and alignment of the fibres and thus influence the probability of a non-uniform arrangement. If Darcy’s law is to be applied in a modelling process it is also important to eliminate the possibility that the applied pressure difference for flow, changes the properties of the porous medium by changing the non-uniformities. Surface effects, for example adsorption, is not likely to be pronounced for Newtonian flow. For randomly arranged fibres, the permeabilities predicted by random cylinder theory are significantly lower than the measured values. Experimental data show that “fine fibres”, with radii between 1 and 9  $\mu\text{m}$ , exhibit higher permeabilities than fibres with larger radii.

### **Tamayol & Bahrami (2009), (2011), and (2012)**

Tamayol & Bahrami (2009) developed an analytical model to predict the permeability of ordered fibrous media for normal and parallel flow. Fibre arrangement is represented by touching and non-touching arrays of cylinders. According to the authors the one-dimensional model, where fibres are parallel to one another (but randomly distributed in the volume) is the most anisotropic model and was used in their 2009 study. Assuming the fibrous medium to be periodic, the chosen unit cells used to analyze the geometry of the porous medium, repeat throughout the material. Creeping, incompressible and steady flow were assumed and an approximate parabolic velocity profile was considered which satisfies the boundary conditions within the chosen unit cell. Tamayol & Bahrami (2009) recognize two limits for fibrous media, namely touching cylinders which can be envisioned as a packed bed and highly porous media with porosities near unity.

In the *limit of touching cylinders*, the normal permeability is zero since the resulting flow can not pass perpendicular to touching fibres. The fluid flow parallel to the axis of touching uni-directional fibres is treated as channel-like flow in a combination of parallel constant cross-sectional channels. Using the Darcy-Weisbach relationship, the permeability was expressed in terms of the Fanning friction factor, porosity, viscosity, density, hydraulic diameter and the volume-averaged superficial velocity. The (parallel) permeability of triangular, square, hexagonal and a combination of octagonal and square arrays of touching cylinders were determined using the numerical Fanning coefficients reported by Shah and London in 1978. The authors chose, in addition, to follow the model of Bahrami et al. (2007) that uses  $\sqrt{A}$  as the length scale, where  $A$  is the cross-sectional area, claiming that this leads to more consistent results when considering random cross-sections such as for the ‘channels’ between ‘touching cylinders’.

In the model of Bahrami et al. (2007) for pressure drop in singly connected micro-channels of arbitrary cross-section, the pressure drop is related to the area of the passage cross-section and the polar moment of inertia. This is based on the Saint-Venant principle that the torsional rigidity of a tube can be approximated by replacing the given tube by a

tube with an elliptic cross-section which has the same cross-sectional area and the same polar moment of inertia as the original shaft. According to Bahrami et al. (2007), this principle can be used since torsion in beams and fully developed, laminar, single-phase flow in ducts are similar in the sense that the governing equation for both problems is Poisson's equation (i.e.  $-\nabla^2 u = f$ ).

Tamayol & Bahrami (2009) calculated the Fanning friction coefficient with  $\sqrt{A}$  as the length scale and combined the model of Bahrami et al. (2007) with Darcy's law to obtain an expression for the non-dimensional permeability of periodic touching fibrous media.

For fibrous media in the *porosity limit near unity*, the **normal permeability** of a *square arrangement of cylinders* was calculated based on a square unit cell with the sides of the square connecting the midpoints of four (circular) cylindrical fibres. (The same approach can be followed for the rectangular unit cell.) The porosity is expressed as the ratio of the difference between the area of the square and the cross-sectional area of a fibre (4 quarters), and the area of the square.

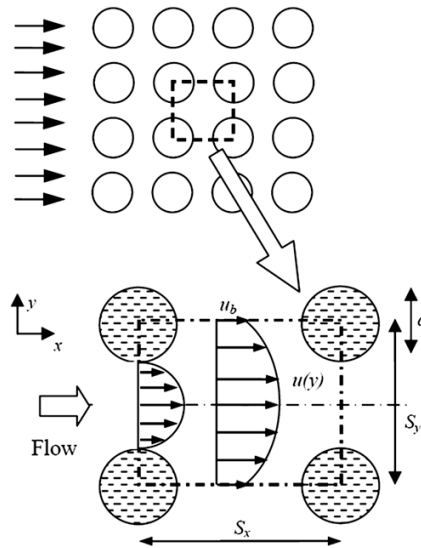


**Figure 3.1:** Unit cell used by Tamayol & Bahrami (2009). [Source: Tamayol & Bahrami (2009)]

Applying Darcy's law, the permeability is related to the total pressure drop through the unit cell as depicted in Figure 3.1. Creeping flow, negligible inertial terms, no-slip condition on the surface of the cylindrical fibres and a zero velocity at the unit cell border line were assumed. A parabolic velocity profile in terms of the 'half thickness' of the unit cell in the  $y$ -direction was assumed and  $dP/dx$  was obtained via the  $x$ -momentum equation. An expression for the total pressure drop over the chosen unit cell was obtained by substituting this velocity-expression into the continuity equation and integrating.

Rewriting Darcy's relation for just one unit cell and substituting the calculated cell pressure drop, the normal permeability is only a function of the geometrical parameters of the porous medium. This is based on the assumption that the 'borderline' velocity is zero everywhere along the boundaries of the unit cell that are parallel to the flow. In

general, this is not the case: It is zero on the edge of the cylinders (no-slip condition) and reaches its maximum value at half the side length (in the direction of flow) of the unit cell. Tamayol & Bahrami (2009) incorporated this in their model by assuming that the maximum border velocity is related to porosity through a linear function of porosity  $g(\epsilon)$  with  $g(0.215) = 0$  and  $g(1) = 1$ . This leads to an expression for the normal permeability of the square arrangement that accounts for the border velocity.

For fibrous media in the *porosity limit near unity*, an expression for the **parallel permeability** of a square arrangement of cylinders was also obtained. The same approach was followed with the same unit cell as described above, but with flow parallel to the length of the cylinders.

The authors also investigated the effect of the unit cell aspect ratio,  $S_x : S_y$ , (refer to Figure 3.1) on the non-dimensional permeability of normal flow through a rectangular fibre-arrangement. The porosity and fibre-diameter were kept constant while the aspect ratio was varied. As the unit cell aspect ratio was increased, the normal permeability decreased considerably for relatively low porosities while for highly porous materials this variation was relatively small. The change of parallel permeability due to the variation of the aspect ratio of the unit cell was not as significant as those for normal flow. This can be explained by the fact that since porosity is kept constant, the permeability is related to the cross-section of the pores (which is also constant) although the aspect ratio is changed. (The one-dimensional fibres parallel to the flow are assumed to produce capillaries with a slip velocity boundary condition.)

According to Tamayol & Bahrami (2009), only the average fibre diameter and the medium porosity are needed to predict the permeability with this model and no tuning parameters are required.

The same authors (Tamayol & Bahrami (2011)) developed a theoretical approach regarding transverse permeability that is applicable to one-, two- and three-dimensional fibrous matrices. A scale analysis technique was applied to different arrangements of unidirectionally aligned fibres, simple two-directional mats and cubic structures. As a result, compact relationships were presented for permeability as a function of porosity and fibre diameter.

In this approach, the scale or the range of variation of the parameters in question were substituted into the governing (continuity- and Stokes') equations. (The pressure drop was assumed to be due to only frictional effects.) The length scale over which rapid changes in velocity occur was chosen as half of the minimum width between two adjacent cylinders.

The average velocity in the section of the unit cell with minimum frontal area was used as the characteristic velocity scale. It is approximately equal to the superficial velocity divided by the ratio of the minimum to total frontal areas in the unit cell. This did not reflect the effect of tortuosity (defined by the authors as the ratio of the average tortuous path length a fluid particle should travel in a porous medium to cover the length of the porous sample). Using Archie's law (equation (2.6)), with applicable values for the tuning parameter, tortuosity was incorporated under the assumption that for a constant pressure drop, the resulting velocity scale is inversely related to the tortuosity.

As a result, the permeability was expressed in terms of scale factors and compact models were developed using the geometrical properties of the one-, two-, and three-dimensional micro-structures.

Tamayol et al. (2012) investigated the effects of mechanical compression on the single phase through-plane permeability of carbon paper gas diffusion layers (GDLs). This was done in the context of proton exchange membrane (PEM) fuel stacks where the cell components are compressed together to prevent gas leakage from the system. In general the GDLs are porous media made of carbon fibres with diameters ranging from 7 to 10  $\mu\text{m}$ . These carbon papers or cloths have a complex micro-structure with a random distribution of fibres. In the experimental approach, the carbon papers were cut into circular samples, compressed and the variation in thickness measured with a micrometer. The airflow rate through the samples were measured and the Reynolds number based on the fibre diameter was lower than 0.1. Therefore, to analyze the experimental results, Darcy's law was applied with the pressure drop across the thickness of the GDL. To account for minor pressure losses at the exit and entrance sections of the sample holder, the pressure drop in the test section was measured once without any GDL samples. This was subtracted from the measured values of the pressure drop.

Based on the models developed for uncompressed fibrous porous media, (as already discussed), a relationship for the dimensionless through-plane permeability for GDLs was obtained in terms of the solid volume fraction. Assuming that during the compression process, the volume of the solid carbon fibre remains constant, the solid volume fraction of a compressed sample was expressed in terms of the original value for an uncompressed carbon paper and the ratio of the uncompressed GDL thickness to the compressed thickness.

As will be discussed in detail in Section 4.1, the relationship between compression and the solid volume fraction is essential in the prediction of the permeability of a porous medium subject to a compressive load.

### **Shou et al. (2011)**

In this study the hydraulic permeability for viscous flow through high porosity ( $\epsilon > 0.7$ ) fibrous porous media was presented. Repetitive unit cells, based on Voronoi tessellations, were employed as well as the volume averaging method. The modelling procedure was based on a geometrical simplification of the fibrous media to arrays of cylinders in one-, two- and three-dimensional structures respectively, in the same sense as the categorization according to Tamayol & Bahrami (2009). Starting from the regular one-dimensional structure and a square unit cell, assuming slip flow (the normal component of velocity vanishes at surfaces but not the tangential component) and neglecting the effect of compressibility and rarefaction (since the Mach number was low enough), a formula for the dimensionless hydraulic permeability was obtained. This was done by employing the Knudsen number, the continuity- as well as Stokes equations, the stream function (and assuming zero vorticity for flow perpendicular to the fibres) as well as Darcy's law. For randomly placed fibres of one-dimensional media, the Voronoi tessellation was applied and a Voronoi cell used as the unit cell.

For the two- and three-dimensional cases, closure modelling of volume averaging was done

by assuming that the porous medium consists of repetitive cubic cells in which the overall fibre orientation is characterized by the fractional length of the fibres orientated in the  $x$ -,  $y$ -, and  $z$ -directions, respectively. The fibre fractional length was determined by the fibre fraction in the same direction of the cubic cell. The results for the one-dimensional structure were used to model the two- and three-dimensional cases by combining the contributions in the three orthogonal directions. This was done by calculating a volume averaged drag coefficient and making approximate corrections for the fact that the hydraulic drag forces of fibres in different directions are inter-dependent. Here the assumption was made that when determining permeability of fibres in one direction the fibres in other directions have a negligible effect, except for their occupation of space in the cubic cell.

Using the resulting formula for dimensionless hydraulic permeability, the investigation of the effect of through-plane fibre orientation on the hydraulic permeability for flow perpendicular to the three-dimensional fibrous media showed that the permeability increases significantly with increase in the through-plane fibre orientation. Another conclusion is that the hydraulic permeability increases with increasing degree of randomness of the fibres although this effect is less significant in the three-dimensional case.

### **Zobel et al. (2007)**

Spun-bonding is a manufacturing technique where filaments are extruded from multiple banks of spinnerets, cooled and drawn to their final diameters and laid down onto a porous conveyer belt. The fibres in the matt do not form bonds at the cross-overs and require subsequent bonding. Thermal calendering is frequently used for bonding spun-bonded webs. Based on this context, virtual three-dimensional non-woven structures were generated and compressed from top and bottom in order to simulate the permeability of fibrous non-woven materials before and after compression. Virtual spun-bonded non-wovens were generated and their structural changes during the calendering process simulated at different compression ratios (in this context, the ratios of the original to final thicknesses).

The permeability of the media was calculated at each step of compression by computing the resistance of the fabric against laminar uniform airflow.

The fibres were modelled as having a square cross-section and laying horizontally in the  $xy$ - plane of the web and only in the  $\underline{i}$ - or  $\underline{j}$ -direction of a rectangular Cartesian coordinate system. An uncompressed three-dimensional web was generated with the fibres represented as a succession of cubes of size 1, with integer coordinates in the  $\underline{i}$ - and  $\underline{j}$ -directions. Anisotropic fibre-webs were generated where the number of fibres in one direction was greater than that in the other direction. For the compression part of the simulation it was essential to 'know' which cube in which fibre is in contact with which other cube in which other fibre since this information was employed in simulating the bending of the fibres during the compression process. The detail falls beyond the scope of the present study.

The fluid flow modelling was based on steady state, laminar and incompressible flow with the Reynolds number (based on the fibre diameter) less than unity. A finite volume method was employed to solve for the airflow field. The underlying methodology is to subdivide the solution domain into a large number of control volumes. The govern-



ing partial differential equations (in this case the continuity and conservation of linear momentum) can, by integration over these control volumes, be converted into a set of algebraic equivalents which is then solved by iterative methods.

Details regarding the computational grid as well as the boundary conditions fall beyond the scope of this study. Important to note is the assumption of a no-slip boundary condition on the fibre surface since slip on the fibre surface was considered negligible. Therefore, at the standard temperature and pressure, the diameter of the fibres being simulated are assumed large enough ( $\sim 10 \mu\text{m}$ ) so that a continuum approach is justified.

The permeability was calculated using Darcy's law with the pressure drop across the porous medium's thickness. The effects of fibre rigidity was also investigated through simulations and it was concluded that when fibres are rigid, the compression process propagate deeper into the media resulting in a more uniform SVF across the thickness of the fabric.

### 3.1.1 Discussion

It is clear from the literature study that Darcy's law is still central to most modelling processes in the lower Reynolds number flow regime. Cylindrical geometry is more often used than rectangular geometry to resemble the shape of the fibres and morphology of the porous medium. The assumption of no-slip at the fluid-solid interfaces is frequently employed. Different forms of unit cells and arrays are used in the modelling procedures. The apparent friction factor and/or tortuosity were incorporated into the modelling procedures by some authors. The solids were assumed to be impenetrable and the porous medium fully saturated, the compression was uni-axial and the fibres itself were not compressed. Fully developed flow was assumed in some cases and developing flow in others. Laminar, steady state and incompressible flow (at low Reynolds numbers) are common assumptions.

In the modelling procedure followed in the present study, the aim is to represent the flow resistance of fibres parallel and perpendicular to flow in a geometric model where the ratio of surface-areas parallel and perpendicular to the streamwise direction is derived from the porosity and the structure of the medium. A weighted average of the resistance to flow parallel and normal to the fibres will be implicitly incorporated through the geometry of the representative solid in the newly proposed model. The solid in the present study will not reflect the fibre shape as such, but rather a minimal resultant distribution of solids represented by a single solid. Also, a *representative* unit cell will be employed and due to the fibrous porous media under consideration, the focus will be on high porosities. The present study will also only take frictional effects into account.

In Chapter 4 detail regarding assumptions will be given which will highlight the similarities and differences with the modelling procedures referred to in this section.

It is clear that, given a certain physical concept (e.g. permeability), different geometries, mathematical concepts and assumptions can be (and are) employed in the modelling process there-of. Relevant concepts from previous models based on rectangular geometry

which serve as a cornerstone for the development of (a) model(s) for the prediction of the effect of compression on the permeability of fibrous porous media will be discussed in the next section.

## 3.2 Literature regarding RRUCs

Originally introduced by Du Plessis and Masliyah as the *Representative Unit Cell* for isotropic foam-like media, the RRUC (extra ‘R’ to emphasize the *Rectangular* geometry) is a geometric pore-scale model developed with focus on mathematical simplicity. In order to fulfil the basic requirements of the geometry of the actual porous structure that it resembles, it respectively takes on different rectangular geometries for granular media, foamlike media and fibre beds (Woudberg (2012a)).

A short summary of earlier RRUC models, with an emphasis on the assumptions made, will be given in this section. The first models, that reflect the original trail of thought, are of special interest, although later refinements of these models will be incorporated where relevant. (The comparative analysis of Woudberg (2012a) provides an extensive overview of the existing RRUC models.)

Since the present study is only concerned with quantifying pressure loss in terms of shear stresses, the focus of the summary will be on how shear stresses were incorporated in the models.

According to Du Plessis & Van der Westhuizen (1993), the RRUC is a schematic (rectangular prism) representation of a hypothetical control volume containing a single solid, which captures the locally averaged essence of the micro-structural parameters in a physically plausible manner. The REV contains several pores and solid parts over which an average is obtained. However, in the case of the RRUC the average geometry is obtained before being embedded into the chosen geometric representation (Du Plessis (1991)).

The RRUC can not be regarded as a repetitive building block since it is practically impossible to construct an isotropic array (Woudberg (2006)) since isotropy and even transverse isotropy can not be justified in the unconsolidated RRUC models (Woudberg (2012a)). The emphasis in the ‘name’ *RRUC* should be on *representative*.

### 3.2.1 Foam RRUC model

Figure 3.2 is a visual representation of the original RRUC model proposed for flow through a rigid, isotropic and consolidated porous medium. Under the assumption of isotropy, the mean pore cross-sectional area is the same in each of the three principal directions and the fluid enters and exits the RRUC in the streamwise direction. The three short mutually perpendicular square duct sections exhibit maximum possible inter-connectivity as well as maximum possible staggering (Du Plessis & Masliyah (1988)).

In the modelling procedure followed by Du Plessis & Masliyah (1988), the tortuosity is

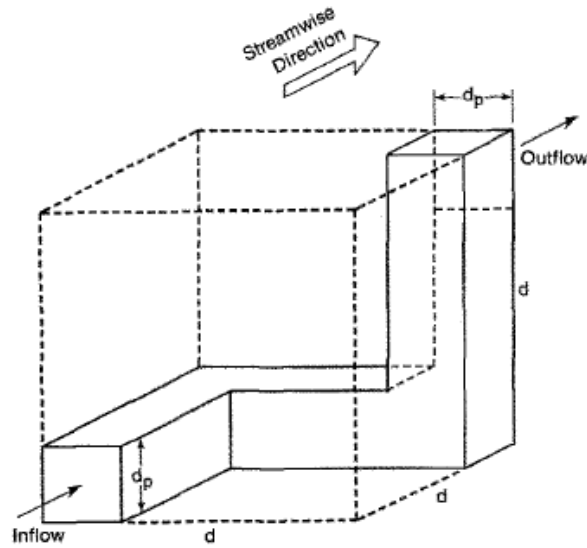


**Figure 3.2:** Original RRUC model proposed for flow through a rigid, isotropic and consolidated porous medium. [Source: Du Plessis & Masliyah (1988)]

defined as the ratio of the linear displacement of fluid in the RRUC to the total flow length in the RRUC. Due to the representation of isotropy in the geometry of the chosen RRUC, the porosity can therefore be expressed uniquely as a function of the tortuosity. The assumption was also made that the average velocities in the transverse and streamwise duct sections are equal in magnitude and that flow conditions may be inferred from analytical results for developing flow in a square duct. Applying an asymptote-matching technique to the expressions for the (apparent) friction factor in the very short- and long duct limits, an equation applicable to any duct length was obtained. Through closure modelling of equation (2.18) (under the assumption that the surface integral term may be approximated by three times the contribution of the shear stresses in the streamwise duct section) a general expression, with no restriction on the porosity range, was derived for the Darcy permeability.

### 3.2.2 Granular RRUC model

For flow through unconsolidated granular porous media, Du Plessis & Masliyah (1991) derived a momentum transport equation for a single phase fluid with constant physical properties. The porous medium was assumed to be stationary, rigid and locally isotropic with respect to the average geometrical properties. It was also assumed that the flow is laminar with no local flow separation within the pores and that the no-slip boundary condition is applicable to all fluid-solid interfaces. Figure 3.3 visualizes the assumption that the average geometrical properties of the solid structure within an REV can be resembled by a cube within a cubic RRUC. In order to maintain isotropy and ensure that the fluid traverses all void sections, the arrangement of neighbouring cubes provided maximum possible staggering.

Under the assumption of a constant cross-sectional flow-area equal to  $d^2 - d_s^2$  (in terms of the dimensions indicated in Figure 3.3) the total tortuous path length was defined as the

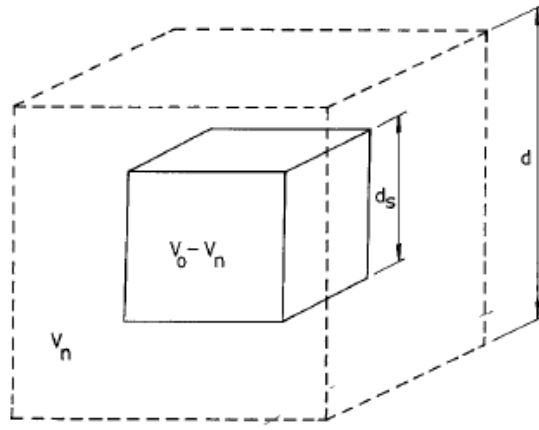


**Figure 3.3:** Original RRUC model proposed for flow through rigid, isotropic granular porous media. [Source: Du Plessis & Masliyah (1991)]

total fluid volume divided by this cross-sectional flow-area. The tortuosity was defined as the side length of the RRUC divided by this tortuous path length.

Closure modelling, commencing from equation (2.18), was done based on the assumption that the cross-sectional mean pore velocity in each duct section is directed axially along that specific duct section and that the duct sections are orientated either perpendicular or parallel to the locally averaged velocity. In the evaluation of the surface integral, the shear stresses which occur along transverse surfaces were manifested through the pressure term and it was assumed that the magnitude of the transverse and streamwise average flow velocities are equal. The frictional effects on the traversing fluid was quantified using an expression for the apparent friction factor - Reynolds number product obtained through interpolation and asymptote matching. This was done by incorporating the friction factor for fully developed laminar flow between infinitely long parallel plates (low porosity) and for flow development along a short flat plate (high porosity) (as proposed by Shah & London (1978)). The distance between the parallel plates was taken as  $(d - d_s)$ .

The fact that two-thirds of the flow length is orientated streamwise and one-third transversally was incorporated. This is a direct result of the geometry of the RRUC in Figure 3.3. It was also assumed that the average wall shear stress gives rise to the total apparent Fanning friction factor between two facing surfaces over a flow developing length of  $d_s$ . An expression for a velocity-independent Darcy-permeability for very low Reynolds number flow was obtained. The theoretical result was also used to predict the inertial effects in the non-Darcy (Forchheimer) regime through the use of the Reynolds number. It was suggested that a shape factor of some kind could be introduced to improve the prediction capability of the model.

### 3.2.3 Fibre RRUC model

Using a rectangular representation of fluid-solid interfaces, such as depicted in Figure 3.4, Du Plessis (1991) derived momentum transport equations for laminar incompressible Newtonian flow to describe saturated crossflow through a two-dimensional porous medium.

This was done based on the condition that the two-dimensional porous medium consists of rigid stationary prisms which are mutually parallel. The prisms were hypothetically positioned in such a way that the assumptions of local isotropy with respect to average geometrical properties in the directions perpendicular to the streamwise direction, as well as maximum spatial staggering of the prisms, were reflected.

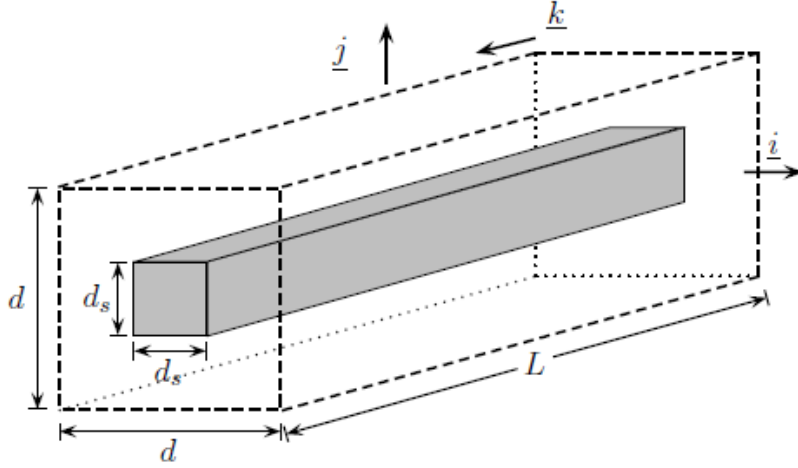


**Figure 3.4:** Fibre RRUC model for predicting the permeability of a fibrous porous medium.

The local specification of streamwise and transverse directions is allowed through an assumption that at any point within the domain under consideration, the RRUC can be orientated in such a manner as to have one side parallel to the local superficial velocity.

The model assumed single phase flow, constant physical properties, flow that takes place in a plane perpendicular to the prism axis and a no-slip boundary condition at the fluid-solid interfaces. Tortuosity was defined in the same way as for the granular- and foam models, and as a function of porosity, highlights the fact that a geometric model must reflect the relevant porous medium type.

Referring to Figure 3.4, some notational definitions applied to the original fibre RRUC model, as well as the partitioning of volumes are given in Table 3.1 for an array without any stagnant volumes. For the sake of mathematical simplicity the RRUC is placed in a Cartesian coordinate system in such a way that the fibre axis is parallel to the  $z$ -axis, as indicated in Figure 3.4.

Du Plessis (1991) obtained a single expression for the product of the apparent friction factor of any straight pore section and the Reynolds number, in terms of the length of the section. This was done by applying an asymptote matching technique to the expressions obtained in the limits of fully developed laminar flow between infinitely long parallel plates (low porosity) and flow development along a short flat plate (high porosity).

A unified expression, applicable to any streamwise surface length, was obtained assuming a uniform entry velocity profile within a parallel plate configuration. The distance between the parallel plates was assigned  $(d - d_s)$ , with  $d_s$  and  $d$  the side lengths of the square solid- and RRUC - bases, respectively, and  $L$  denoting the lengths of both the RRUC

Parameter	Fibre RRUC model
$U_o$ (total volume)	$d^2 L$
$U_s$ (total solid volume)	$d_s^2 L$
$U_f$ (total fluid volume)	$(d^2 - d_s^2)L$
$U_t$ (total transfer volume: no wall shear stresses)	$(d - d_s)^2 L$
$U_{\parallel}$ (total streamwise volume)	$d_s(d - d_s)L$
$S_{fs}$ (fluid-solid interfacial area)	$4 d_s L$
$S_{\parallel}$ (surface area adjacent to streamwise fluid volume)	$2 d_s L$
$U_{\perp}$ (total transverse volume)	$d_s(d - d_s)L$
$S_{\perp}$ (surface area adjacent to transverse fluid volume)	$2 d_s L$
$\epsilon$ (volumetric porosity)	$(d^2 - d_s^2)(d^{-2})$

**Table 3.1:** Volume and surface partitioning referring to the original fibre RRUC model.

and the solid (as indicated in Figure 3.4). This expression was employed to evaluate the surface integral in the closure modelling of equation (2.18).

Assuming that the cross-sectional mean pore velocity in each duct section is directed axially along that specific duct, the direction of the local average velocity determines the orientation of the duct sections. The shear stresses which occur along the transverse surfaces were manifested as an additional pressure drop in the streamwise direction through the pressure deviation term. It was further assumed that the local wall shear stress per unit length in transverse pores is equal to that in streamwise pores and that the total streamwise pressure drop over the RRUC results from the wall shear stress contained in the integral term of equation (2.18).

From equation (A.8), the interstitial velocity was related to the apparent friction factor. The Reynolds number was then introduced, and an expression for the intra-pore shear influence of the solid on the fluid was obtained in terms of the porosity and  $d$ . Incorporation thereof into the momentum transport equation produced a velocity independent Darcy permeability for very low Reynolds number flow.

Based on the three original models described, further enhancements, refinements and applications of the RRUC model ensued:

Du Plessis & Van der Westhuizen (1993) defined the tortuosity as in equation (2.5) and the tortuous path length as the ratio of the fluid volume enclosed by the RRUC to the *minimum* pore cross-sectional flow area in the RRUC which yielded the characteristic functional relationship between porosity and tortuosity for prismatic porous media. In the unified model of Du Plessis & Van der Westhuizen (1993) the effect of recirculation was incorporated.

Du Plessis & Diedericks (1997) defined an effective streamwise volume which consists only

of that portion of the volume of a REV which contributes to the streamwise displacement of the particles of an extensive quantity. It was done as follows: An average pore velocity was introduced in the REV having the same direction as the interstitial velocity at each point, with restriction that it results in the same superficial velocity. From the method of volume averaging and projection of the average pore velocity onto the streamwise direction, an effective streamwise volume ( $\mathcal{U}_{\parallel}$ ) within the REV was obtained and defined. The average flux in a streamwise channel was consequently regarded as the volume integral of the actual microscopic flux weighted over the effective streamwise volume. The ratio between the average streamwise pore velocity and the superficial velocity could then be expressed in terms of the ratio between the total fluid volume and the effective streamwise volume. After embedding the averages of the REV into the RRUC, the average streamwise pore velocity in the effective streamwise volume is represented by  $\underline{w}_{\parallel}$ .

Lloyd (2003) presented a result for the pressure integral evaluated over the total fluid solid interfaces of staggered and non-staggered arrays of squares that includes, what became known as, the Lloyd correction. In principle it states that

$$\frac{1}{U_0} \iint_{S_{fs}} \underline{n} p dS = \left( \frac{U_{\parallel} + U_t}{U_f} - 1 \right) \nabla \langle p \rangle. \quad (3.1)$$

Under the assumption that all the properties of the REV may be embedded into the RRUC, equation (2.20) has been expressed in general RRUC notation (i.e. no calligraphic font) as:

$$-\nabla \langle p \rangle_f = \frac{1}{U_f} \iint_{S_{fs}} (\underline{n} p - \underline{n} \cdot \underline{\tau}) dS. \quad (3.2)$$

In the closure modelling of volume averaged equations for flow through two-dimensional arrays of squares, Lloyd et al. (2004) obtained

$$\begin{aligned} -\nabla \langle p \rangle &= \frac{1}{U_0} \iint_{S_{\parallel}} (-\underline{n} \cdot \underline{\tau}) dS + \frac{1}{U_0} \iint_{S_{\perp}} (\underline{n} p) dS \\ &+ \frac{1}{U_0} \iint_{S_{\parallel}} (\underline{n} p) dS + \frac{1}{U_0} \iint_{S_{\perp}} (-\underline{n} \cdot \underline{\tau}) dS, \end{aligned} \quad (3.3)$$

under the conditions of a stationary and uniform porous structure, uniform porosity and uniform averaged flow. The last two terms on the righthand side of the equality sign, which contribute to the transverse direction, were assumed to be zero since the macroscopic pressure gradient is in the streamwise direction. In evaluating the remaining surface integrals, a weighted average, of the contribution of all possible squares associated with different streamwise displacements for unconsolidated porous structures, was incorporated.

For each transverse channel section (in the Darcy regime) it was assumed that the interstitial pressure on the fluid-solid interface can be decomposed into an average channel wall pressure and a wall pressure deviation from this channel average (Lloyd et al. (2004)). It was further assumed that the pressure deviations are caused by shear stresses at the

transverse surfaces (although, due to the randomness of the porous medium, the transverse shear stresses cancel vectorially) and that the remaining surface integral of the wall average pressures in the transverse channels in the RRUC is expressible in terms of the Lloyd correction. (It must be noted that only RRUCs that do not cut through the solids and therefore include different transverse channels, contributed to this integral.)

According to Woudberg (2012a) the inclusion of the Lloyd correction validates the direct modelling procedure if it is assumed that this result can be generalized to other rectangular geometric representations of the REV. The direct modelling procedure (for low Reynolds number flow) entails the following: considering the RRUC as a unit cell (since the word ‘representative’ refers to representing the REV of volume averaging), the magnitude of the total force over the unit cell can be expressed as the product of the total pressure drop over the unit cell and the streamwise cross-sectional flow area. The magnitude of this force may also be expressed as the sum of the magnitude of the forces exerted by the solids on the fluid in the unit cell (Woudberg (2012a)).

In the modelling of airflow through a stack in a timber-drying kiln, Smit et al. (2007) did not make use of the Lloyd correction. For the Darcy flow regime it was assumed (in the closure modelling of equation (2.19)) that the pressure deviation term in the integrand can be replaced by the shear stresses encountered by the fluid in the transverse channel, since the pressure loss is a direct result of the wall shear stresses. In the intermediate Reynolds number flow regime the pressure part of equation (2.19) was assumed to be predominant and a form drag condition for flow over obstacles were employed.

Woudberg (2012b) presented a geometric pore-scale model for predicting the permeability of three-dimensional flow through fibrous porous media. An unconsolidated fibrous medium was represented by the fibre RRUC as infinitely long, straight, uniform and solid square-based prisms. Flow perpendicular to unidirectional fibres and flow parallel to unidirectional fibres were considered separately. Instead of orientating the fibres simultaneously in three directions perpendicular to one another, the fibres were always orientated (referring to Figure 3.4) in the  $\underline{k}$  direction and the streamwise direction was respectively chosen in the  $\underline{i}$ ,  $\underline{j}$  and  $\underline{k}$  directions.

The description of **flow perpendicular to fibres** involved the  $\underline{i}$ - and  $\underline{j}$ -directions. Only one of these directions was considered since both directions produce the same analytical result. Assuming flow between parallel plates and defining the hydraulic diameter in the RRUC context yielded

$$D_h = 4 \frac{(d - d_s)L}{2L} = 2(d - d_s). \quad (3.4)$$

Using the concept of total volumetric fluid discharge through the RRUC, the magnitude of the streamwise average channel velocity was written in terms of the magnitude of the superficial velocity:

$$w_{\parallel} = \frac{q d}{d - d_s}. \quad (3.5)$$

Staggering of the RRUCs was considered only in the streamwise direction. In order to account for the effect of stagnant fluid volumes (where the fluid velocity is assumed to be zero once the porous medium is fully saturated) a regular array was considered in which no staggering occurs. In order to take into account the fact that a tortuous path is more



probable than a straight one, a fully staggered array was considered. A geometric factor was, in addition, introduced to account for the tortuous flow path.

For **flow parallel to fibres** a high porosity model, with the solid as indicated in Figure 3.4, as well as a low porosity model, were considered. In the low porosity model the fluid (void) volume was represented by a duct with the same dimensions as that of the solid volume in the high porosity model. For the high porosity model flow between parallel plates was once again assumed with a corresponding hydraulic diameter and magnitude of the streamwise average channel velocity in terms of the superficial velocity. For the low porosity model flow in a rectangular duct was assumed.

Assuming fully developed flow in the Darcy regime, the pressure drop was expressed in terms of the shear stresses for each of the above cases and the corresponding permeabilities expressed in terms of the solid volume fraction and  $d_s$ . A unified parallel flow model was obtained by application of a power addition technique to the permeabilities obtained for the high- and low porosity parallel flow models. A three-dimensional model was obtained by performing a weighted average over the models for flow parallel and perpendicular to the fibres. Assuming that two thirds of the flow in a fibrous porous medium has a direction perpendicular to the fibres and a third is directed parallel to the fibres, a weight of one third was given to the model prediction for (unified) parallel flow and a weight of two thirds to that for transverse flow. The effect of developing flow and pore blockage were, in addition, incorporated into the model.

Woudberg (2012a) adapted a RRUC model that was originally developed for predicting the permeability of metallic foams, and used it to predict the effect of compression on the permeability of *non-woven fibres*. Figure 3.5 visualizes this anisotropic *foam* model of which a detailed description can be found in Woudberg (2012a). Henceforth, this adapted model (as depicted in Figure 3.5) will be referred to as the *three-strut fibre RRUC model*.

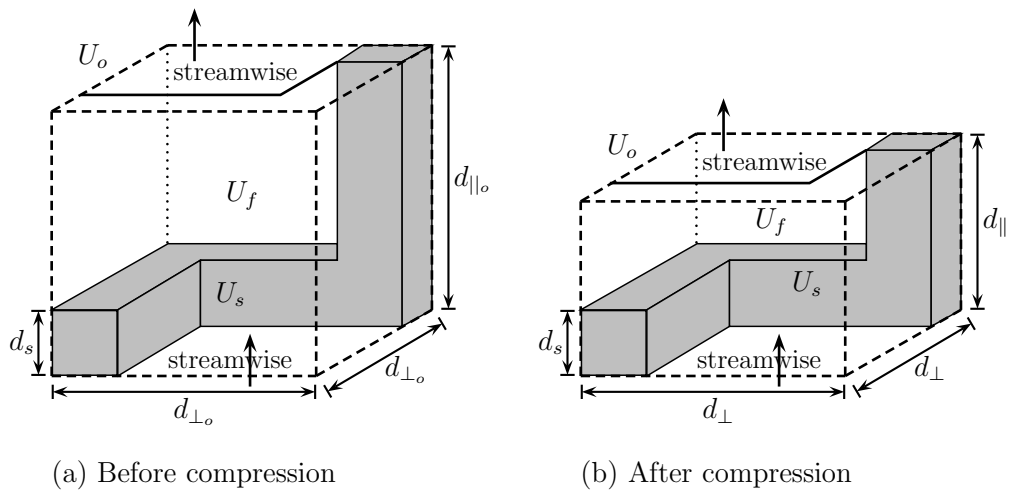


**Figure 3.5:** Three-strut fibre RRUC model (a) before and (b) after compression. [Source: Woudberg (2012a)]

Woudberg (2012a) used this model to predict the effect of compression on glass fibre non-wovens as well as soft fibrous porous media. The modelling steps applied for the above mentioned predictive model will form the basis of the modelling process in the present study. Refinements to the model of Woudberg (2012a) will be suggested and the results will be compared to the results of this study.

The conceptualization of the RRUC in general includes the following:

- The RRUC is positioned with its volumetric centroid corresponding with that of the REV that it represents and it is restricted to rectangular geometry;
- The size of the RRUC is the minimum size into which the statistical average geometry of the corresponding REV can be imbedded;
- The orientation of the RRUC is always such that the normal vector of one of its faces is in the streamwise direction (as defined in the REV);
- It is assumed that the RRUC forms a streamtube associated with the RRUC's downstream face;
- The porosity of the porous medium is reflected within the RRUC;
- Arrays of RRUCs staggered in different ways are used to include effects of stagnant volumes and tortuosity in the modelling.
- Neighbouring RRUC's fit tightly, do not overlap and have no gaps between them and any flow section of a RRUC (or part there-of) is bordered by the solid material of the adjacent RRUC;
- Directional priorities may be induced by choosing a particular arrangement of the solid in a single RRUC and this is accounted for by considering the effect of complementary RRUC's and using a relevant average;
- The solid material is rigid, smooth, impermeable and stationary;
- There is no staggering in the transverse directions: the solid surfaces parallel to the streamwise direction are aligned in the transverse directions, and
- Piece-wise straight streamlines are applicable between and parallel to the solid surfaces.

As is evident, an underlying assumption is that there is no channeling and that there are no external boundaries.

The following two articles to be discussed is of special importance since data from these studies will be employed to highlight the effect of changing variables on the prediction capability of the new geometric model introduced in Chapter 4. The data from Le Coq (2008) will be referred to throughout Chapters 4 and 5 and the data from Akaydin et al. (2011) will be referred to in Chapter 6.

## 3.3 Experiments pertaining to the present study

### 3.3.1 Influence of structural parameters on permeability (Le Coq (2008))

The influence of the structural parameters of heterogeneous porous media on the permeability was assessed by Le Coq (2008). For the micro-structural characterization of filtering fibrous media, the methods of mercury porosimetry and image analysis were compared. A short reference to these methods will be sufficient for the purpose of discussing possible discrepancies between the results obtained by Le Coq (2008) and those obtained through the analytical modelling process of this study.

**Mercury porosimetry** is, according to Giesche (2006), a very useful characterization technique providing the pore size distribution, porosity, apparent and skeletal density as well as the specific surface area of a porous medium sample. It must be kept in mind that this technique determines the largest connection from the sample surface towards a pore and not the actual inner size of a pore. Thus mercury porosimetry results will show smaller pore sizes compared to those determined through Scanning Electron Microscopy (SEM).

All mercury porosimeters essentially work according to the assumption that the porous medium can be characterized as a set of *cylindrical*, straight capillaries (through which the non-wetting liquid mercury must be forced). The modified Young-Laplace equation (referred to as the Washburn equation) relates the pressure difference across the curved mercury interface to the corresponding pore size, using the surface tension of mercury and the contact angle between the solid and mercury. (The cylinder pore assumption can lead to major differences between the analysis and reality.)

Giesche (2006) highlights different aspects to take into consideration in order to ensure the correctness of readings for key measurement parameters, e.g.: the sample porous medium must be well-defined and unambiguous; the creation of artificial pores due to the packing of the sample should be minimized; pore size as well as pore volume can be greatly influenced by the intrusion rate settings and the compressibility of the porous medium.

When converting the pore volume data into the corresponding surface area (under the assumption of a reversible intrusion process) minor measurement errors, especially in the high pressure or small pore size range can affect the calculated surface area to a very large degree. During mercury porosimetry measurements, hysteresis between the intrusion (increasing pressure) and extrusion (decreasing pressure) is observed in essentially all samples (Giesche (2006)).

**Image analysis** requires preparation of a porous medium sample which usually involves consolidation of the medium with a resin that fills the pore space of the medium. Acquisition of images of media cross-sections is followed by image processing and image measurement. Montillet & Le Coq (2003) present characteristic information that can be determined from image analysis as well as the procedure involved to obtain it. Le Coq

(2008) compared data obtained through mercury porosimetry regarding the uncompressed state of the porous medium in question to data acquired through image analysis.

When using experimental data, or information regarding an experiment, it is essential that one should take note of the aims of the experiment since it has an influence on the assumptions made. Comparison of data (results) from two different contexts (i.e. experimental procedures and analytical modelling), must reflect the awareness of the different (and sometimes not explicit) assumptions underlying the respective contexts.

In this respect, the experimental procedure of Le Coq (2008) will be discussed, of which part of the data will be employed during the present study.

The effect of compression of a fibrous porous medium on the structural parameters thereof, and therefore on the medium's permeability, was established using mercury porosimetry. For comparison with the analytical model to be proposed in this study, it is important to note that in this context the concept of 'consolidated porous medium' is described as "bonded together in the form of a non-woven or woven membrane".

The production of the glass fibre non-wovens (of which a detailed description can be found in Le Coq (2008)) was performed by following a paper-making process. A chemical binder was used to ensure the mechanical cohesion of the fibrous web. The pictures in Figure 3.6 give an actual micro-structural representation of the fibrous porous media used. Due to the manufacturing process of paper prototypes, the fibrous media obtained can be considered isotropic in the sheet plane but anisotropic in the thickness.

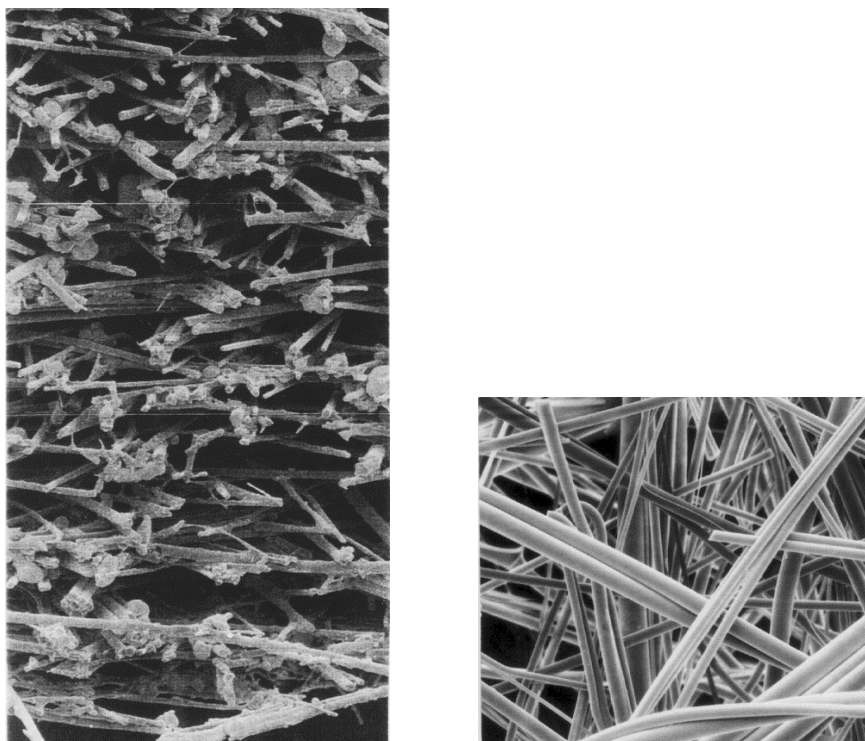


**Figure 3.6:** Glass fibre non-wovens. [Source: Le Coq (2008)]

In order to study the influence of fibre diameter and -length for media made of one or two grades of fibres, eight different fibrous compositions of different lengths and diameters were produced and their textural and mechanical parameters obtained. The apparent density of each fibrous medium was represented by the ratio of its specific weight to its thickness. Although the latter ratio shows no significant variation with changes in fibre diameter, it showed an increase with decreasing fibre length.

Of interest for this study is the effect of compression on the permeability of a non-woven fibrous porous medium consisting (only) of fibres with a mean diameter of 2.7  $\mu\text{m}$  and a mean length of 0.9 mm. Only information, which can be of value when comparing results regarding this porous medium (Le Coq (2008)) with the analytical results of the present study, will be summarized.

The definition of the hydraulic diameter used to verify the experimental values reported for this parameter, i.e.

$$D_h = \frac{4\epsilon}{\text{volume specific surface area}} = \frac{4\epsilon}{(1 - \epsilon)\left(\frac{\text{fibre surface}}{\text{fibre volume}}\right)}, \quad (3.6)$$

implies an unconsolidated fibrous porous medium since the whole surface area of each fibre is used. The tortuosity was defined according to the mean flow path direction, i.e. according to medium thickness. The porosity, pore hydraulic diameter and tortuosity were determined by post-processing the mercury porosimetry results. This provided the structural parameters of the *overall* medium at different levels of compression. (Stereological analysis of images obtained from media cross-sections provided local structural parameters.) Three reproducibility experiments (mercury porosimetry measurements) were performed for each sample (including the one relevant for this study). The mercury volume penetrating the porous medium was measured at different pressures to obtain a porosity versus pore size curve based on the Washburn theory. The glass - mercury contact angle of  $153^\circ$  and surface tension of  $0.48 \text{ Nm}^{-1}$  were used for data interpretation.

For the glass fibre prototypes, the experimental data of porosity versus pore size were modelled, bearing in mind that there are two levels of pore size, namely surface roughness and media internal pores. Details of the mathematics (e.g. iterative algorithm based on a Newton method used to solve a least squares problem) and theories (e.g. ‘equivalent pore’ theory) involved in determining the porosity, tortuosity and volume specific surface area fall beyond the scope of this study. It does, however, highlight the fact that behind the percentage errors indicated, there are assumptions and calculations that indicate a trail of thought.

In estimating the permeability, the permeability coefficient was deduced in terms of porosity, tortuosity and volume specific surface area. The permeability was also determined from the pressure drop measurements for airflow through the medium based on Darcy’s law (referred to as permeametry). A summary of data which is utilized in the modelling processes in this study is given in Table 3.2. The data was deduced from mercury porosimetry and permeametry measurements for a fibrous porous medium which was compressed in the streamwise direction. Le Coq (2008) tabulated the relative variation in thickness and indicated it as positive numbers although the material is compressed. Traditionally, as in Case (1957), the strain (deformation), which is a purely geometrical concept, is defined as the *increase* of length per unit length. This leads to a negative

number indicating that the material has been compressed. The experimental values for the filter thickness relative to its uncompressed state,  $e_{\text{exp}}$ , is calculated from the relative variation in thickness given by Le Coq (2008). Incorporating the negative sign in, for example, a relative variation of 15% e.g.,

$$\frac{h - h_0}{h_0} = -0.15, \quad (3.7)$$

leads to  $e_{\text{exp}} = 0.85$ . In equation (3.7)  $h$  is the height of the sample under compression and  $h_0$  is the corresponding initial uncompressed height. It is important to clarify that Le Coq (2008) indicates the *thickness* of the porous medium with the letter ‘e’, not to be confused with the compression fraction to be introduced in Section 4.4.

	Mercury porosimetry			Permeametry
	$\epsilon$	$D_h$ ( $\mu\text{m}$ )	$k_{\text{exp}}$ ( $\mu\text{m}^2$ )	$k_{\text{exp}}$ ( $\mu\text{m}^2$ )
$e_{\text{exp}}$				
1.00	0.94	28.0	8.20	10.0
0.85	0.92	17.0	2.00	2.1
0.75	0.89	16.5	1.40	-
0.55	0.86	16.0	0.17	-

**Table 3.2:** Selection of data from Le Coq (2008) regarding glass fibre non-wovens (average diameter 2.7  $\mu\text{m}$ ; average length 0.9 mm).

In the modelling process, only the empirical data based on mercury porosimetry will be used as input to determine the relationship between compression and porosity. The data based on permeametry will be compared with the results of the analytical model(s), without employing it as input variables.

### 3.3.2 Permeability of soft porous media (Akaydin et al. (2011))

Determining the permeability of a fibrous porous medium under variable longitudinal compression was done with a novel (according to the author) experimental approach. A new permeameter was fabricated and tested with this specific aim in mind. It consists of an electrically driven piston which slides vertically with a controlled velocity inside a long Plexiglas tube. The piston velocity was measured and assumed to be equal to the superficial (bulk) velocity.

The fibrous porous medium in this context was regular polyester pillow material composed of fibres with an average diameter of 10  $\mu\text{m}$  and with low flexural rigidity. The compression of the porous medium was done by sandwiching several circular cut-out layers between two plastic holding grids and adjusting the distance between the two grids. Two samples of material with initial uncompressed heights of 330 mm and 110 mm were tested to determine whether the permeability of a medium after compression is a function of the initial sample height of the medium.

The tests led to the assumption that the cylinder boundaries and holding grids did not contribute to the pressure drop. The pressure measurements were facilitated by an array of 13 pressure ports placed within small intervals from one another. With four pressure transducers (connected to one of the pressure ports) the pressure within the porous medium was measured at four different positions with which the pressure gradient within the medium was estimated.

The total volume of the uncompressed layers was obtained from the measured diameter and the height in the uncompressed state. The volume of the solid was measured by immersing it into a solution of dishwashing liquid water. The material is classified as hydrophobic and therefore molecular diffusion of the solute into the solid structure was assumed to be negligible. The initial volume was noted and the displaced volume (after immersion of the uncompressed layers and removal of bubbles) removed and its volume calculated from its density and weight. From the solid- and total volume values corresponding to the uncompressed state, the porosity of the porous medium in the uncompressed state was calculated.

Akaydin et al. (2011) defined the compaction (or compression) ratio as

$$\frac{-\Delta h}{h_0} = \frac{-(h - h_0)}{h_0}, \quad (3.8)$$

which is the negative of the strain that Case (1957) refers to in the context of materials in general. As with the data regarding glass fibre non-wovens, the experimental values for the filter thickness relative to its uncompressed state,  $e_{\text{exp}}$ , were calculated from the compression ratio given by Akaydin et al. (2011), which for a value of 0.85 leads to

$$\frac{-(h - h_0)}{h_0} = 0.85, \quad (3.9)$$

yielding  $e_{\text{exp}} = 0.15$ . The porosities associated with different levels of compression were calculated from the relationship between the compression ratio and porosity, given the porosity in the uncompressed state. In Table 3.3 a selection of the data pertaining to the soft porous medium sample with initial (uncompressed) sample height of 110 mm is provided. The permeability is expressed in  $\mu\text{m}^2$ .

The flow was assumed to be incompressible and the porous medium stationary, uniform and isotropic. Care was taken to have a uniform porosity sample and the measured pressures through the sample did not show large deviations from linearity. Therefore the porosity was assumed to be uniform, also due to the fact that the pressure gradient was not strongly affected by changes in porosity due to compression. Darcy's law was employed (assuming that the pressure gradient is always aligned with the flow direction) to determine the permeability with the measured pressure gradient since it was assumed that inertial effects are negligible.

Experiments were performed to establish whether hysteresis of permeability was present and whether the permeability was in any way dependent on the initial thickness of the sample. It was concluded that the effect of initial geometry of the porous sample on the permeability (when compressed), is negligible. It was found that no hysteresis was present in the pressure gradient between compression and decompression of the medium.

h (mm)	$e_{\text{exp}}$	$\epsilon$	Permeability ( $\mu\text{m}^2$ )
110	1.00	0.9968	9220
86	0.78	0.9959	6170
60	0.55	0.9941	3720
50	0.45	0.9930	2820
41	0.37	0.9914	2110
30	0.27	0.9883	1340
16	0.15	0.9780	620

**Table 3.3:** Selection of data from Akaydin et al. (2011) regarding regular polyester pillow material (average diameter 10  $\mu\text{m}$ ).

In the next chapter the newly proposed model, employing rectangular geometry, will be presented for predicting the influence of compression of a fibrous porous medium on the permeability in the discharge direction. As with all analytical models which in general require input variables that characterize the porous medium in question, the porosity in the uncompressed state as well as the (average) fibre diameter are required in the model. When information regarding the hydraulic diameter and/or the porosity of the medium in one or more compressed states are known, it can be incorporated in the model with the aim of enhancing the prediction capability there-of.



## Chapter 4

# Two-strut fibre RRUC model

Given a certain fibrous porous medium with an empirically determined porosity in the uncompressed state, the aim is to predict the effect of one-dimensional compression (i.e. in the streamwise direction) on the porosity and consequently the permeability of the fibrous porous medium in question. For application purposes, it is therefore important to note that the porosity of the material is altered in a very specific manner (via uniaxial compression). Although the new fibre RRUC model presented in this chapter is based on characteristics of previous RRUC models, there are fundamental differences which will be emphasized throughout the chapter. This chapter will focus on the development of the newly proposed RRUC model as well as on the comparison of the permeability prediction capability with that of the three-strut fibre RRUC model.

Since the effect of perturbation of fibre micro-structure is particularly important in high porosity materials, the change in permeability due to a compressed state (relative to the original structure), is of special interest for e.g. filters.

In this study the change in fibre micro-structure will be assumed to be only due to the compression of the material itself (before fluid flow through the medium) and not because of the fluid flow through the medium in a (pre-determined) compressed state.

Three mathematical relationships, all describing the influence of compression on the porosity of a porous medium, will be obtained and used in the modelling steps referring to the new geometric model. The model presented by Woudberg (2012a) is based only on a linear relationship between the level of compression (sample thickness relative to its uncompressed state) and porosity. The two other relationships will also respectively be employed in the geometric model of Woudberg (2012a) and the results will be compared to each other. This will highlight the effect that the choice of relationship has on the permeability prediction of a specific geometric model. This comparison will also be done for the new geometric model. Simultaneously, the effect of a specific choice of geometric model on the predictive capability there-of will be highlighted, by comparing results of the newly proposed geometric model, for each compression-porosity relationship, with those of the geometric model proposed by Woudberg (2012a).

As already mentioned in Chapter 1, using the same empirical data in the different models highlights the effect(s) of changes in the model on the prediction capability of the model. This is done to improve the prediction capability of a model within a chosen (data) context by making clear the causality between (for example) changes in geometry and prediction accuracy. The data in Table 3.2 (Le Coq (2008)) will be used for this purpose.

In general, the deformation of a porous medium under compression may not be uniform and/or aligned with the compressive force. In the modelling process it is assumed that incorporating an (on average) uniform compression will still render a prediction capability applicable to porous media where the compression is not necessarily uniform.

The new geometric model is chosen with the specific aim of representing the pressure losses in terms of the effect of shear stresses. During the development of the analytical model through changes in parameters, conditions associated with the asymptotic limit of low Reynolds number flow in the Darcy regime will be applied to predict the effect of compression on the permeability of the porous medium.

## 4.1 Relationship between porosity and compression fraction

In this study the **compression fraction** ( $\epsilon$ ) is defined as the *ratio of the post-compression filter thickness to the uncompressed filter thickness*. This definition highlights the fact that the post-compression filter thickness is a fraction of the uncompressed filter thickness.

In the experiments described by Dukhan (2006), an open-cell aluminum (or aluminium) foam is compressed in the flow direction to lower the porosity. Here the word strain is employed to signify the ratio of the pre-compression to post-compression height of the foam and is indicated by Dukhan (2006) as the compression factor in the table referring to the foam parameters. The porosity of the foam in the compressed state was calculated with the formula

$$\frac{h_0}{h} = \frac{100 - \epsilon}{100 - \epsilon_{\text{initial}}}, \quad (4.1)$$

in which the porosity is expressed as a percentage. This clarifies the fact that equation (4.1) is the reciprocal of the relationship expressed in equation (4.6).

When using experimental data to establish a relationship between variables, linear regression (usually implying an assumption of normally distributed errors) is often applied. The reasons for this are that relationships between variables can often be described by a linear function if the domain (and range) are chosen appropriately, and because a linear relationship between variables is the simplest non-trivial relationship to use. (In the present context, given certain data points, a linear function will not correctly represent the relationship between the compression fraction and porosity for the entire possible porosity interval, i.e. (0, 1).)

## Linear regression relationship

Modelling the relationship between the compression fraction ( $e$ ) and the porosity ( $\epsilon$ ) with *simple linear regression*, (using the four data points ( $\epsilon$  ;  $e_{\text{exp}}$ ) obtained through mercury porosimetry in Table 3.2), results in the following equation with porosity as the explanatory variable and the compression fraction as the response variable:

$$e = -4.03 + 5.34 \epsilon . \quad (4.2)$$

(If  $e$  is taken as the explanatory variable and  $\epsilon$  as the response variable, a different equation will be obtained which is not the re-arrangement of equation (4.2).)

The  $R^2$ -value for the relationship expressed in equation (4.2) is 0.98. This means that within a chosen porosity domain of  $[0.85; 0.95]$ , equation (4.2) gives a reasonable prediction for the deviation of the compression fraction from its mean, given the deviation of porosity from its mean.

However, taking into account information regarding the experiment with which the values of  $e$  and  $\epsilon$  were obtained, as well as the physical properties that these mathematical variables represent, a different relationship between these variables is also valid.

## General non-linear relationship

Assuming that the porous medium to be compressed is in a rigid container, i.e. the porous medium can not expand in the two ‘non-compressed’ directions, the theoretical relationship between the compression fraction and the porosity can be derived as follows:

Let the original total volume be denoted by  $V_0 = A h_0$ , with  $h_0$  the uncompressed height of the porous medium. Let  $A$  denote the base-area of the porous medium (and container) and let  $V = A h$ , with  $h$  the height of the medium after compression, denote the subsequent total volume after compression.

The *constant* (in this context) solid volume ( $V_s$ ) is given by the difference between the original total volume and the original fluid volume ( $V_{f_0}$ ) and can therefore be written as:

$$V_s = V_0 - V_{f_0} = V_0 (1 - \epsilon_0) , \quad (4.3)$$

with  $\epsilon_0$  the porosity of the material in the uncompressed state. The fluid volume after compression is given by

$$V_f = A h - A h_0 (1 - \epsilon_0) , \quad (4.4)$$

which leads (after dividing by  $A h$ ) to the following relationship between  $\epsilon_0$ , the compression fraction ( $e = h/h_0$ ) and the subsequent porosity ( $\epsilon$ ):

$$\epsilon = 1 - \frac{(1 - \epsilon_0)}{e} . \quad (4.5)$$

Equation (4.5) will also be used in the following form:

$$e = \frac{(1 - \epsilon_0)}{1 - \epsilon} , \quad (4.6)$$

with the compression fraction as a function of porosity, given the porosity in the uncompressed state. Since a porosity value is never equal to unity, equation (4.6) is mathematically sound. This provides an alternative to the linear regression relationship between the compression fraction and porosity for porous media where the solid volume does not change during compression and with a known porosity in the uncompressed state.

In a study on compression-induced morphological changes of non-woven fibrous materials, Jaganathan et al. (2009) introduced an image-based modelling technique to study the changes caused by compression of a fibrous porous medium on the pore size distribution. A miniature compression cell was employed that allowed for the porous medium to be compressed to a desired level and kept in place for the subsequent resin impregnation as well as for the serial section-imaging with a so-called Digital Volumetric Imaging (DVI) instrument. It was assumed that the resin (low viscosity) impregnation did not cause significant changes in the micro-structure of the fibrous porous medium, i.e. hydro-entangled non-woven medium consisting of polyester fibres with a fibre length of 3 cm and average diameter of 15  $\mu\text{m}$ . The samples were constrained in one direction and it was assumed that the expansion in the other direction was negligible since the Poisson ratio of non-wovens are usually very small. This is also the assumption on which equation (4.6) is based.

In Table 4.1, the values obtained by Jaganathan et al. (2009) for the SVF (rewritten as porosity) at each level of compression, is compared with the porosity values obtained when substituting the experimental values for the compression fraction in equation (4.5). The percentage difference between the porosity values gives an indication of the correctness of the assumption underlying the use of the formula which is applicable when compression is uni-axial and the porous medium does not expand in other directions. The percentage difference is given relative to the values obtained by equation (4.5) because if the assumption is valid for the porous medium in question, then this relationship should hold. From the percentage differences it can be concluded that it is justified to assume that for a non-woven fibrous porous medium the general non-linear formula is applicable.

Data (Source: Jaganathan et al. (2009))			Eq. (4.5)	% difference
h	$e_{\text{exp}}$	$\epsilon_{\text{exp}}$	$\epsilon$	$(\epsilon_{\text{exp}} - \epsilon)/\epsilon$
1971	1	0.9388	0.9388	n/a
1064	0.54	0.8805	0.8867	-0.70
730	0.37	0.8240	0.8346	-1.3
404	0.21	0.6558	0.7086	-7.5

**Table 4.1:** Verification of the use of the non-linear relationship between  $e$  and  $\epsilon$ .

If empirically determined porosity values at different stages of compression are available, the formula describing the relationship between the compression fraction and the porosity can be ‘refined’. Due to experimental errors when measuring the porosity of a porous medium, the level of correctness of the relationship expressed in equation (4.6) depends on the percentage error in the measurement of the porosity in the uncompressed state.

Although different measurements of a certain property fall within an interval determined by the percentage error, the individual measurements do not each include exactly the same error. Based on this fact that some data points were possibly measured with more accuracy than others, yet another relationship between the compression fraction and porosity can be obtained for media for which measured data regarding porosity at different stages of compression is available.

### Specific non-linear relationship

Assuming that the relationship takes on the form

$$e = \frac{C}{1 - \epsilon}, \quad (4.7)$$

the data from a specific experiment can be used to determine the value of  $C$  which is valid for the porous medium in question. Substituting the data points ( $\epsilon$ ;  $e_{\text{exp}}$ ) from the experiment used in this study (Le Coq (2008)), into equation (4.7), the constant  $C$  can be calculated by taking the average of the different values for  $C$  obtained for each data point. This ‘averaged’ value is based on more than one measurement and therefore captures the possible different errors within a percentage error range in a simple but representative way. This leads to the relationship

$$e = \frac{0.07}{1 - \epsilon}, \quad (4.8)$$

which is valid for the porous medium considered with a porosity of 0.94 in the uncompressed state and with three additional empirically obtained data points with which the relationship was established: (0.92 ; 0.85), (0.89 ; 0.75) and (0.86 ; 0.55). For this relationship the compression *fraction* will be larger than unity when the measured porosity for the uncompressed state is substituted since the obtained average constant leads to a formula representing a porous medium with a smaller uncompressed porosity than the measured value.

In Figure 4.1 a graphical comparison between the three relationships expressed in equations (4.2), (4.6) and (4.8) are shown. Equation (4.2) will be referred to as the linear regression relationship; equation (4.6) as the general non-linear relationship and equation (4.8) as the specific non-linear relationship. The latter three relationships will respectively be used in the prediction of permeability employing the same geometrical model, empirical data and modelling steps. The results will be compared to those of the geometric model presented by Woudberg (2012a).

In Figure 4.1 a visual comparison of the three relationships and the actual data points are presented. The linear regression relationship produces the ‘best fit’ for the data points on a restricted domain. It does not, however, reflect the actual non-linear relationship between the variables or the fact that the compression fraction can not be negative. The general non-linear relationship provides a more accurate reflection of the relationship over the whole (porosity) domain and is theoretically correct assuming that the porosity in the uncompressed state was measured with 100% accuracy. It is clear from Figure 4.1 that (except for the porosity in the uncompressed state) the general non-linear relationship

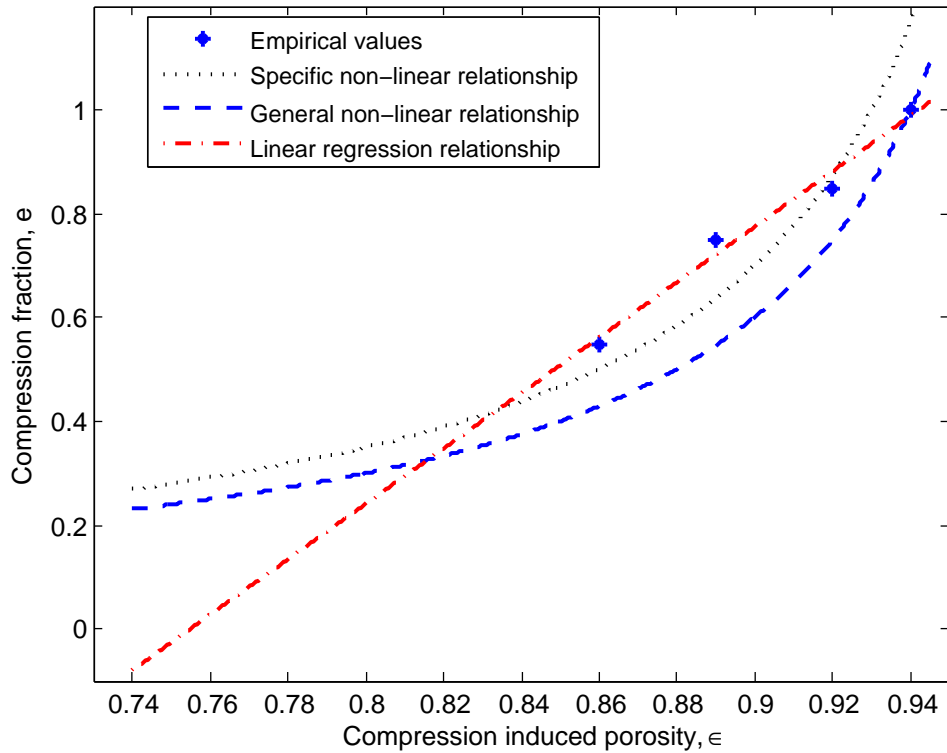


**Figure 4.1:** Different relationships between the compression fraction (filter thickness relative to its uncompressed state) and the compression induced porosity.

does not represent the experimentally obtained data points (for the porous medium in question) as accurately as the linear regression relationship where all the data points were used to determine equation (4.2).

From Figure 4.1 it can be deduced that when porosity measurements other than that in the uncompressed state are available, the general non-linear relationship can be ‘improved’ by incorporating all the data points to obtain the specific non-linear relationship. After employing the three relationships respectively in the modelling process, a further discussion on the choice of relationship will be done.

In the next section a new geometric model, as well as the rationale behind it, will be presented. (All directions indicated refers to that of a rectangular Cartesian coordinate system.)

## 4.2 Geometric model

The word geometry originates from the Greek words *geos* (meaning earth) and *metron* (meaning measure). In line with this, the geometry of the proposed mathematical model is chosen with the explicit aim of ‘measuring’ the permeability via the ‘measuring’ of shear stresses. The choice of geometry must also be in line with the definition of a RRUC, which, according to Du Plessis (1991), is “a minimal volumetric body into which the locally averaged porosity, characteristic length scale and porous medium type can be embedded”. The shape of the solid, representing the morphology of the porous medium, reflects the idea that the solids (fibres) in filters are more aligned in the directions perpendicular to the net flow than parallel to the net flow (as can be seen in Figure 3.6). This means that the minimal solid length in the RRUC, representing fibre-solids parallel to the flow, is assumed to be more closely related to the fibre diameter than to the fibre length.

The newly proposed model is visualized in Figure 4.2 and will be employed with the purpose of modelling the effect of compression on the permeability of an unconsolidated fibrous medium. Representing porosity geometrically, this choice of model reflects the effect of compression as a narrowing of the spaces through which fluid has to flow. This model will be referred to as the *two-strut fibre RRUC model* to distinguish it from the three-strut fibre RRUC model (Figure 3.5) presented by Woudberg (2012a). The (Cartesian) reference frame is chosen in such a way that the streamwise direction and the pressure gradient (Darcy regime) coincide, as indicated by the bold arrows in Figure 4.2.

When embedding the (vector) averages obtained from the REV into a RRUC, the specific choice of geometry means that the directions of the (vector) averages can not be represented in a single RRUC. This influence the way in which closure modelling is done for the volume-averaged equations. Since the corresponding REV contains different solids while the RRUC contains only one (minimal) representative solid with corresponding directional ‘preference’, care has to be taken when quantifying the vector equation (3.2). In previous RRUC closure modelling, the flow in the porous medium was represented with piecewise straight (equal length) streamlines and it became clear that using a single RRUC leads to induced directional priorities by the particular channels in the chosen RRUC. Conceptually this means, as suggested by Du Plessis & Diedericks (1997), that it is necessary to use a set of complimentary RRUCs in the modelling procedure. By taking weighted averages over these complimentary RRUCs, account is taken of the effect of induced directional preference.

The new two-strut fibre RRUC model should be seen as a **rectangular geometric minimal representation of the averages** obtained for the corresponding REV and **not** as a representation of the actual solids and (possible) streamlines of the fluid in the porous medium itself. The geometric model is used to provide the scope of proportions which, through the reflection of porosity, length scale and medium type, in a rectangular prism, can be employed to determine relevant areas, velocities and shear stresses. This choice of representation also lends itself to (the aim of) predicting pressure losses only in terms of shear stresses. It highlights the fact that uni-axial compression of a fibrous porous medium has a large impact on the void space available for flow perpendicular to the streamwise direction which in turn affects the permeability. The fact that the channels in a (compressed) fibrous porous medium are not of equal cross-sectional area, is represented by the

difference in RRUC side lengths parallel and perpendicular to the streamwise direction.

The representation of the total surface area in the corresponding REV was done with one solid in the RRUC with proportionally reduced ‘resultant’ surfaces normal and parallel to the streamwise direction. (The shortest length in the two-strut fibre RRUC will be equated to the average fibre diameter.) This geometric model also reflects the assumption of a rigid, stationary (after each phase of compression) fibrous porous medium which is not necessarily isotropic before or after compression.

For the purpose of this study, a single RRUC will be considered, but not without incorporating the surfaces of solids of neighbouring RRUCs. These surfaces could (but does not have to) be staggered relatively to the solids of the RRUC in question since the RRUC is not a unit cell but a representative there-of. In Figure 4.2 only one neighbouring surface is shown on the bounding surface of the RRUC in the streamwise direction.

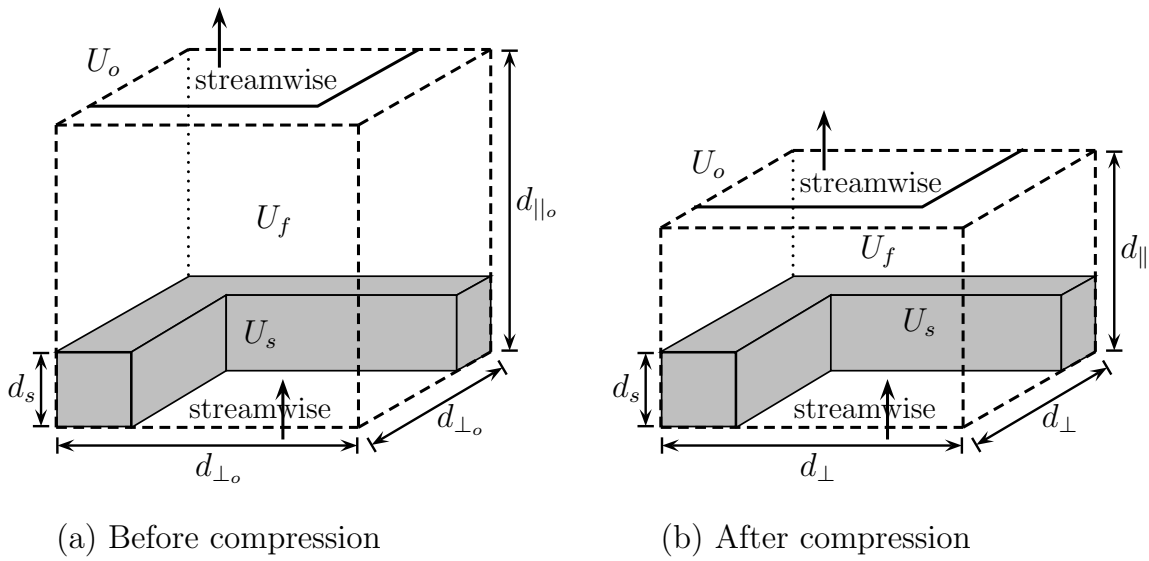


**Figure 4.2:** Two-strut fibre RRUC model (a) before and (b) after compression.

Next an equation for predicting the effect of one-dimensional compression in the streamwise direction on the permeability of non-woven fibres will be derived. The derivation commences with basic definitions referring to the newly proposed RRUC model (Figure 4.2(b)). The total volume ( $U_0$ ), total solid volume ( $U_s$ ) and the total fluid volume ( $U_f$ ) of the two-strut fibre RRUC can respectively be expressed as

$$U_0 = (d_{\perp})^2 d_{\parallel}, \quad (4.9)$$

$$U_s = 2(d_s)^2 d_{\perp} - (d_s)^3 \text{ and} \quad (4.10)$$

$$U_f = (d_{\perp})^2 d_{\parallel} - 2(d_s)^2 d_{\perp} + (d_s)^3, \quad (4.11)$$

which leads to the porosity being written as

$$\epsilon = \frac{U_f}{U_0} = \frac{(d_{\perp})^2 d_{\parallel} - 2(d_s)^2 d_{\perp} + (d_s)^3}{(d_{\perp})^2 d_{\parallel}}. \quad (4.12)$$



(For clarification: The value for  $d_{\parallel}$  (or  $d_{\perp}$ ) in the uncompressed state is  $d_{\parallel_0}$  (or  $d_{\perp_0}$ ) and  $U_0$  refers to the total volume in any state.) The hydraulic pore diameter associated with the corresponding REV will be represented in RRUC notation by

$$D_h = d_{\perp} - d_s, \quad (4.13)$$

which can be visualized in Figure 4.2 as the minimal streamwise opening width of the RRUC. The rationale behind this choice of a ‘streamwise direction’ hydraulic diameter is mathematical simplicity and also because it coincides with the hydraulic diameter for flow in a square duct of dimension  $d_{\perp} - d_s$ . This complies with the choice of hydraulic diameter in previous RRUC models based on the assumption of isotropy. Even though the compression of a fibrous porous medium excludes the assumption of isotropy, the above mentioned hydraulic diameter is employed with the awareness that this choice of definition must be revisited (which will be done in Section 5.2).

Referring to the two-strut fibre RRUC (Figure 4.2), the representation of the pressure loss in the corresponding REV will be done as follows: It is assumed that the validation of the direct modelling procedure, through the Lloyd correction and closure modelling regarding the RRUCs discussed in Section 3.2, can be extended to the present two-strut fibre model without introducing a significant margin of error.

Almost invariably, according to Korteland et al. (2010), it is (implicitly) assumed that the intrinsic phase-volume average pressure corresponds to the pressure that is actually measured (macroscale pressure). Expressing the gradient of the intrinsic phase-volume average pressure as the negative of the pressure drop across the streamwise length of the RRUC divided by the streamwise length, leads to

$$(d_{\perp} - d_s)^2 \Delta p = S_{\parallel} \tau_{w_{\parallel}} + S_{\perp} \tau_{w_{\perp}}, \quad (4.14)$$

which corresponds to the ‘direct modelling procedure’ as described by Woudberg (2012a) for other RRUC types. Here  $S_{\parallel}$  and  $S_{\perp}$  represent the total surface areas available for shear stresses in the streamwise and transverse directions, respectively, and  $\tau_{w_{\parallel}}$  and  $\tau_{w_{\perp}}$  represent the magnitude of the wall shear stresses in the two respective directions. Equation (4.14) will be employed in the modelling steps described in the following section.

According to Shah & London (1978) the pressure drop in fully developed flow is caused by the wall shear stresses and therefore equation (4.14) does not reflect developing flow and accompanying inertial effects. Equation (4.14) also supports the fact that when it is assumed that the flow in each pore channel is in dynamic equilibrium, the net force should be zero and since only shear forces are considered, the force exerted by the pressure over the inlet and outlet areas of a channel section and the shear forces are in balance. Form drag for flow over obstacles will not be employed since the assumption is made that flow in a compressed fibrous porous medium resembles more closely flow *through* a conduit than flow *over* an obstacle. The above described geometric model will now be used to ‘scale’ the velocities, surface areas and shear stresses according to the geometric representation of the porosity and hydraulic diameter of the porous medium in question.

The steps in the modelling procedure (to be presented in Section 4.3) are similar to the steps used by Woudberg (2012a), but will refer to the two-strut geometric model depicted in Figure 4.2. The procedure will be described (using the data of Le Coq (2008) given in

Table 3.2) in order to highlight corresponding assumptions and the rationale behind it. The modelling steps to be presented in Section 4.3 are applicable when the fibre diameter, the porosity in the uncompressed state and the different compression fractions are known. These steps also rely on the availability of data regarding the hydraulic diameter and porosity at different stages of compression for the determination of the streamwise length representing the uncompressed state of the porous medium.

### 4.3 Modelling steps

The permeability will be written in terms of the compression fraction (explicitly) and the porosity (implicitly through the dimensions of the two-strut fibre RRUC). For the geometrical representation of the porosity in the uncompressed state it is necessary to determine an applicable uncompressed streamwise side length of the RRUC. From this the streamwise side lengths corresponding to different compressed states will be derived. If empirically determined values of the hydraulic diameter for different stages of compression are available, as is the case for the porous medium modelled in this chapter, it will be employed as follows:

Incorporating the representative hydraulic diameter,  $D_h = d_\perp - d_s$ , equation (4.12) can be expressed as:

$$\epsilon = \frac{U_f}{U_0} = \frac{(D_h + d_s)^2 d_\parallel - 2(d_s)^2 (D_h + d_s) + (d_s)^3}{(D_h + d_s)^2 d_\parallel}, \quad (4.15)$$

from which it follows that

$$d_\parallel = \frac{2(d_s)^2 (D_h + d_s) - (d_s)^3}{(1 - \epsilon)(D_h + d_s)^2}. \quad (4.16)$$

The assumption is made that the effect of compression is spread homogeneously throughout the porous medium. Therefore the filter thickness after compression relative to its uncompressed state (i.e. the compression fraction), is taken as the percentage with which the side length of the RRUC in the streamwise direction will shorten relative to its uncompressed length. With  $d_{\parallel_0}$  denoting the uncompressed streamwise length of the RRUC, this assumption can be expressed mathematically as:

$$e = \frac{d_\parallel}{d_{\parallel_0}}. \quad (4.17)$$

A value for  $d_{\parallel_0}$  may be obtained in the following way: Substituting the data from the experiments of Le Coq (2008) in Table 3.2 into equation (4.16), the streamwise length of the two-strut fibre RRUC for the four stages of compression is determined. The value used for  $d_s$  is 2.7  $\mu\text{m}$ , which is the fibre diameter of the porous medium referred to in the modelling process.

Corresponding values for  $d_{\parallel_0}$  are obtained from equation (4.17), yielding an average value of  $d_{\parallel_0} = 8.9 \mu\text{m}$ . This value will be used as the streamwise length of the RRUC in the

uncompressed state. Therefore, based on the empirical data used,

$$d_{\parallel} = 8.9 \text{ e} . \quad (4.18)$$

It must be noted that the value of  $d_{\parallel 0}$  depends on the choice of definition for the hydraulic diameter as well as on the empirically determined values for this structural parameter.

The side length of the RRUC perpendicular to the streamwise direction ( $d_{\perp}$ ), can be obtained from equation (4.12) for a specific porosity, using the corresponding value for  $d_{\parallel}$ , given by equation (4.18):

$$0 = \epsilon (d_{\perp})^2 d_{\parallel} - (d_{\perp})^2 d_{\parallel} + 2(d_s)^2 d_{\perp} - (d_s)^3 , \quad (4.19)$$

with roots

$$d_{\perp} = \frac{d_s \left( d_s \mp \sqrt{(d_s)^2 + d_{\parallel} d_s (\epsilon - 1)} \right)}{d_{\parallel} (1 - \epsilon)} . \quad (4.20)$$

Since  $d_s + d_{\parallel}(\epsilon - 1) \geq 0$ , it follows that:

$$d_s \geq (1 - \epsilon) d_{\parallel} = (1 - \epsilon) d_{\parallel 0} \text{ e} . \quad (4.21)$$

This restriction follows from the reflection of the choice of geometric model in the definition of porosity. For the different relationships between the compression fraction and porosity to be implemented, based on the choice of  $d_s = 2.7 \text{ } \mu\text{m}$  as well as  $d_{\parallel 0} = 8.9 \text{ } \mu\text{m}$ , this restriction will be used to show for which porosities the different relationships are valid.

Only the addition of the square root in equation (4.20) is considered since the subtraction there-of leads to impractical small values for  $d_{\perp}$ . (Since in practice the porosity is never 100%, the equation is valid over the whole porosity range.) Therefore,

$$d_{\perp} = \frac{d_s \left( d_s + \sqrt{(d_s)^2 + d_{\parallel} d_s (\epsilon - 1)} \right)}{d_{\parallel} (1 - \epsilon)} . \quad (4.22)$$

Although there is no macroscopic nett flow in the directions perpendicular to the streamwise direction, the shear stresses due to velocity gradients in the micro-channels perpendicular to the streamwise direction also contribute to pressure loss in the streamwise direction. Flow in the directions perpendicular to the streamwise direction is represented in the RRUC by an average transverse velocity,  $\underline{w}_{\perp}$ , of which the magnitude is assumed to be the same in both transverse directions, as is reflected in the geometric model. The relationships between the magnitudes of the velocities  $\underline{w}_{\parallel}$  (representing the average streamwise pore velocity in the effective streamwise volume in the corresponding REV),  $\underline{w}_{\perp}$  and  $\underline{q}$  are written in terms of the dimensions of the RRUC. This is done based on the definition of the superficial velocity within the volume averaging context (i.e. equation (2.15)), as well as on the principle of mass conservation.

Using the dimensions of the two-strut fibre RRUC (Figure 4.2(b)) as ‘prescribed’ by the porosity, the mathematical expressions of these relationships are:

$$w_{\parallel} = \frac{q (d_{\perp})^2}{(d_{\perp} - d_s)^2} , \quad (4.23)$$

and

$$\frac{w_{\perp}}{w_{\parallel}} = \frac{(d_{\perp} - d_s)^2}{(d_{\parallel} - d_s)(d_{\perp})}. \quad (4.24)$$

As a result, the magnitude of the average transverse velocity can be expressed as:

$$w_{\perp} = \left( \frac{q (d_{\perp})^2}{(d_{\perp} - d_s)^2} \right) \left( \frac{(d_{\perp} - d_s)^2}{(d_{\parallel} - d_s)(d_{\perp})} \right) = \frac{q d_{\perp}}{(d_{\parallel} - d_s)}. \quad (4.25)$$

In general, for two infinitely wide (e.g. in the  $\underline{k}$ -direction) parallel plates, stationary relative to each other, a distance  $d$  (in the  $\underline{j}$ -direction) apart, with flow in the  $\underline{i}$ -direction, the velocity profile for *fully developed plane Poiseuille flow* is given by:

$$u(y) = \frac{y}{2\mu} \left( -\frac{dp}{dx} \right) (d - y). \quad (4.26)$$

The mean velocity between the plates is then expressed as

$$u_m = \frac{d^2}{12\mu} \left( -\frac{dp}{dx} \right), \quad (4.27)$$

and the wall shear stress is given by:

$$\tau_{\text{wall}} = \frac{6 \mu u_m}{d}. \quad (4.28)$$

In the context of the two strut fibre RRUC model, equation (4.28) is used to approximate the magnitude of the total wall shear stresses represented via the chosen geometry of the RRUC. The underlying assumption is therefore that a formula, that refers to uniform and constant wall shear stresses with fully developed flow between parallel plates, will produce an approximation of which the margin of error falls within the same order of magnitude as that of other approximations made in the modelling process. This is done although the ‘parallel plates’ (note that the one plate is always part of a neighbouring RRUC) are not infinitely wide (or long) and can be ‘shifted’ relative to each other.

The use of equation (4.28) also highlights the assumption of steady (velocity, pressure and cross-section may differ from point to point but do not change with time at a specific point), laminar flow. This is despite the fact that in practise there are usually slight variations in velocity and pressure over time at a specific point.

Four sets of equal area parallel plates (of which the two sets parallel to the streamwise direction are not shifted in the transverse directions) will be employed to quantify the shear stresses. Based on the above mentioned assumptions, the wall shear stresses in the streamwise and two transverse directions can respectively be expressed as:

$$\tau_{w_{\parallel}} = \frac{6 \mu w_{\parallel}}{d_{\perp} - d_s} \quad \text{and} \quad \tau_{w_{\perp}} = \frac{6 \mu w_{\perp}}{d_{\parallel} - d_s}. \quad (4.29)$$

The relationship between the total pressure drop over the RRUC and the shear stresses (equation (4.14)) then becomes:

$$(d_{\perp} - d_s)^2 \Delta p = [4 d_s (d_{\perp} - d_s)] \tau_{w_{\parallel}} + [4 d_s (d_{\perp} - d_s) + 2(d_s)^2] \tau_{w_{\perp}}. \quad (4.30)$$

Incorporating equation (4.29) and then equations (4.23) and (4.25) into equation (4.30), lead to an expression for the total pressure drop over the RRUC in terms of the magnitude of the superficial velocity, viscosity and the dimensions of the RRUC:

$$\begin{aligned}\Delta p &= \mu q \left[ \frac{24 d_s (d_{\perp})^2}{(d_{\perp} - d_s)^4} + \frac{24 d_s (d_{\perp})^2 - 12 (d_s)^2 d_{\perp}}{(d_{\perp} - d_s)^2 (d_{\parallel} - d_s)^2} \right] \\ &= \mu q \left[ \frac{24 d_s (d_{\perp})^2 (d_{\parallel} - d_s)^2 + 12 d_s d_{\perp} (2 d_{\perp} - d_s) (d_{\perp} - d_s)^2}{(d_{\perp} - d_s)^4 (d_{\parallel} - d_s)^2} \right].\end{aligned}\quad (4.31)$$

Assuming that the pressure drop across the streamwise length of the RRUC ( $d_{\parallel}$ ) is the same as the pressure gradient across the length of the filter and that Darcy's law is applicable in this low Reynolds number flow regime, it follows that

$$\frac{\Delta p}{d_{\parallel}} = \frac{\mu q}{k}, \quad (4.32)$$

with  $k$  the (hydrodynamic) permeability of the fibrous porous medium. From equations (4.31) and (4.32) the permeability can be expressed as

$$k = \frac{d_{\parallel} (d_{\perp} - d_s)^4 (d_{\parallel} - d_s)^2}{24 d_s (d_{\perp})^2 (d_{\parallel} - d_s)^2 + 12 d_s d_{\perp} (2 d_{\perp} - d_s) (d_{\perp} - d_s)^2}. \quad (4.33)$$

Based on the choice of compression fraction - porosity relationship, equation (4.33) can be re-written in terms of the uncompressed length of the RRUC, the compression fraction and the fibre diameter. In the next section the different relationships and the influence there-of on the prediction efficiency of the geometric model will be compared. The three relationships will also be applied in the three-strut fibre model (Woudberg (2012a)) and in each case the permeability predictions will be compared to that of the two-strut fibre model.

Although during comparison of results the word 'error' will be used, it should rather (in the context of this study) be regarded as a percentage difference. As is evident from the literature study, experiments also involve calculations and manipulations with measured values - all based on assumptions. In the context of this study the use of the word 'error' does not imply that the experimental values (relative to which the percentage differences are calculated) are assumed to be 'correct' in the absolute sense.

## 4.4 Permeability prediction based on different compression fraction - porosity relationships

In this section the three different relationships for the inter-dependence of the compression fraction and porosity, discussed in Section 4.1, will be incorporated in the modelling steps outlined in Section 4.3 pertaining to the two-strut fibre RRUC model depicted in Figure 4.2. Woudberg (2012a) discussed the three-strut fibre RRUC model *using only the linear regression relationship*. The two non-linear relationships will also be applied to the three-strut model (without showing all the steps and restrictions) and the results will be compared to that of the two-strut model.

#### 4.4.1 Linear (regression) relationship between compression fraction and porosity (equation (4.2))

Combining equations (4.18) and (4.2) an expression for the RRUC thickness in the stream-wise direction is obtained in terms of the calculated value of  $d_{\parallel_0}$  and the porosity:

$$d_{\parallel} = d_{\parallel_0} (-4.03 + 5.34 \epsilon) = 8.9 (-4.03 + 5.34 \epsilon). \quad (4.34)$$

It must be noted that since length is a positive real number in this context, writing  $d_{\parallel}$  as a function of  $\epsilon$  in equation (4.34) implies that  $\epsilon > 0.755$ . This model where linear regression is used, is therefore only applicable for compression induced porosities larger than 0.755. The latter condition also ensures that equation (4.21), which leads to

$$2.7 \geq 8.9 (-4.03 + 5.34 \epsilon)(1 - \epsilon), \quad (4.35)$$

is not violated.

Using equation (4.22) to calculate corresponding values for  $d_{\perp}$  and then substituting lengths corresponding to a specific porosity into equation (4.33) leads to the information given in Tables 4.2 and 4.3.

Experiment		Pore size, $D_h$ ( $\mu\text{m}$ )		
$e_{exp}$	$\epsilon$	Exp.	Two-strut: $d_{\perp} - d_s$	Three-strut: $d_{\perp} - d_s$
1.00	0.94	28.0	23.5	23.7
0.85	0.92	17.0	19.1	19.4
0.75	0.89	16.5	16.5	16.6
0.55	0.86	16.0	16.7	16.3

**Table 4.2:** Values for the hydraulic diameter corresponding to the four stages of compression (experiment), based on a linear relationship between  $e$  and  $\epsilon$ .

The values for the hydraulic diameter in Table 4.2 are given to highlight the fact that the hydraulic diameter for the two models is in correspondence with the experimental values when  $d_{\perp}$  is calculated using a linear relationship between the compression fraction and the porosity. The values of the hydraulic diameter is coupled to those of  $d_{\perp}$  since  $d_s$  is taken as a constant. For each of the three different relationships between the compression fraction and porosity, as described in Section 4.1, the variation of  $d_{\perp}$  will be visualized graphically. The percentage errors of the two-strut fibre RRUC model relative to the experimental values of Le Coq (2008) are shown in Table 4.3. The permeability is expressed as a number rounded to 2 significant digits. For comparison purposes the modelling steps were also applied to the three-strut fibre model (Woudberg (2012a)) and the results are also presented in Table 4.3. The percentage errors regarding the prediction with the two-strut fibre model show a better distribution ‘around’ the empirical data than those of the three-strut fibre model.

Permeability ( $\mu\text{m}^2$ ) (Linear $e - \epsilon$ relationship)				
Experiment	two-strut RRUC	% error	three-strut RRUC	% error
8.2	4.0	-51	5.4	-34
2.0	2.5	25	3.3	65
1.4	1.0	-29	1.5	7
0.17	0.32	88	0.51	200

**Table 4.3:** Relative percentage error in the permeability prediction of the two-strut- and three-strut fibre RRUC models. (Linear relationship between  $e$  and  $\epsilon$ .)

Figure 4.3 depicts a comparison of the predictions of the effect of compression on the permeability using the three-strut (Woudberg (2012a)) and two-strut RRUC models. The permeability is plotted against the compression induced porosity and the empirical values from the experiment of Le Coq (2008) are also shown.

The reason for using the compression induced porosity as the ‘independent’ variable (instead of the compression fraction), is to highlight the fact that porosity is the medium-specific property and not the level of compression. The largest percentage error, although not revealed in Figure 4.3, is at the smallest compression fraction. A general comparative discussion on the permeability prediction of the two- and three-strut RRUCs will be given in Section 4.4.4.

A visualization of the manner in which variables in different geometric models change, has a potential informative role regarding the correctness of the assumptions which were made and the domain for which a model is applicable. For this reason, certain properties of the two types of RRUC’s are plotted against the compression induced porosity based on the linear relationship between  $e$  and  $\epsilon$ .

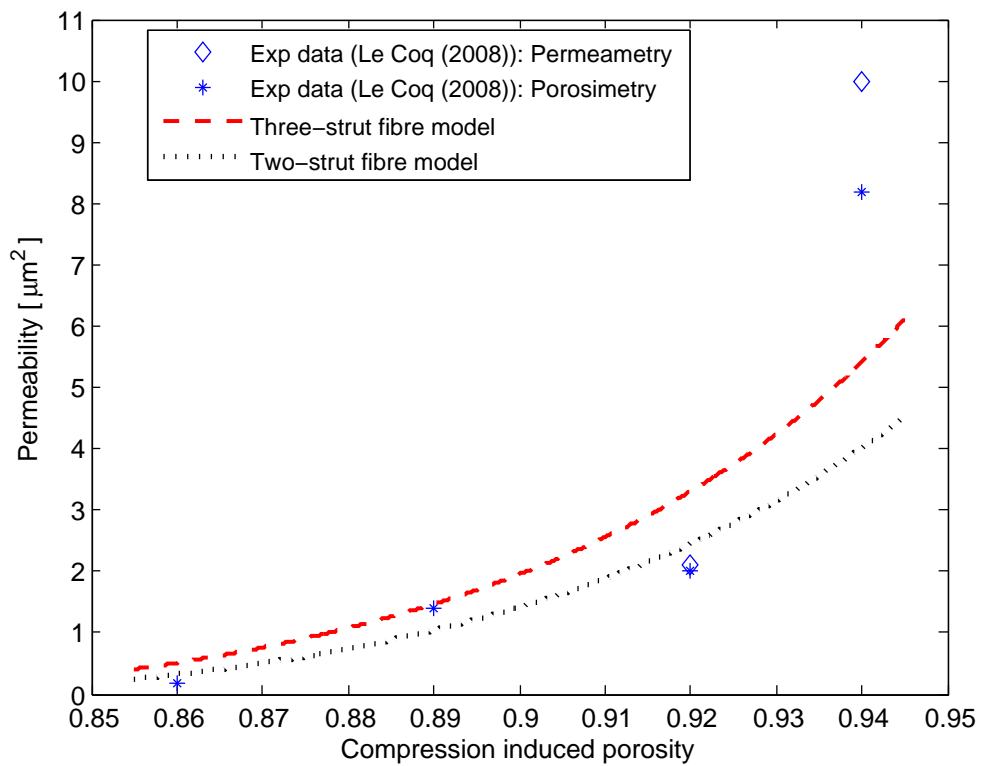


**Figure 4.3:** Permeabilities predicted by the two-strut- and three-strut fibre RRUC models, based on a linear relationship between  $e$  and  $\epsilon$  (equation (4.2)).



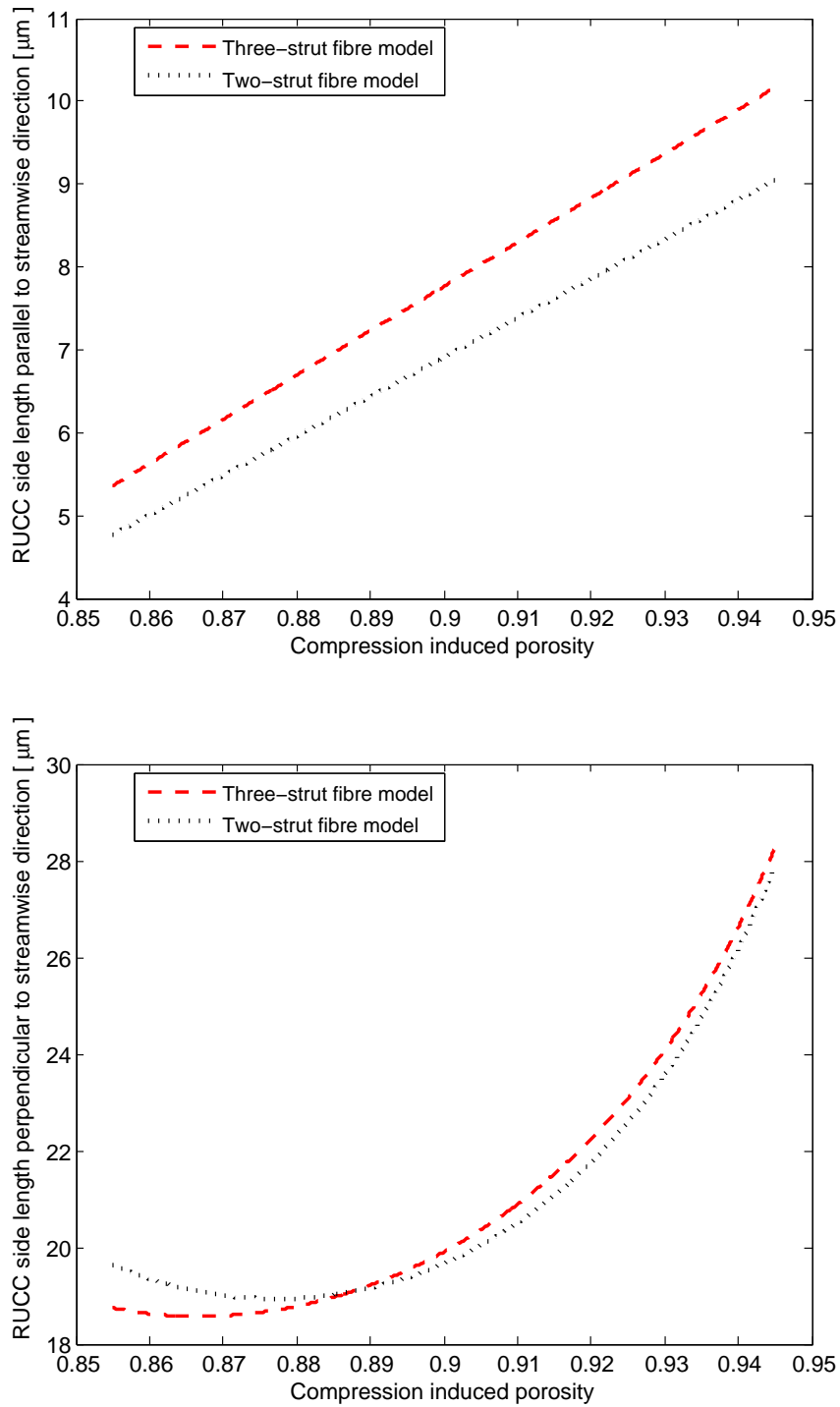


**Figure 4.4:** RRUC side lengths parallel (top) and perpendicular (bottom) to the stream-wise direction, as a function of compression induced porosity. (Linear relationship between  $e$  and  $\epsilon$ .)

Because of the chosen linear relationship between  $e$  and  $\epsilon$ , the relationship between the RRUC side length parallel to the streamwise direction and porosity is linear, as is evident in Figure 4.4. The difference between the two linear trends representing the two- and three-strut models, lie in the different values for  $d_{\parallel 0}$ . The trends are in line with the fact that the RRUC reflects the compression of the porous medium in the streamwise direction.

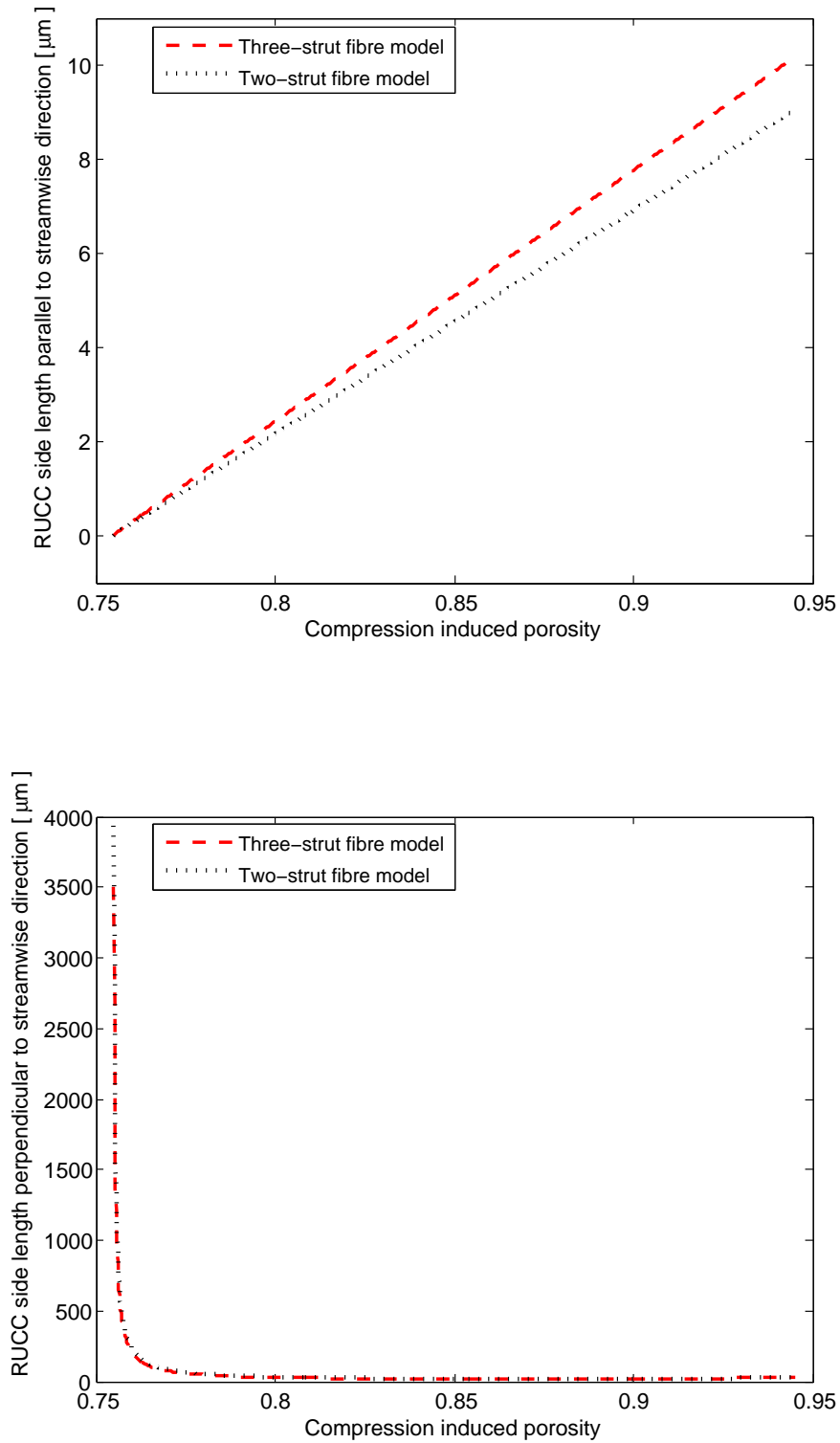
The difference in the variation of the RRUC side length perpendicular to the streamwise direction of the two models is due to the different geometrical models used. The choice of the geometry of the solid in the RRUC determines the relationship between the different side lengths of the chosen geometric model and porosity. The linear relationship between  $e$  and  $\epsilon$  causes the side length perpendicular to the streamwise direction initially to decrease with increasing porosity and then to increase with increasing porosity. From equation (4.22), with a linear  $e - \epsilon$  relationship, it is evident that the relationship between  $d_{\perp}$  and the compression induced porosity is not quadratic or cubic. (Woudberg (2012a) mentioned a quadratic relationship with porosity but the porosity dependence of  $d_{\parallel}$  was not taken into account.) In order to highlight the non-quadratic behaviour, the graphs depicting the change in RRUC side lengths are drawn on a larger (mathematically valid) porosity domain in Figure 4.5.

It is clear that the behaviour of the geometric model itself is an indicator of the applicability thereof on a mathematically valid porosity domain. To emphasize this, the change in volume with compression induced porosity as well as the permeability prediction are visualized on a larger porosity domain in Figures 4.6 and 4.7.

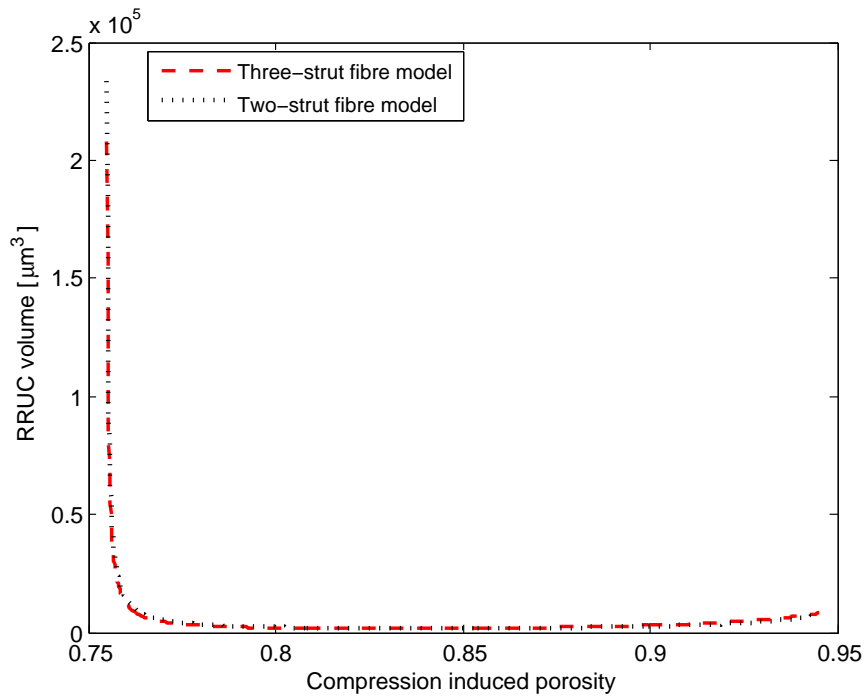
A non-linear decrease in the volumes of both RRUCs is expected when the porosity is decreased *through compression* since the geometric model is employed as a ‘description’ of the compression of a porous medium. This is the case for the porosity interval [0.85; 0.95] but not at lower porosities.

Figure 4.7 confirms the fact that the relationship between the porosity and compression fraction obtained through linear regression renders a model that is not valid in general. The linear relationship between the compression fraction and porosity is statistically sound for a predetermined domain (i.e.  $0.86 \leq \epsilon \leq 0.94$  in this context) but leads to negative permeability values corresponding to porosities lower than 0.755. As functions of porosity, the behaviour of the side lengths of the RRUCs and consequently the volumes of the RRUCs, indicate that another relationship between  $e$  and  $\epsilon$  may produce a more ‘stable’ model which renders no negative values for permeability. It is also important to note that the choice of domain when visualizing the relationship between variables or parameters, has to be carefully thought through.

For further analysis, other relationships between  $e$  and  $\epsilon$  will be employed, keeping the geometric model and modelling steps unaltered.



**Figure 4.5:** RRUC side lengths parallel (top) and perpendicular (bottom) to the stream-wise direction, as a function of compression induced porosity, for the porosity domain [0.75; 0.95]. (Linear relationship between  $e$  and  $\epsilon$ .)



**Figure 4.6:** RRUC volumes as a function of compression induced porosity for the porosity domain [0.75; 0.95]. (Linear relationship between  $e$  and  $\epsilon$ .)

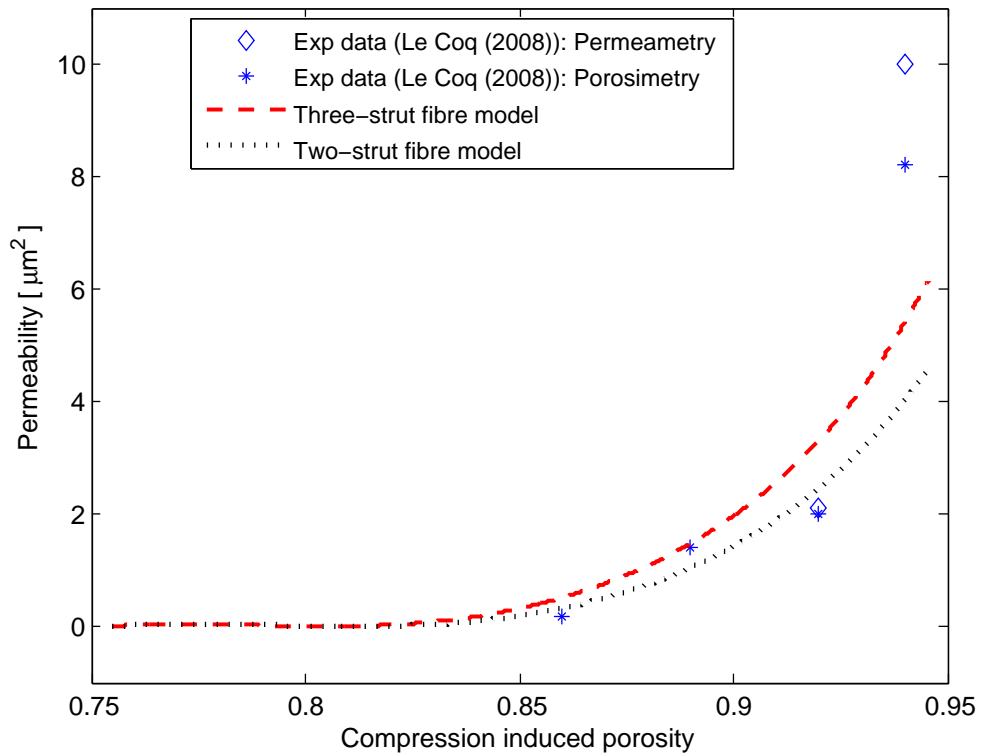


**Figure 4.7:** Permeabilities predicted by the two-strut- and three-strut fibre RRUC models for the porosity domain [0.75; 0.95]. (Linear relationship between  $e$  and  $\epsilon$ .)

#### 4.4.2 General non-linear relationship between compression fraction and porosity (equation (4.6))

The effect of the mathematical relationship between  $e$  and  $\epsilon$  on the prediction capability of the models will be highlighted by using the general non-linear relationship whilst keeping all other aspects of the model the same as in Section 4.4.1. Combining equations (4.6) and (4.18), an expression for the RRUC thickness in the streamwise direction is obtained in terms of the calculated value of  $d_{\parallel 0}$  and porosity:

$$d_{\parallel} = 8.9 \left( \frac{1 - 0.94}{1 - \epsilon} \right), \quad (4.36)$$

where  $\epsilon_0 = 0.94$  is the porosity associated with the uncompressed state of the medium. Adhering to the restriction expressed in equation (4.21), with  $d_s = 2.7 \mu\text{m}$ , leads to:

$$2.7 \geq (1 - \epsilon) 8.9 \left( \frac{0.06}{1 - \epsilon} \right), \quad (4.37)$$

which is true for all possible values of porosity. Again referring to the visualization of the model in Figure 4.2 and following the modelling steps stipulated in Section 4.3, equation (4.22) is used to calculate the corresponding values for  $d_{\perp}$ . The permeability for a specific porosity is calculated using equation (4.33).

Subsequently, using equation (4.6) for the three-strut fibre RRUC model and applying the modelling steps as in Woudberg (2012a), a corresponding prediction for the effect of compression on the permeability is obtained. In Figure 4.8 the comparison of the prediction results of the two-strut and three-strut geometric models are visualized. The empirical values from the experiment of Le Coq (2008) are also shown.

Permeability ( $\mu\text{m}^2$ ) (General non-linear $e - \epsilon$ relationship)				
Experiment	two-strut RRUC	% error	three-strut RRUC	% error
8.2	4.2	-49	5.6	-32
2.0	1.3	-35	2.0	0
1.4	0.29	-79	0.49	-65
0.17	0.06	-65	0.13	-24

**Table 4.4:** Relative percentage error in the permeability prediction of the two-strut and three-strut fibre RRUC models. (General non-linear relationship between  $e$  and  $\epsilon$ .)

As is evident from Table 4.4 and Figure 4.8, the permeabilities predicted by both geometric models show negative margins of error. The fact that both models under-predict the permeability as opposed to the predictions using the linear relationship between  $e$  and  $\epsilon$ , indicate a high dependence of the models on the relationship between the compression fraction and porosity. The relationship between  $e$  and  $\epsilon$ , as expressed in equation (4.6), is highly dependent on the measured value of the porosity of the porous medium in the

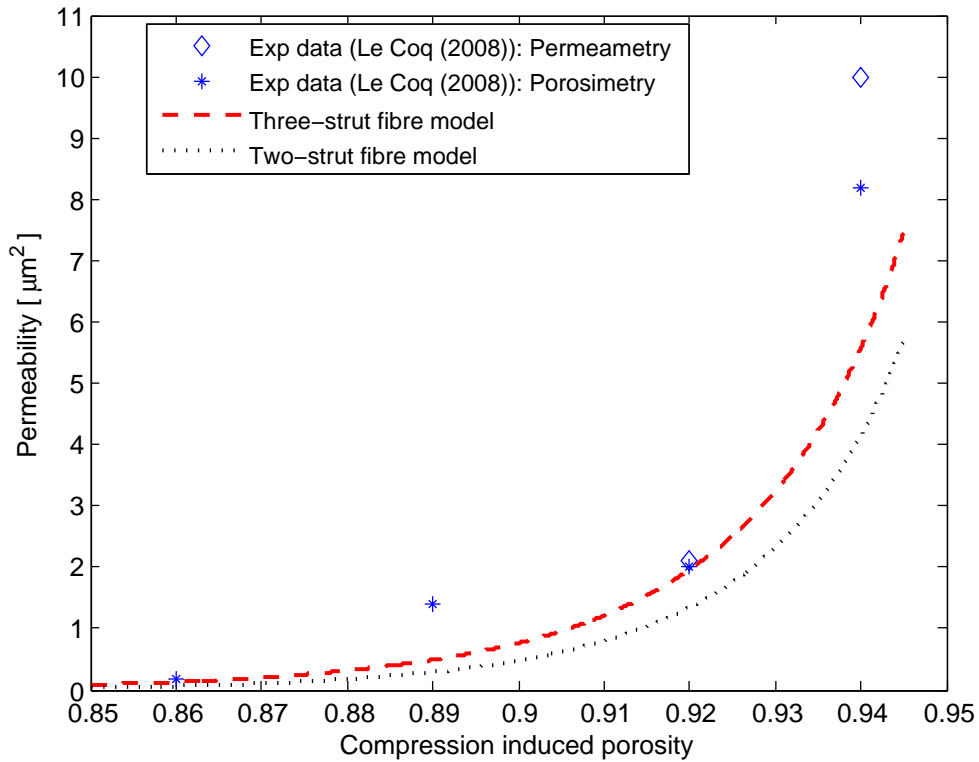


**Figure 4.8:** Permeabilities predicted by the two-strut- and three-strut fibre RRUC models, based on the general non-linear relationship between  $e$  and  $\epsilon$  (equation (4.6)).

uncompressed state. An ‘insignificant’ error in  $\epsilon_0$  could result in a significant error in the permeability prediction of the model. (Further discussion will follow in Section 4.4.4.)

Again the variation of the dimensions of the RRUC’s are visualized through graphs with compression induced porosity as the independent variable (Figure 4.9). It is to be expected that the side length parallel to the streamwise direction follows a similar trend as the relationship between the compression fraction and porosity. The difference between the two models lies in the value for  $d_{||0}$ . For the two-strut fibre RRUC, the side length perpendicular to the streamwise direction is constant since it depends only on the value of the porosity in the uncompressed state of the porous medium. (This implies a constant value for the hydraulic diameter which will be elaborated on in Section 5.2.) The geometry of the three-strut fibre RRUC leads to a porosity dependency of  $d_{\perp}$ . On a larger chosen porosity domain, the  $d_{\perp}$ -curves do not show the same trend as in the case of the linear regression  $\epsilon$  -  $e$  relationship. The side lengths, as functions of compression induced porosity, are continuous and differentiable functions for  $0 < \epsilon < 1$ . In order to visualize this,  $d_{\perp}$  as well as the permeability are plotted as a function of  $\epsilon$  on an extended porosity domain in Figures 4.10 and 4.11, respectively. The graph depicted in Figure 4.11 indicates that the non-linear relationship between the compression fraction and porosity leads to a more representative reflection of the permeability-concept, although the margin of error is larger than that of the linear relationship. The hypothesis is that a relationship that more accurately describes the  $e$  -  $\epsilon$  relationship for a specific porous medium will lead to smaller margins of error in the permeability prediction. This will be investigated in the next section.

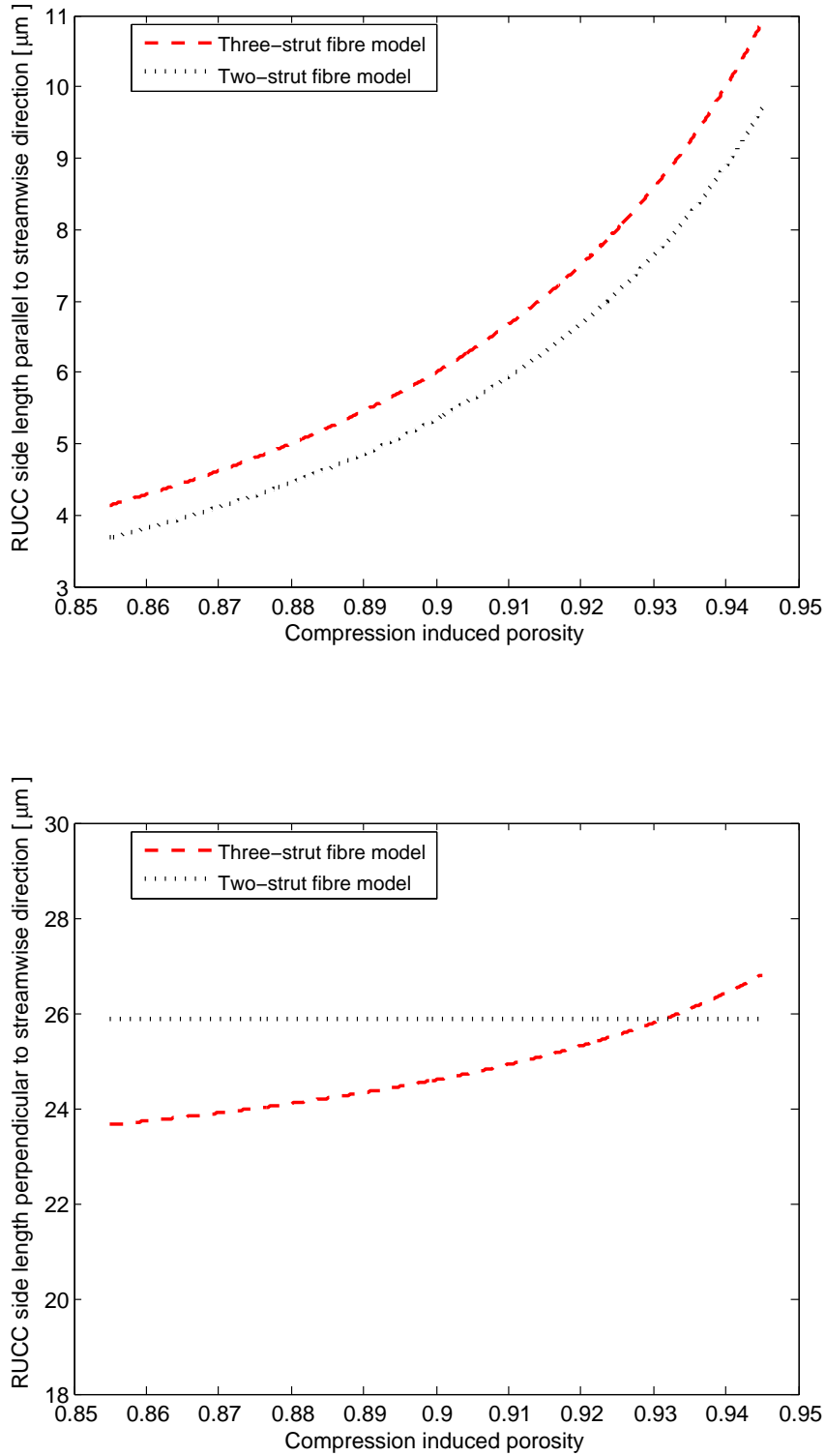


**Figure 4.9:** RRUC side lengths parallel (top) and perpendicular (bottom) to the stream-wise direction as a function of compression induced porosity. (General non-linear relationship between  $e$  and  $\epsilon$ .)

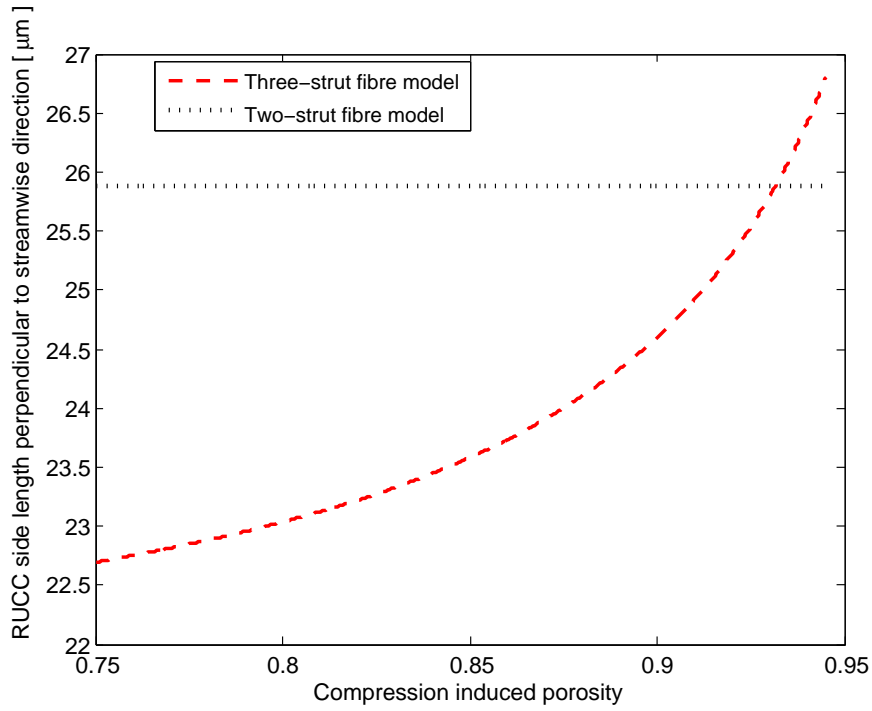


**Figure 4.10:** RRUC side length perpendicular to the streamwise direction as a function of compression induced porosity for the porosity domain [0.75; 0.95]. (General non-linear relationship between  $e$  and  $\epsilon$ .)

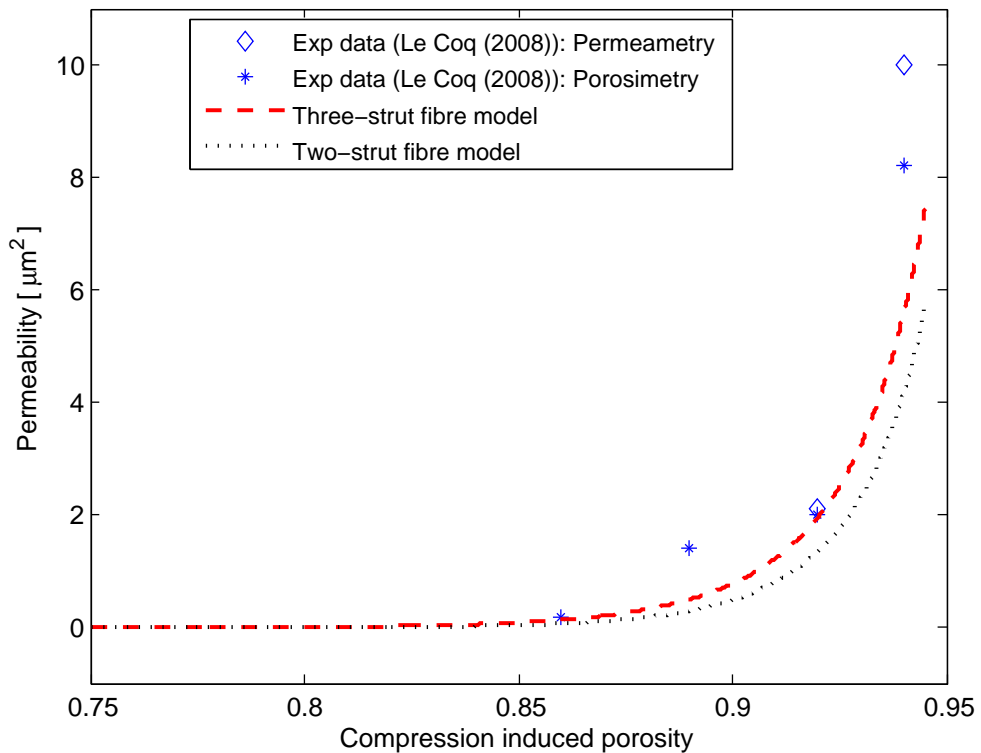


**Figure 4.11:** Permeabilities predicted by the two-strut- and three-strut fibre RRUC models for the porosity domain [0.75; 0.95]. (General non-linear relationship between  $e$  and  $\epsilon$ .)



### 4.4.3 Specific non-linear relationship between compression fraction and porosity (equation (4.8))

Using the relationship between the compression fraction and the porosity as given in equation (4.8), under the assumption expressed in equation (4.17), the expression for the RRUC thickness in the streamwise direction becomes:

$$d_{\parallel} = 8.9 \left( \frac{0.07}{1 - \epsilon} \right). \quad (4.38)$$

Adhering to the restriction expressed in equation (4.21), with  $d_s = 2.7 \mu\text{m}$ , leads to:

$$2.7 \geq (1 - \epsilon) 8.9 \left( \frac{0.07}{1 - \epsilon} \right), \quad (4.39)$$

which is true for all possible values of porosity.

The steps in the modelling procedure remain the same as in Section 4.3 and therefore equation (4.33) is valid using the relevant side lengths of the two-strut fibre RRUC. Using equation (4.8) for the three-strut fibre RRUC model, a corresponding prediction of the effect of compression on the permeability is obtained. In Figure 4.12 the comparison of the results of the two-strut and three-strut geometric models is visualized. Again the permeability is plotted against the compression induced porosity and the empirical values from the experiment of Le Coq (2008) are also shown.

As anticipated, a more representative (of a specific porous medium) relationship between compression and porosity leads to smaller margins of error (as given in Table 4.5) in the permeability prediction of both geometric models. The variation of the two side lengths of the two types of RRUCs are plotted against the compression induced porosity in Figure 4.13, based on equation (4.8).

Permeability ( $\mu\text{m}^2$ ) (Specific non-linear $e - \epsilon$ relationship)				
Experiment	two-strut RRUC	% error	three-strut RRUC	% error
8.2	6.6	-19	8.3	1.2
2.0	2.4	20	3.2	60
1.4	0.61	-56	0.93	-34
0.17	0.17	0	0.30	76

**Table 4.5:** Relative percentage error in the permeability prediction of the two-strut and three-strut fibre RRUC models. (Specific non-linear relationship between  $e$  and  $\epsilon$ .)

Due to the relationship between  $e$  and  $\epsilon$  (i.e. equation (4.8)), the relationship between the RRUC side length parallel to the streamwise direction and porosity is non-linear and again the difference between the two models lies in the different values for  $d_{\parallel 0}$ .

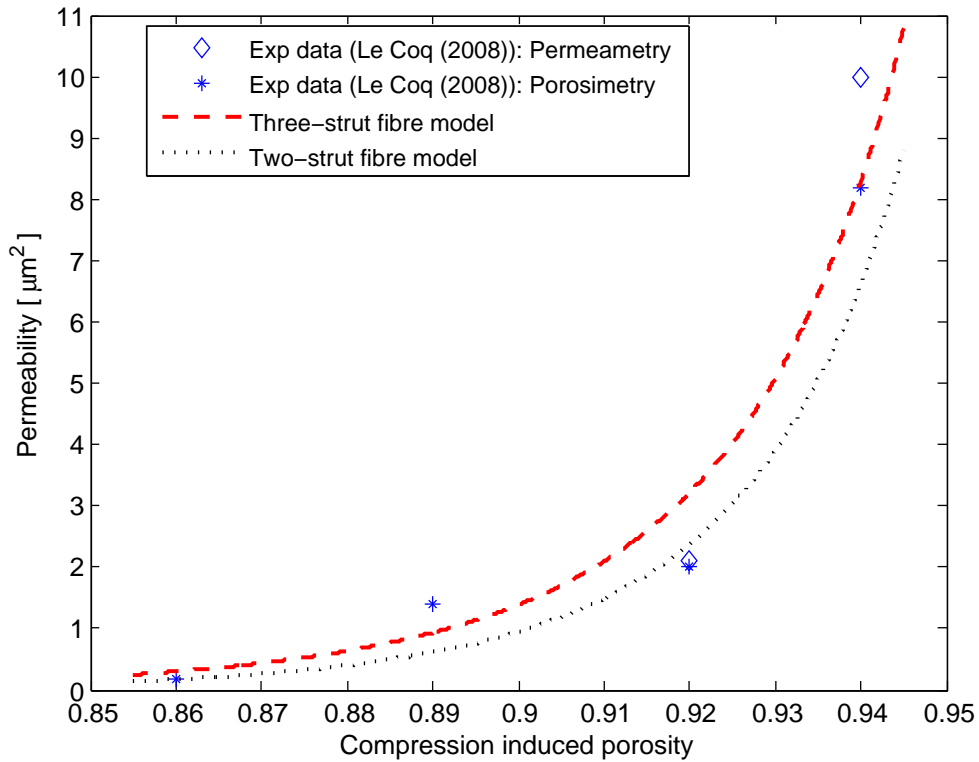


**Figure 4.12:** Permeabilities predicted by the two-strut- and three-strut fibre RRUC models based on a specific non-linear relationship between  $e$  and  $\epsilon$  (equation (4.8)).

The difference between the two models regarding the side lengths perpendicular to the streamwise direction, is due to the different model-geometries. The respective geometries directly determines the relationship between the porosity and the different side lengths of the RRUCs. The fact that in the two-strut model the side length perpendicular to the streamwise direction is a constant for a given uncompressed porosity, can also be deduced from equation (4.22) by substituting the side length parallel to the streamwise direction (given by equation (4.38)). This leads to an equation for  $d_{\perp}$  which is independent of the compression induced porosity, where-as this is not the case with the three-strut model. Since the  $\epsilon - e$  relationship used is a ‘refinement’ of the general relationship, the dimensions of the RRUC’s are (again) continuous, differentiable functions over the whole porosity domain. Graphs are therefore not presented for extended porosity-domains since the specific non-linear relationship (equation (4.8)) renders a representative reflection of the permeability-concept.

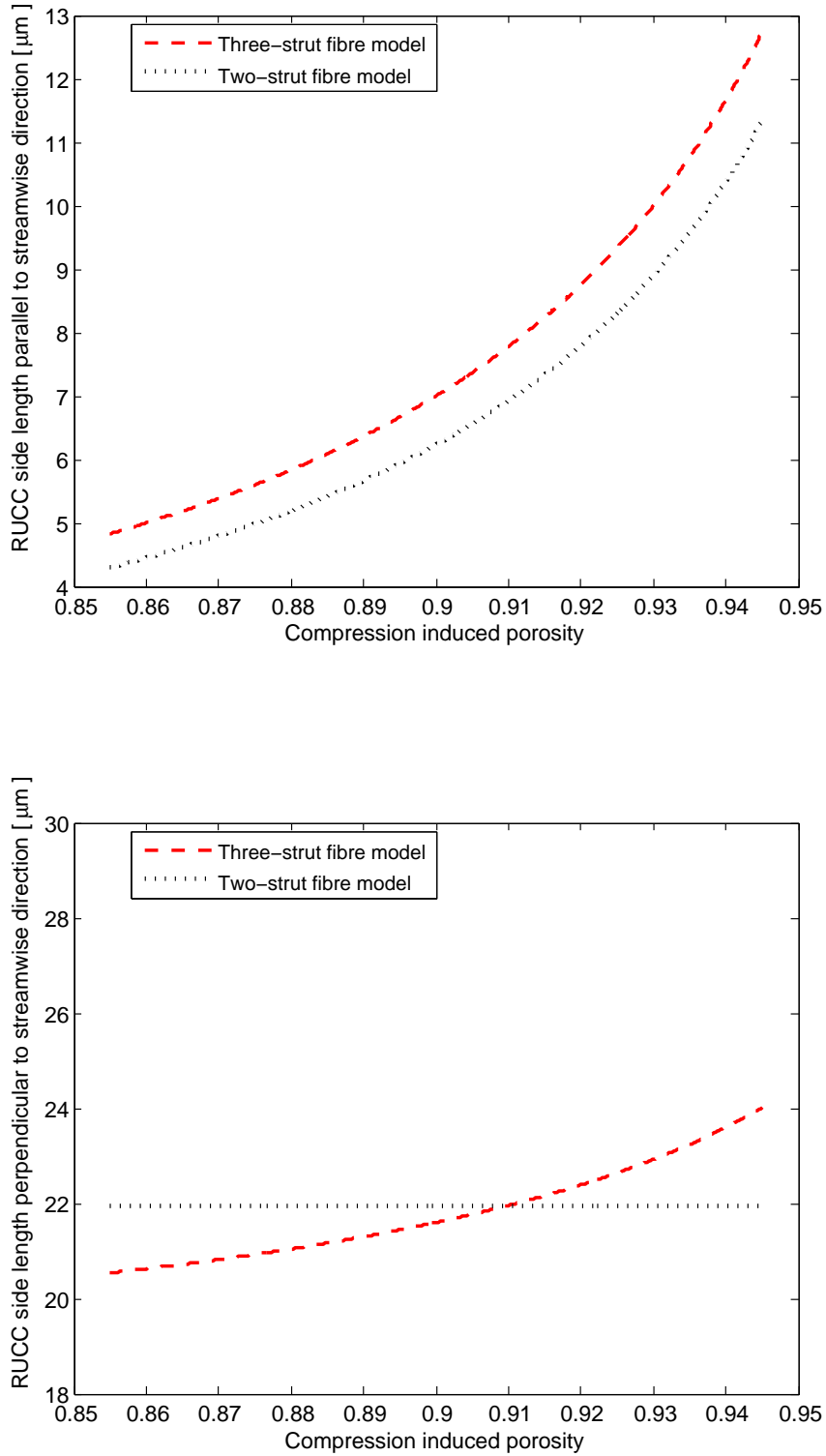


**Figure 4.13:** RRUC side lengths parallel (top) and perpendicular (bottom) to the streamwise direction as a function of compression induced porosity. (Specific non-linear relationship between  $e$  and  $\epsilon$ .)

#### 4.4.4 Summary

All the model predictions show a significant effect of compression on permeability which is in line with the experimental permeability data. It is important to note that the porosity associated with the uncompressed state is not necessarily the porosity of an isotropic porous medium. The permeability predictions are very sensitive to the porosity of the medium in the uncompressed state, which is in line with what Akaydin et al. (2011) stated. This is also highlighted by the difference in the predictions of the two- and three-strut fibre models when the porosity of the uncompressed state and a more refined coefficient were respectively used to determine the general and specific relationship between  $e$  and  $\epsilon$ .

Figures 4.14 and 4.15 are presented to visualize the effect of the choice of relationship between the compression fraction and the porosity on the prediction capability of a chosen geometric model.

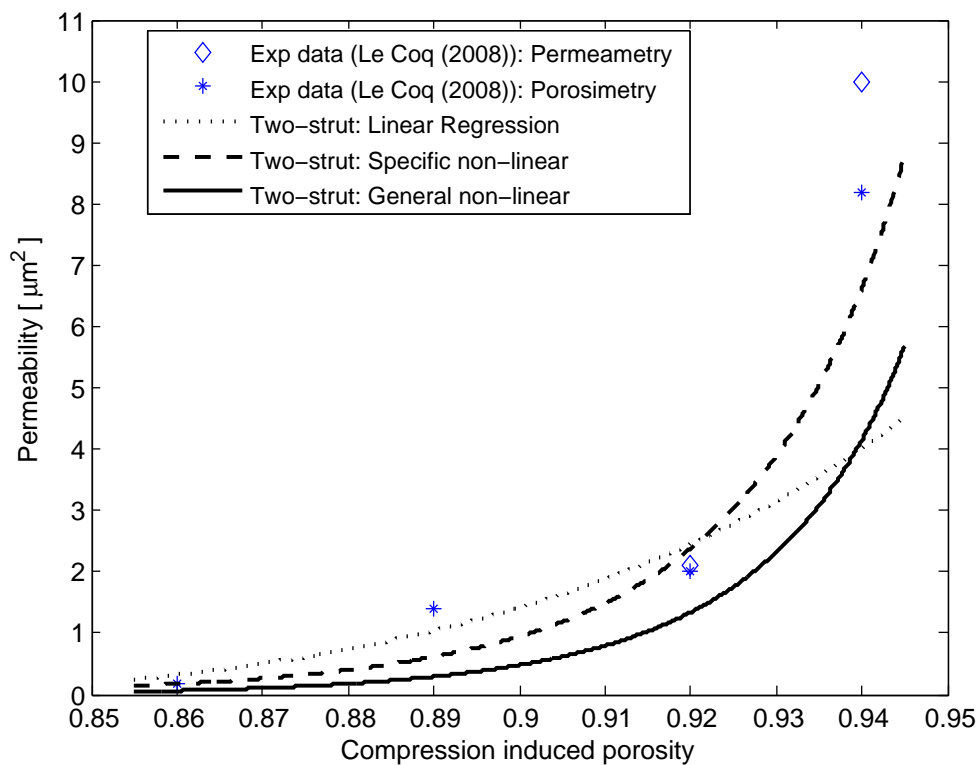


**Figure 4.14:** Influence of the relationship between  $e$  and  $\epsilon$  on the permeability-prediction of the two-strut fibre RRUC model.

The percentage errors are reflected in Tables 4.3, 4.4, and 4.5 but it is clear from Figures 4.15 and 4.14 that the specific non-linear relationship renders the more accurate prediction curve for both geometric models.

Employing the specific non-linear relationship leads to an improvement of the three-strut fibre RRUC model presented by Woudberg (2012a).

The general relationship is valid whenever the porous medium is uniaxially compressed.

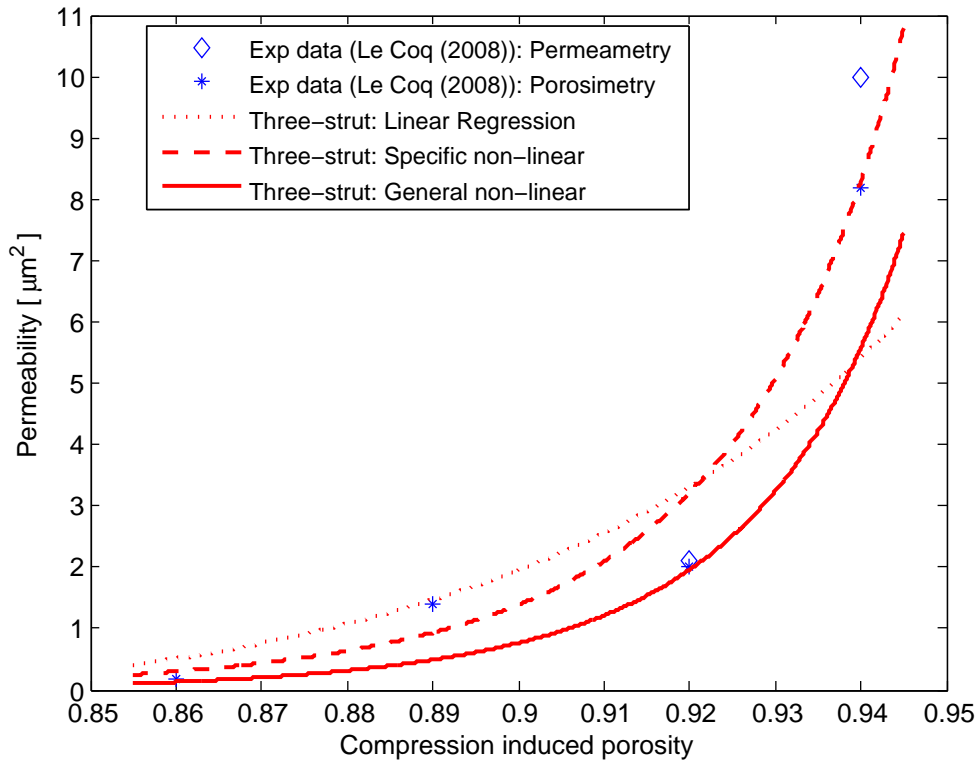


**Figure 4.15:** Influence of the relationship between  $e$  and  $\epsilon$  on the permeability prediction of the three-strut fibre RRUC model.

It must be mentioned that when this relationship is employed, the accuracy in the measurement of the porosity in the uncompressed state is extremely important since a small error in this value is amplified to much larger percentage errors in the permeability prediction. This is why, when porosity data is available for different stages of compression, the data is used to minimize the possible error in the constant used in the specific non-linear relationship (equation (4.7)).

When experimental data regarding the porosity and hydraulic diameter is available, and therefore the modelling steps described in this chapter are applicable, the two-strut fibre model produces a lower permeability prediction than the three-strut model for all three  $e - \epsilon$  relationships. For each of the three relationships used, the streamwise length of the two-strut RRUC is shorter than that of the three-strut RRUC which is due to the fact that the three-strut RRUC gives rise to a higher value for the uncompressed length in each case. This also indicates that the value for  $d_{\parallel 0}$  has a significant influence on the permeability prediction.

As can be deduced from equations (4.17) and (4.22), for the two-strut geometry and chosen relationship between  $e$  and  $\epsilon$ , a larger value of  $d_{\parallel 0}$  will consequently result in smaller streamwise channels and larger transverse channels being represented in the geometric model. In the two-strut model,  $d_{\perp}$  is a constant for a given  $\epsilon_0$  when a non-linear (general or specific) relationship between  $e$  and  $\epsilon$  is employed. Consequently  $w_{\parallel}$  stays constant for all the levels of compression considered, while  $w_{\perp}$  increases as the compression fraction ( $d_{\parallel}/d_{\parallel 0}$ ) decreases.

Since the hydraulic diameter was employed to determine  $d_{\parallel 0}$ , the underlying assumptions and corresponding formulas used for the hydraulic diameter in the modelling as well as experimental procedures will influence the margin of difference between the analytical model predictions and the experimentally obtained data.

In the modelling steps, the experimental values for the hydraulic diameter were employed to obtain initial values for  $d_{\perp}$  with which  $d_{\parallel 0}$  was calculated using the experimental data pertaining to the porosity and corresponding compression fraction. The obtained value for  $d_{\parallel 0}$  was then employed to determine the side lengths of the RRUC for each level of compression in order to predict the corresponding permeability. An alternative to employing the hydraulic diameter for determining  $d_{\parallel 0}$  will be investigated in Section 5.3, referring only to the two-strut fibre RRUC introduced in this study.

The constant value for  $d_{\perp}$  in the two-strut model (with a non-linear relationship between  $e$  and  $\epsilon$ ) has, as consequence, the fact that the hydraulic diameter is constant for all phases of compression in this model. In the three-strut fibre RRUC model the hydraulic diameter does change with compression. The hydraulic diameter will be revisited in Section 5.2.

The comparison done between the two-strut and three-strut models for each of the three different relationships, highlights the fact that the prediction capability of the models are also influenced by the choice of geometry for the RRUC solid. The visualization of this effect in Figures 4.4, 4.5, 4.6, 4.9, 4.10 and 4.13, comparing the dimensions of the RRUCs, emphasize this influence. It is therefore evident that the solid geometry which determines the expression for porosity, is a crucial factor influencing the other dimensions of the RRUC. In Chapter 5, this will be investigated further, referring only to the two-strut fibre model.

## Chapter 5

# Modified two-strut fibre RRUC model

The porosity is an indicator of the volume available for flow in a porous medium. As is evident from Chapter 4, the porosity can be modelled with the aid of different solid geometries. When the porous medium is compressed, not only does the volume available for flow decrease, but the geometry of this volume changes. In modelling the effect of compression on the permeability of a porous medium, special attention must be given to the effect of change of solid geometry on the prediction capability of a model. It is possible that one type of geometry is a better representation of the morphology of the medium than another geometry. To investigate this, the experimental data of Le Coq (2008), presented in Table 3.2, as well as the two-strut model, will be used throughout this chapter. An alternative strategy for obtaining the value of  $d_{\parallel 0}$  will also be presented.

### 5.1 Solid-change in the two-strut fibre RRUC

In general the availability of porosity data at different stages of compression will influence the choice of relationship between the compression fraction and porosity to be used. Since experimental porosity data for different compressed states of the porous medium in question is available (through mercury porosimetry), the optimal option for the relationship between  $e$  and  $\epsilon$  in this context, is the specific relationship given by equation (4.8), as discussed in Chapter 4. The specific relationship will therefore be used throughout this section in order to determine the effect of solid-geometry on permeability prediction.

In the two-strut RRUC model the cross-sectional area (parallel to streamwise direction) of the solid part, was chosen as  $(d_s)^2$ , with  $d_s$  set equal to the mean average diameter of the fibres in question. This implies that the compression had no effect on the *distribution* of solids in the two-strut RRUC model. The change in porosity due to compression was reflected by a change in the volume available for fluid flow.

The RRUC is a representation of the geometry (morphology) of the porous medium in question and the aim is to enhance this representation. This can be investigated by

changing the representation, within the geometric two-strut fibre model, of the fractions of solid surfaces that are aligned with the streamwise and transverse directions in the corresponding REV.

The decision was made to investigate a change in the side lengths of the solid in the RRUC whilst keeping the cross-sectional area (cut parallel to streamwise direction) of the solid constant. This implies that the distribution of solid surface areas is altered without changing the other dimensions of the RRUC significantly.

The reason for not wanting to change the dimensions of the RRUC significantly is the following: If the solid volume is increased in the two-strut fibre RRUC, the total volume must increase if the porosity is to be kept constant. Due to the choice of the geometry of the two-strut model, and the consequent constant  $d_{\perp}$ , the volume is then increased in an asymmetric manner leading to impractical values for the streamwise sidelength. From Chapter 4 it is reasonable to assume that the modelling of the widths of the transverse and streamwise channels in the two-strut fibre RRUC provides satisfactory first order permeability predictions. The aim is to investigate possible enhancements of this model. Changing the dimensions of the solid part of the two-strut fibre RRUC without changing the RRUC side lengths significantly, implies that the contribution of shear stresses in the streamwise and transverse directions is altered mainly through a change in surface-areas (and not just by changing the volume available for flow). The change in the solid geometry does not imply a change in the geometry of the actual fibres - the representation of the average solid surface distribution in the directions perpendicular and parallel to the streamwise directions is done via different ratios.

Rough sketches will be used to show the changes in the representative solid geometry - in essence the model is still represented by Figure 4.2. Two options will be considered and discussed separately in the following two subsections.

### 5.1.1 Solid with side lengths $d_{\perp}$ , $\frac{1}{\sqrt{2}} d_s$ and $\sqrt{2} d_s$

The effect of changing the contribution of shear stresses (through a change in geometry of the solid part of the RRUC) on the prediction capability of the two-strut fibre RRUC will be investigated. This will be done by employing the specific non-relationship between the compression fraction and porosity (equation (4.8)) and the same modelling steps as in Section 4.3. The first solid-change to be investigated is shown in Figure 5.1 with the cross-sectional area equal to  $(d_s)^2$ .

The first choice is made for a 2:1 ratio. This is done to balance mathematical simplicity and choice of solid geometry with the concept of the RRUC as a minimal volumetric body into which the type of porous medium can be embedded. The minimal length represented in the RRUC is ideally a dimension resembling the diameter of the fibres in question. Choosing a 2:1 ratio with cross-sectional area equal to  $(d_s)^2$  implies that the minimal length in the dimensions of the RRUC is  $\frac{1}{\sqrt{2}} d_s$ . Increasing this ratio leads to a decreasing minimal length.

The two-strut fibre RRUC with solid geometry as depicted in Figure 5.1, will be referred



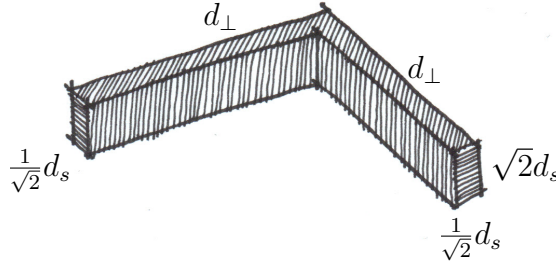


**Figure 5.1:** Solid with dimensions  $d_{\perp}$ ,  $\frac{1}{\sqrt{2}} d_s$  and  $\sqrt{2} d_s$  for two-strut fibre RRUC model.

to as the two-strut sqrt(2) fibre RRUC model. The modelling steps will be repeated in order to highlight the effect that the change in geometry have on the parameters (such as the shear stresses) used in the permeability prediction. The total volume ( $U_0$ ) and total solid volume ( $U_s$ ) of this model can respectively be expressed as

$$U_0 = (d_{\perp})^2 d_{\parallel} \quad \text{and} \quad (5.1)$$

$$U_s = 2(d_s)^2 d_{\perp} - \frac{1}{\sqrt{2}} (d_s)^3, \quad (5.2)$$

which leads to the porosity being written as

$$\epsilon = \frac{U_f}{U_0} = \frac{(d_{\perp})^2 d_{\parallel} - [2(d_s)^2 d_{\perp} - \frac{1}{\sqrt{2}} (d_s)^3]}{(d_{\perp})^2 d_{\parallel}}. \quad (5.3)$$

Combining the hydraulic diameter  $D_h = d_{\perp} - \frac{1}{\sqrt{2}} d_s$  (in RRUC notation), with the expression for porosity (equation (5.3)), leads to

$$d_{\parallel} = \frac{2(d_s)^2 (D_h + \frac{1}{\sqrt{2}} d_s) - \frac{1}{\sqrt{2}} (d_s)^3}{(1 - \epsilon)(D_h + \frac{1}{\sqrt{2}} d_s)^2}. \quad (5.4)$$

Determining an uncompressed streamwise side length of the RRUC in the same way as in Section 4.3, leads to:

$$d_{\parallel} = 9.4 e. \quad (5.5)$$

Incorporating the relationship

$$e = \frac{0.07}{1 - \epsilon}, \quad (5.6)$$

yields:

$$d_{\parallel} = 9.4 \frac{0.07}{1 - \epsilon}. \quad (5.7)$$

The expression for the side lengths of the RRUC perpendicular to the streamwise direction, i.e.

$$d_{\perp} = \frac{d_s \left( d_s + \sqrt{(d_s)^2 + \frac{1}{\sqrt{2}} d_{\parallel} d_s (\epsilon - 1)} \right)}{d_{\parallel} (1 - \epsilon)}, \quad (5.8)$$

can thus be written as:

$$d_{\perp} = \frac{d_s \left( d_s + \sqrt{(d_s)^2 - \left(\frac{1}{\sqrt{2}}\right) (9.4) (0.07) d_s} \right)}{(9.4) (0.07)}. \quad (5.9)$$

The constant values are not multiplied in order to keep the assumptions explicit.

Under the same assumptions as in Section 4.3, the magnitudes of the velocities can respectively be expressed as

$$w_{\parallel} = \frac{q (d_{\perp})^2}{\left(d_{\perp} - \frac{1}{\sqrt{2}} d_s\right)^2}, \quad (5.10)$$

and

$$w_{\perp} = \left( \frac{q (d_{\perp})^2}{\left(d_{\perp} - \frac{1}{\sqrt{2}} d_s\right)^2} \right) \left( \frac{\left(d_{\perp} - \frac{1}{\sqrt{2}} d_s\right)^2}{\left(d_{\parallel} - \sqrt{2} d_s\right) (d_{\perp})} \right) = \frac{q d_{\perp}}{\left(d_{\parallel} - \sqrt{2} d_s\right)}. \quad (5.11)$$

Again it is assumed that, for dynamic equilibrium, the shear stresses can be utilized to approximate the pressure loss in a porous medium and that the formulas associated with parallel plates may be employed. In terms of the dimensions of the two-strut sqrt(2) fibre RRUC with the solid as in Figure 5.1, the assumptions lead to:

$$\left(d_{\perp} - \frac{d_s}{\sqrt{2}}\right)^2 \Delta p = \left[4 \sqrt{2} d_s \left(d_{\perp} - \frac{d_s}{\sqrt{2}}\right)\right] \tau_{w_{\parallel}} + \left[4 \frac{d_s}{\sqrt{2}} \left(d_{\perp} - \frac{d_s}{\sqrt{2}}\right) + (d_s)^2\right] \tau_{w_{\perp}}, \quad (5.12)$$

with

$$\tau_{w_{\parallel}} = \frac{6 \mu w_{\parallel}}{d_{\perp} - \frac{1}{\sqrt{2}} d_s} \quad \text{and} \quad \tau_{w_{\perp}} = \frac{6 \mu w_{\perp}}{d_{\parallel} - \sqrt{2} d_s}. \quad (5.13)$$

Therefore:

$$\begin{aligned} \left(d_{\perp} - \frac{d_s}{\sqrt{2}}\right)^2 \Delta p &= \left[4 \sqrt{2} d_s\right] 6 \mu w_{\parallel} + \left[2\sqrt{2} d_s d_{\perp} - (d_s)^2\right] \frac{6 \mu w_{\perp}}{d_{\parallel} - \sqrt{2} d_s} \\ \Delta p &= \left[4 \sqrt{2} d_s\right] \frac{6 \mu q (d_{\perp})^2}{\left(d_{\perp} - \frac{1}{\sqrt{2}} d_s\right)^4} + \left[2\sqrt{2} d_s d_{\perp} - (d_s)^2\right] \frac{6 \mu q d_{\perp}}{\left(d_{\parallel} - \sqrt{2} d_s\right)^2 \left(d_{\perp} - \frac{1}{\sqrt{2}} d_s\right)^2} \\ \Delta p &= \frac{6 \mu q \left[4 \sqrt{2} d_s (d_{\perp})^2 (d_{\parallel} - \sqrt{2} d_s)^2 + \left(2\sqrt{2} d_s (d_{\perp})^2 - (d_s)^2 d_{\perp}\right) \left(d_{\perp} - \frac{1}{\sqrt{2}} d_s\right)^2\right]}{\left(d_{\parallel} - \sqrt{2} d_s\right)^2 \left(d_{\perp} - \frac{1}{\sqrt{2}} d_s\right)^4} \end{aligned} \quad (5.14)$$

As previously, based on the assumptions expressed in equation (4.32), the permeability in this context can be written as:

$$k = \frac{d_{\parallel} (d_{\parallel} - \sqrt{2} d_s)^2 \left(d_{\perp} - \frac{1}{\sqrt{2}} d_s\right)^4}{24 \sqrt{2} d_s (d_{\perp})^2 (d_{\parallel} - \sqrt{2} d_s)^2 + 6 \left(2\sqrt{2} d_s (d_{\perp})^2 - (d_s)^2 d_{\perp}\right) \left(d_{\perp} - \frac{1}{\sqrt{2}} d_s\right)^2}. \quad (5.15)$$

Figure 5.2 gives a comparison between the permeabilities predicted by the two-strut fibre RRUC model and the two-strut  $\sqrt{2}$  fibre RRUC model. Table 5.1 presents the percentage errors. Recall that the permeability predictions are based on a specific non-linear relationship between  $e$  and  $\epsilon$  (equation (4.8)).

It is evident that, as was also observed in the comparison between the two-strut and three-strut models, a change in the solid geometry affects the permeability prediction of the RRUC models. The two-strut  $\sqrt{2}$  fibre RRUC model renders a more accurate permeability prediction for porosities close to the porosity associated with the uncompressed state while the initial two-strut fibre RRUC model is more accurate for porosities associated with compressed states of the porous medium.

Assuming that compression has an effect on the resultant surfaces available for shear in the three principal directions, it can be deduced from Figure 5.2 that the two-strut  $\sqrt{2}$  fibre RRUC model resembles the structure of the fibrous porous medium in the uncompressed state and the initial two-strut fibre RRUC model the compressed state. The representation of the solid (re-)distribution (note: NOT necessarily deformation of fibres) can be made a continuous function of the compression fraction by incorporating the compression fraction in the dimensions of the solid part of the RRUC whilst keeping the cross-sectional area of the solid equal to  $(d_s)^2$ .

Permeability ( $\mu\text{m}^2$ ) (Specific non-linear $e - \epsilon$ relationship)				
Experiment	two-strut RRUC	% error	two-strut $\sqrt{2}$ RRUC	% error
8.2	6.6	-19	8.2	0
2.0	2.4	20	2.7	35
1.4	0.61	-56	0.52	-63
0.17	0.17	0	0.07	-59

**Table 5.1:** Relative percentage error in the permeability prediction of the two-strut- and two-strut  $\sqrt{2}$  fibre RRUC models. (Specific non-linear relationship between  $e$  and  $\epsilon$ .)

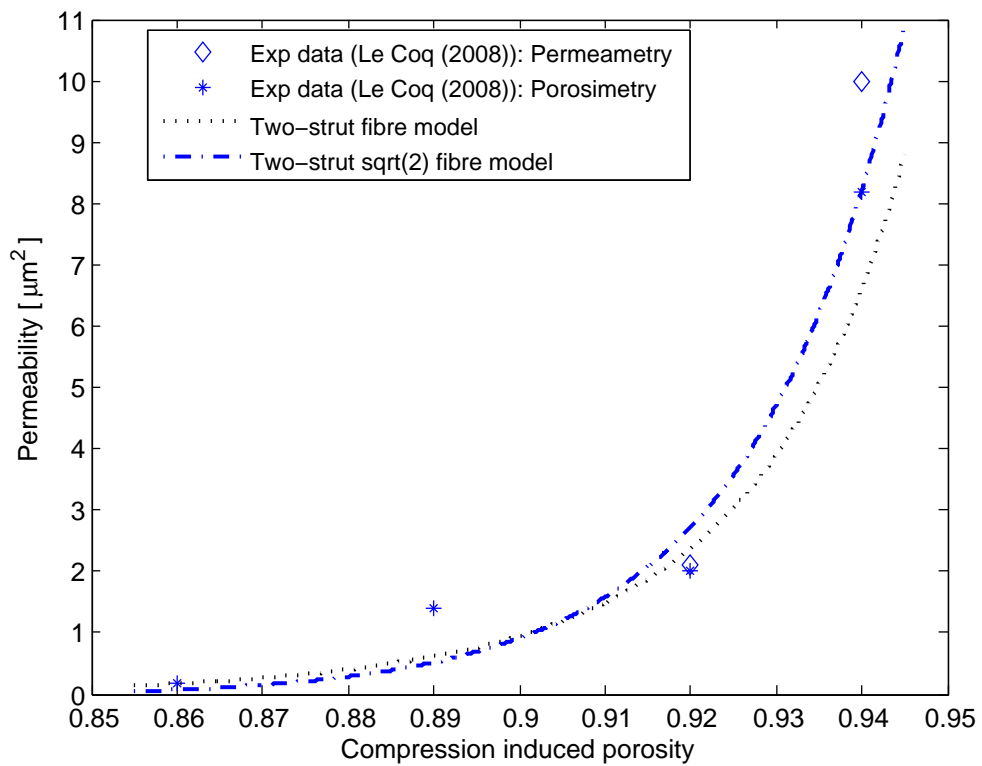


**Figure 5.2:** Permeabilities predicted by the two-strut- and two-strut sqrt(2) fibre RRUC models. (Specific non-linear relationship between  $e$  and  $\epsilon$ .)

### 5.1.2 Solid with side lengths $d_{\perp}$ , $\frac{1}{\sqrt{2e}} d_s$ and $\sqrt{2e} d_s$

Changing the dimensions of the solid in the two-strut fibre RRUC in the manner as depicted in Figure 5.3, keeping the assumptions and the modelling steps the same as in Section 5.1, leads to a value of  $9.2 \mu\text{m}$  for the uncompressed streamwise length. The two-strut fibre RRUC model with dimensions as depicted in Figure 5.3 will be referred to as the two-strut sqrt(2e) fibre RRUC model.

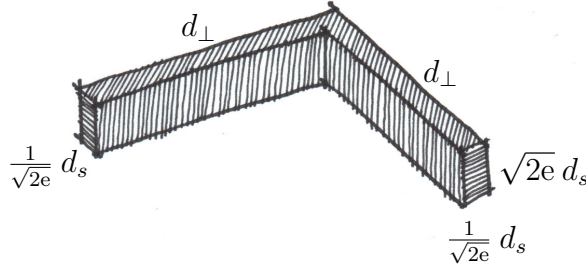


**Figure 5.3:** Solid with dimensions  $d_{\perp}$ ,  $\frac{1}{\sqrt{2e}} d_s$  and  $\sqrt{2e} d_s$  for two-strut fibre RRUC model.

The expression for the permeability where the resultant solid distribution changes with the level of compression can then be written as follows:

$$k = \frac{d_{\parallel} (d_{\parallel} - \sqrt{2e} d_s)^2 (d_{\perp} - \frac{1}{\sqrt{2e}} d_s)^4}{24 \sqrt{2e} d_s (d_{\perp})^2 (d_{\parallel} - \sqrt{2e} d_s)^2 + 6 \left( \frac{2\sqrt{2}}{\sqrt{e}} d_s (d_{\perp})^2 - \frac{1}{e} (d_s)^2 d_{\perp} \right) (d_{\perp} - \frac{1}{\sqrt{2e}} d_s)^2}, \quad (5.16)$$

with  $d_{\parallel} = d_{\parallel_0} e = 9.2 e$  and

$$d_{\perp} = \frac{d_s \left( d_s + \sqrt{(d_s)^2 - \left( \frac{1}{\sqrt{2e}} \right) (9.2) (0.07) d_s} \right)}{(9.2) (0.07)}. \quad (5.17)$$

As is evident from Figure 5.4 and Table 5.2, there is little difference between the predictions of the two-strut sqrt(2e) fibre RRUC and the initial two-strut fibre RRUC model other than respectively being more accurate on the upper and lower boundaries of the porosity domain.

It is expected that the two-strut sqrt(2e) and two-strut sqrt(2) fibre RRUC models provide the same prediction for  $e = 1$ . The difference in permeability prediction for the uncompressed state is (in the present context) due to different values obtained for  $d_{\parallel_0}$  through the steps described in Section 4.3.

Changing the dimensions of the solid whilst keeping the modelling steps as well as the relationship between  $e$  and  $\epsilon$  constant, leads to a change in permeability prediction regarding a chosen porous medium. The aim is not to draw a conclusion on the ‘best’

model for fibrous porous media in general, since a fixed set of data regarding glass fibre non-wovens was used through-out. A general discussion leading to conclusions regarding the applicability of the different RRUC models will be given in Chapter 7.

In the comparative investigation regarding the influences of parameter-changes on the permeability prediction of the different RRUC models, the hydraulic diameter was (up until now) employed to determine an uncompressed streamwise length. This concept will be revisited to highlight possible discrepancies between the experimental and analytical modelling processes.

<b>Permeability (<math>\mu\text{m}^2</math>) (Specific non-linear e - <math>\epsilon</math> relationship)</b>				
Experiment	two-strut RRUC	% error	two-strut sqrt(2e) RRUC	% error
8.2	6.6	-19	7.7	-6.1
2.0	2.4	20	2.6	30
1.4	0.61	-56	0.65	-54
0.17	0.17	0	0.21	24

**Table 5.2:** Relative percentage error in the permeability predictions of the two-strut- and two-strut sqrt(2e) fibre RRUC models. (Specific non-linear relationship between e and  $\epsilon$ .)

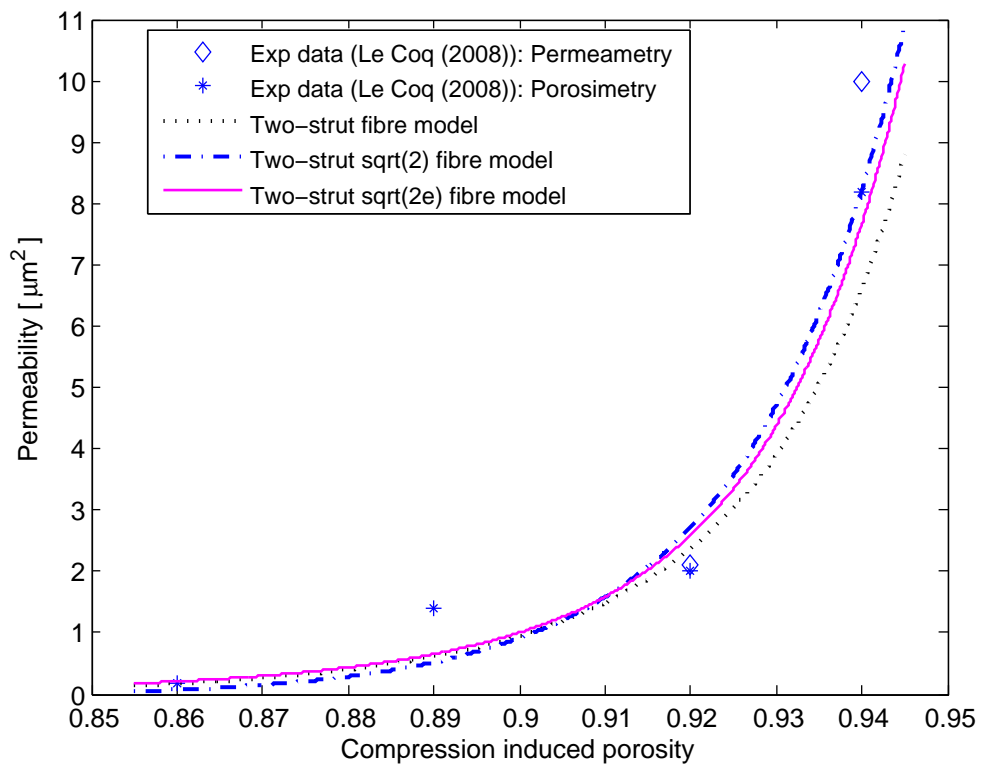


**Figure 5.4:** Permeabilities predicted by the two-strut-, the two-strut sqrt(2)- and the two-strut sqrt(2e) fibre RRUC models. (Specific non-linear relationship between  $e$  and  $\epsilon$ .)

## 5.2 The choice of hydraulic diameter revisited

Since the hydraulic diameter forms an essential part of the modelling process, the choice there-of should be a subject of reflection. For flow in a fully filled circular pipe of constant cross-sectional area, the pressure loss per unit length can be written as the average (if the wall surface is not uniform) wall shear stress multiplied by the ratio of the circumference to the cross-sectional area of the pipe. In this case the latter ratio is equal to four divided by the diameter of the pipe. For fully filled **non**-circular pipes of **constant** cross-sectional area, the above mentioned equality leads to the definition of the hydraulic diameter:

$$D_h = 4 \left( \frac{\text{cross-sectional area}}{\text{perimeter}} \right). \quad (5.18)$$

This means that a non-circular pipe can be replaced with a circular pipe with diameter  $D_h$  for the same pressure loss per unit length.

The hydraulic diameter is often used as characteristic length when considering flow in non-circular tubes and channels. For example, assuming flow in a straight duct, Shah & London (1978) express the Reynolds number in terms of the hydraulic diameter.

It is clear that when the numerator and denominator in equation (5.18) are both multiplied with a constant cross-sectional length, the definition becomes:

$$D_h = 4 \left( \frac{\text{total fluid volume}}{\text{wetted surface area}} \right), \quad (5.19)$$

which is the formula used in the context of porous media (although the channels/pores in general do not have a constant cross-sectional area).

Since pore size distributions are often employed in obtaining values for the hydraulic diameter, it is important to clarify that the definition of pore size depends on the application of the porous medium in question. As previously mentioned, in liquid porosimetry, a pore is assumed to be a cylindrical capillary with its diameter calculated through the measurement of the pressure required to intrude (or extract) a non-wetting (or wetting) fluid into (from) the porous medium. This concept of pore-size is often used to characterize unsaturated media where two immiscible fluids simultaneously occupy the void spaces in the porous medium. When, however, the porous medium is applied in a filtering process (e.g. removing solid particles from a liquid), the pore size definition is based on the size of the particles that can traverse through the medium without getting trapped. In the case of a saturated fibrous porous medium (as assumed in the present analytical modelling process), the pore size depends only on the internal structure of the material while in porosimetry it also depends on the paths with which the different void spaces can be accessed (Jaganathan et al. (2009)).

According to Le Coq (2008) the fibrous media used in the characterization process show a pore size gradient in the thickness, although in the case of the 100% 2.7  $\mu\text{m}$  samples (of which the data was employed in this study) only a slight pore gradient was recorded. Jaganathan et al. (2009) states that most of the theoretical pore size distribution models are obtained for homogenous structures and could not be applied in predicting the pore



size distribution of a typical hydro-entangled fabric since there is a SVF gradient in the thickness direction. By increasing the compression, the porous medium tends to become more uniform in this regard.

Based on an image analysis technique, known as the full-morphology method, Jaganathan et al. (2009) obtained a geometric pore size distribution via a modified full-morphology algorithm. This approach is based on the assumption that all pores are spherical and that a continuous void domain can be approximated by a number of discrete spherical volumes. It was concluded that the geometric pore size distribution narrows and the tail of the distribution reduces with increased compression.

It is therefore evident that the underlying assumptions are not always explicit and that discrepancies between experimental and analytical results may be a consequence thereof.

In the context of the RRUC the hydraulic diameter is taken as the side length of the square (normal vector in the streamwise direction) associated with the smallest entrance to the RRUC in the streamwise direction. This is in line with the hydraulic diameter of a square duct as well as with the notion of the average pore hydraulic diameter obtained through mercury porosimetry (where the smallest opening towards a pore is measured). The hydraulic diameter obtained through mercury porosimetry or image analysis represents the average pore diameter in any direction. In line with previous RRUC models (discussed in Section 3.2) the choice is made to represent this average by equating it to the sidelength of the square face of the RRUC that is associated with the smallest streamwise entrance to the RRUC.

The hydraulic diameter does not change in the two-strut (with cross-sectional area  $d_s \times d_s$ ) and the two-strut  $\sqrt{2}$  ( $(\sqrt{2} d_s) \times (\frac{1}{\sqrt{2}} d_s)$ ) fibre models (with a non-linear relationship between  $e$  and  $\epsilon$ ) since both  $d_{\perp}$  and  $d_s$  are constant for a specific porous medium. The two-strut  $\sqrt{2e}$  fibre model, with the cross-sectional area given by  $(\sqrt{2e} d_s) \times (\frac{1}{\sqrt{2e}} d_s)$  (non-linear relationship between  $e$  and  $\epsilon$ ), reflects small changes in the hydraulic diameter since the compression fraction is incorporated into the dimensions of the solid in the RRUC. The constant hydraulic diameter of the two-strut- and two-strut  $\sqrt{2}$  fibre models should be seen as an average of the experimentally obtained hydraulic diameters associated with each level of compression.

As can be seen from experimental data, e.g. Le Coq (2008), it is possible that the percentage change in permeability is much more profound than the change in hydraulic diameter. The change in hydraulic diameter and porosity are not proportional to the change in permeability. The manner in which the hydraulic diameter is experimentally obtained can obscure the actual change in the geometry of the porous medium. If, due to compression, the pore-size of the smaller pores decrease, it doesn't reflect in the average pore hydraulic diameter or in the porosity with the same significance as in the permeability.

It is very important to note that the change in the solid geometry (two-strut  $\sqrt{2e}$  fibre RRUC model) does not necessarily imply fibre deformation. It reflects a change in solid distribution in the corresponding REV due to compression and the ratios of solid surfaces in different directions are reflected by a change in solid in the RRUC. The fibre diameter is chosen as the fixed length relative to which the rest of the dimensions are scaled to represent the averages of the corresponding REV in the RRUC.

As mentioned by Woudberg (2012a), the anisotropic foam (and fibre) RRUC model(s) distinguishes between the hydraulic diameter associated with the streamwise and transverse directions. Since the hydraulic diameter presented by Le Coq (2008) represents the streamwise and transverse pores, there could be a discrepancy between the experimental values and the choice of a ‘streamwise’ hydraulic diameter for the two-strut fibre RRUC model. Based on the original concept of the hydraulic diameter, an average of streamwise and transverse hydraulic diameters is not meaningful. In the two-strut fibre RRUC context the choice of hydraulic diameter is associated with streamwise flow, being aware that this choice influences the percentage error of the permeability predictions of this model.

It is clear that the difference between the permeability prediction of the analytical model(s) and the permeability values presented by Le Coq (2008) could be assigned to differences in the application of the hydraulic diameter concept.

When experimental values for the hydraulic diameter are not available a different strategy for obtaining  $d_{\parallel 0}$  is necessary. This will be discussed in the next section.

### 5.3 Alternative method for determining $d_{\parallel 0}$

Referring to the two-strut fibre RRUC, as visualized in Figure 4.2, a different strategy for determining  $d_{\parallel 0}$  will be introduced in this section (as opposed to employing the hydraulic diameter).

This is important since porosity and hydraulic diameter data regarding one or more compressed states of a fibrous porous medium are not necessarily available to characterize the medium in question. Furthermore, if there is no available data with which to obtain a linear regression or specific non-linear relationship, only the general non-linear relationship between the compression fraction and the porosity is applicable.

In the event that porosity data at different levels of compression were not obtained empirically, but calculated using equation (4.5), as was done by e.g. Akaydin et al. (2011), both the permeability as well as the porosity can be regarded as functions of the compression fraction. All the porosity values, each corresponding to a compression fraction, are dependent on the measured value of the porosity of the medium in the uncompressed state:

$$\epsilon = \frac{e - (1 - \epsilon_0)}{e}. \quad (5.20)$$

For convenience, Figure 4.2 is duplicated in Figure 5.5 for the purpose of quick reference for the reader. (For clarification: as discussed in Chapter 4, for the general non-linear relationship between  $\epsilon$  and  $e$ , the side length perpendicular to the streamwise direction,  $d_{\perp}$ , has the same value for the uncompressed state as well as all phases of compression.)

Following the same modelling steps as in Section 4.3, apart from the method used to obtain a value for  $d_{\parallel 0}$ , again leads to equation (4.33) as an expression of the permeability in terms of the dimensions of the two-strut fibre RRUC. The crucial choice of the dimensions of the RRUC is as previously discussed: The side length parallel to the streamwise direction

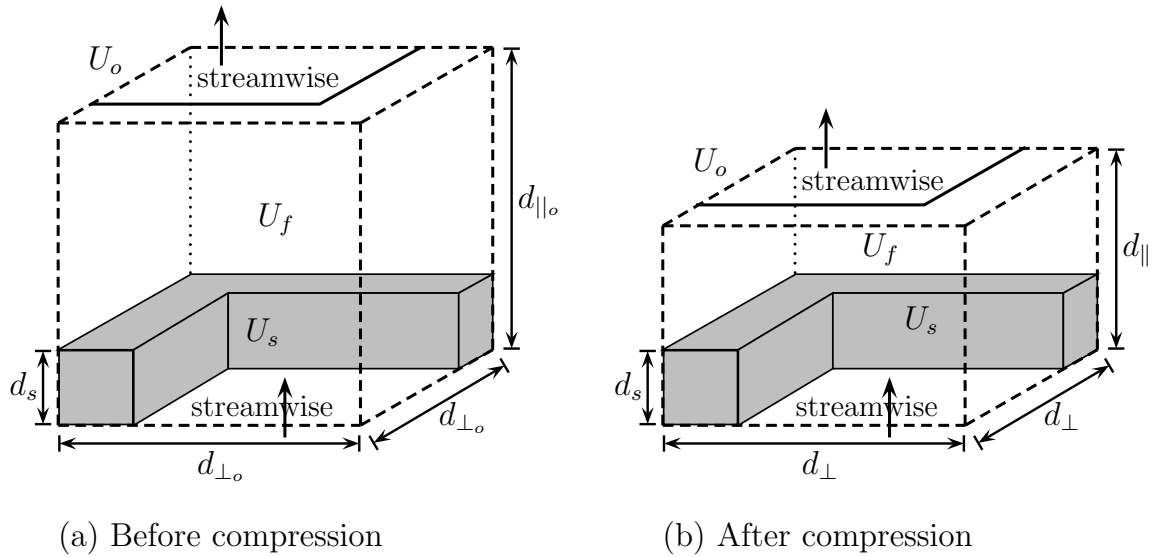


**Figure 5.5:** Two-strut fibre RRUC model (a) before and (b) after compression.

is given by  $(e d_{\parallel_0})$  and  $d_s$  is equated to the average diameter of the fibres of the porous medium. The side length perpendicular to the streamwise direction, in terms of  $d_{\parallel_0}$ , is given by

$$d_{\perp} = \frac{d_s \left( d_s + \sqrt{(d_s)^2 + e d_{\parallel_0} d_s (\epsilon - 1)} \right)}{e d_{\parallel_0} (1 - \epsilon)}. \quad (5.21)$$

Based on equation (5.20), for the chosen geometric model visualized in Figure 5.5,  $d_{\perp}$  is determined only by the values of  $d_s$ ,  $d_{\parallel_0}$  and  $\epsilon_0$  and is therefore constant for a given fibrous porous medium:

$$d_{\perp} = \frac{d_s \left( d_s + \sqrt{(d_s)^2 - (1 - \epsilon_0) d_{\parallel_0} d_s} \right)}{(1 - \epsilon_0) d_{\parallel_0}}. \quad (5.22)$$

The concept of porosity as an indicator of the void volume to total volume ratio of the porous medium will be employed in determining a value for  $d_{\parallel_0}$ . The porosity of a medium is a macroscopic parameter which, up until now, was represented in the RRUC as a void volume to total volume ratio. Due to the choice of geometry of the RRUC the solid material is not spread uniformly throughout the RRUC. In order to determine the dimensions of the two-strut fibre RRUC representing the uncompressed state of the fibrous porous medium, a choice is made that the top- and side views of the RRUC must both display the same void-total ratio (based on areas) as the corresponding volume ratio. This choice is based on the assumption that the porosity in the corresponding REV will be reflected in the (hypothetical) cross-sectional areas of the corresponding REV. The top- and side views (not drawn to scale) are shown in Figure 5.6.

In terms of the dimensions of the RRUC representing the uncompressed state of the medium, the mathematical expression for the choice that the top- and side-views must

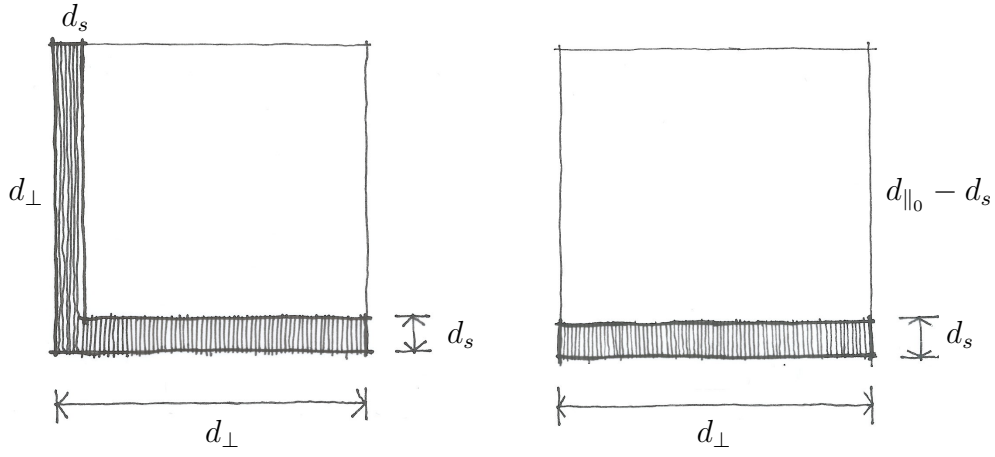


**Figure 5.6:** Top view (left) and side view (right) of the two-strut fibre RRUC for the uncompressed state ( $e=1$ ).

have the same void-total ratio (based on area) is:

$$\frac{d_{\parallel 0} d_{\perp} - d_{\perp} d_s}{d_{\parallel 0} d_{\perp}} = \frac{(d_{\perp})^2 - (2d_{\perp} d_s - (d_s)^2)}{(d_{\perp})^2}, \quad (5.23)$$

which can be written as:

$$d_{\parallel 0} = \frac{(d_{\perp})^2}{2d_{\perp} - d_s}. \quad (5.24)$$

The mathematical expression for the porosity of the medium in the uncompressed state i.e.,

$$\epsilon_0 = \frac{(d_{\perp})^2 d_{\parallel 0} - 2(d_s)^2 d_{\perp} + (d_s)^3}{(d_{\perp})^2 d_{\parallel 0}}, \quad (5.25)$$

can be written as

$$\begin{aligned} (d_{\perp})^4 (\epsilon_0 - 1) + 2(d_s)^2 d_{\perp} (2d_{\perp} - d_s) - (2d_{\perp} - d_s)(d_s)^3 &= 0 \\ (\epsilon_0 - 1)(d_{\perp})^4 + 4(d_s)^2 (d_{\perp})^2 - 4d_{\perp} (d_s)^3 + (d_s)^4 &= 0, \end{aligned} \quad (5.26)$$

after combining it with equation (5.24). For the present context ( $d_s = 2.7 \mu\text{m}$  and  $\epsilon_0 = 0.94$ ), the applicable solution to the simultaneous equations (5.24) and (5.25) is  $d_{\perp} = 20.6 \mu\text{m}$  and  $d_{\parallel 0} = 11 \mu\text{m}$ .

In terms of  $d_{\parallel 0}$  and the compression fraction the permeability can then be expressed as

$$k = \frac{d_{\parallel 0} e (d_{\perp} - d_s)^4 (d_{\parallel 0} e - d_s)^2}{24 d_s (d_{\perp})^2 (d_{\parallel 0} e - d_s)^2 + 12 d_s d_{\perp} (2d_{\perp} - d_s) (d_{\perp} - d_s)^2}, \quad (5.27)$$

with  $d_{\perp}$  a constant for a specific porous medium (equation (5.22)) which in this context is  $20.6 \mu\text{m}$ . The permeability can therefore be expressed as a function of the mean diameter of the fibres, the compression fraction and  $d_{\parallel 0}$ . Implicitly the permeability is a function of the porosity in the uncompressed state since  $d_{\parallel 0}$ ,  $d_{\perp}$  and  $e$  are functions thereof.

The two-strut fibre RRUC model associated with determining  $d_{\parallel 0}$  through this method will be referred to as the two-strut alternative  $d_{\parallel 0}$  fibre RRUC model.

Permeability ( $\mu\text{m}^2$ ) (General non-linear $e - \epsilon$ relationship)				
Experiment	two-strut RRUC	% error	two-strut alternative $d_{\parallel 0}$ RRUC	% error
8.2	4.2	-49	7.7	-6.1
2.0	1.3	-35	2.9	45
1.4	0.29	-77	0.79	-44
0.17	0.06	-65	0.24	41

**Table 5.3:** Relative percentage error in the permeability prediction of the two-strut- and two-strut alternative  $d_{\parallel 0}$  fibre RRUC models. (General non-linear relationship between  $e$  and  $\epsilon$ .)

Again it must be emphasized that the accuracy of the measurement of the porosity in the uncompressed state is crucial.

It is clear from Table 5.3 that the general non-linear relationship in combination with employing the hydraulic diameter to determine  $d_{\parallel 0}$ , does not perform as well as when  $d_{\parallel 0}$  is determined through the void-total-area ratio concept.

As is evident from Table 5.3 and Figure 5.7, the permeability prediction capability of the two-strut alternative  $d_{\parallel 0}$  fibre RRUC model is reasonable. When the porosity in the uncompressed state is the determining factor for obtaining the value of  $d_{\parallel 0}$  and not the hydraulic diameter, the accuracy of the permeability prediction is highly influenced by the accuracy of the porosity value for the uncompressed state of the fibrous porous medium.

An overview of the percentage differences relative to the set of experimental values obtained by Le Coq (2008) will be given in Chapter 7, as a basis for conclusions and recommendations. In Chapter 6 the prediction capability of the alternative  $d_{\parallel 0}$  fibre RRUC model will be investigated for other fibrous porous media by employing data sets from Akaydin et al. (2011) and Jackson & James (1986).

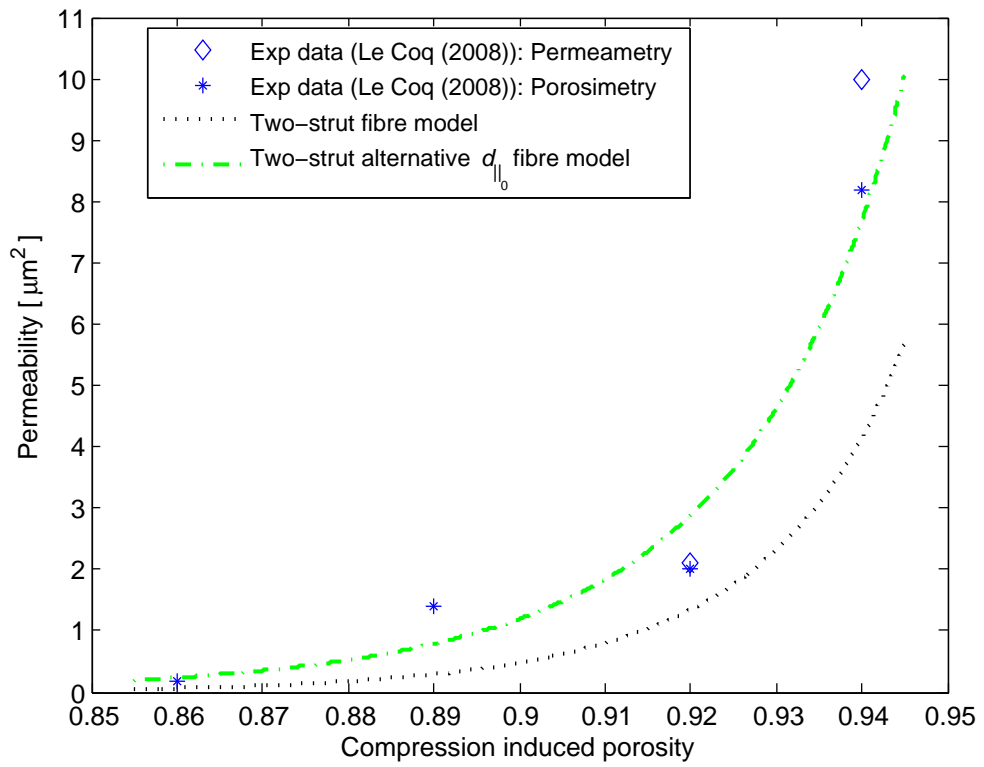


**Figure 5.7:** Permeabilities predicted by the two-strut- and two-strut alternative  $d_{||0}$  fibre RRUC models. (General non-linear relationship between  $e$  and  $\epsilon$ .)

# Chapter 6

## Model validation

Data regarding the hydraulic diameter and porosity values for compressed states of the fibrous porous medium, formed an essential part of the modelling process discussed thus far. An alternative method for determining the dimensions of the two-strut fibre RRUC was introduced in Section 5.3 and will be employed in the permeability prediction process for soft porous media. Although the model is developed with the specific aim of predicting the influence of compression on the permeability of a fibrous porous medium, evidence will be provided that the model has, in addition, the potential for predicting the permeability of anisotropic fibrous porous media.

### 6.1 Soft fibrous porous medium

The characterization of the structural parameters for the soft fibrous porous medium, investigated by Akaydin et al. (2011), was not done with the aid of mercury porosimetry or image analysis. In addition, experimental data regarding the hydraulic diameter and porosities corresponding to different levels of compression were also not provided. As was discussed in Section 3.3.2, the porosity of the medium in the uncompressed state was determined ( $\epsilon_0 = 0.9968$ ) and the porosities at different levels of compression were calculated from the relationship between the compression ratio and porosity. The average fibre diameter in this context is 10  $\mu\text{m}$ .

Therefore, an analytical model prediction for the permeability must be obtained without employing the hydraulic diameter of the porous medium in question. The general non-linear relationship has to be employed, which, for the porous medium in question (Akaydin et al. (2011)) is given by:

$$\epsilon = \frac{e - (1 - 0.9968)}{e}. \quad (6.1)$$

Based on the same set of assumptions and constraints regarding the fluid and the flow regime made explicit thus far, the two-strut alternative  $d_{||0}$  fibre RRUC model will be used in predicting the effect of compression on the permeability of a soft fibrous porous medium.

The same modelling steps as in Section 5.3 will be followed with  $d_s = 10 \mu\text{m}$ , referring to the geometry visualized in Figures 5.5 and 5.6. The solution to the simultaneous equations (5.24) and (5.25) that is applicable in the current context is  $d_{\perp} = 348.5 \mu\text{m}$  and  $d_{\parallel_0} = 176.8 \mu\text{m}$ .

Equation (5.27) was used to predict the permeability corresponding to the respective compression fractions. The porosity values corresponding to the compression fraction values were calculated with the aid of equation (6.1). The results are presented in Table 6.1 and Figure 6.2.

To investigate the prediction capability of the two-strut alternative  $d_{\parallel_0}$  fibre RRUC model in combination with the solid geometry reflected in Figure 5.3, the modelling steps as set out in Section 5.3 are again followed with  $d_s = 10 \mu\text{m}$ .

For this choice of solid geometry the simultaneous equations, with  $e = 1$  and reference to Figure 6.1, are:

$$d_{\parallel_0} = \frac{\sqrt{2} (d_{\perp})^2}{\sqrt{2} d_{\perp} - \frac{1}{2} d_s} \quad (6.2)$$

and

$$\epsilon_0 = \frac{(d_{\perp})^2 d_{\parallel_0} - 2(d_s)^2 d_{\perp} + \frac{1}{\sqrt{2}} (d_s)^3}{(d_{\perp})^2 d_{\parallel_0}}. \quad (6.3)$$

It then follows that

$$(\epsilon_0 - 1)(d_{\perp})^4 + 2(d_s)^2 (d_{\perp})^2 - \sqrt{2} d_{\perp} (d_s)^3 + \frac{1}{4} (d_s)^4 = 0. \quad (6.4)$$

The applicable solution to the simultaneous equations is  $d_{\perp} = 246 \mu\text{m}$  and  $d_{\parallel_0} = 250 \mu\text{m}$ .

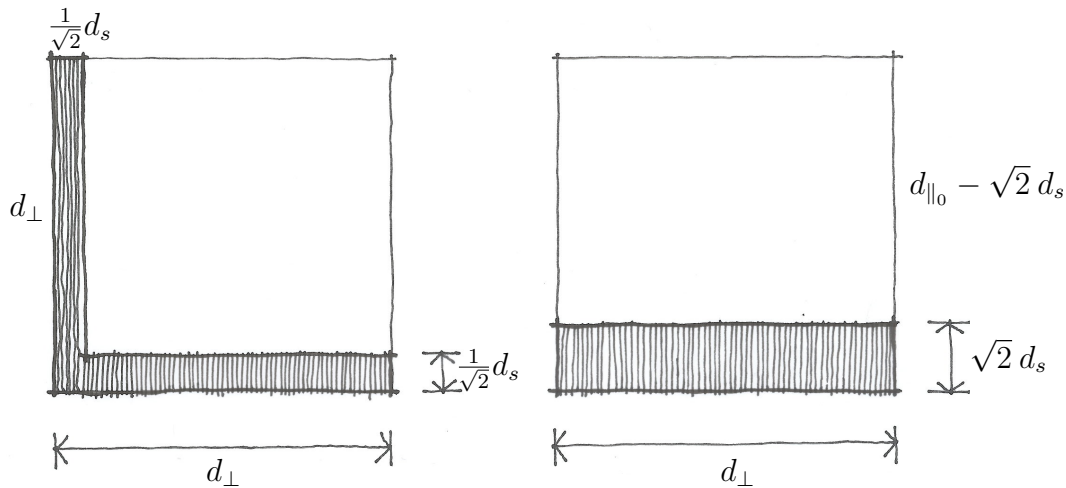


**Figure 6.1:** Top view (left) and side view (right) of the two-strut  $\sqrt{2e}$  fibre RRUC for the uncompressed state ( $e=1$ ).

The permeability is expressed by equation (5.16) with  $d_{\perp} = 246 \mu\text{m}$  and  $d_{\parallel} = 250 e$ .

In Figure 6.2 the permeability prediction of the two-strut alternative  $d_{\parallel_0}$ - and the two-strut  $\sqrt{2e}$  alternative  $d_{\parallel_0}$  fibre RRUC models for a soft porous medium are compared with



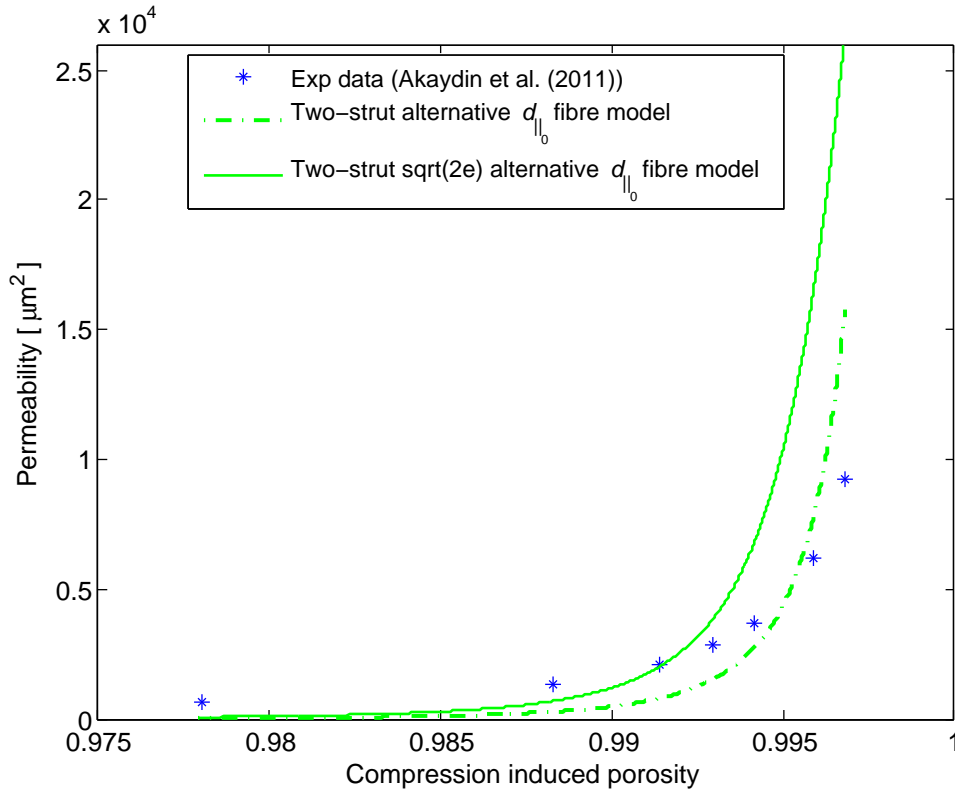


**Figure 6.2:** Permeabilities predicted by the two-strut alternative  $d_{||_0}$ - and the two-strut sqrt(2e) alternative  $d_{||_0}$  fibre RRUC models for a soft porous medium. (General non-linear relationship between  $e$  and  $\epsilon$ .)

the experimental permeability values obtained by Akaydin et al. (2011). The percentage differences calculated with respect to the experimental data are given in Table 6.1.

The permeability prediction of the two-strut alternative  $d_{||_0}$  fibre RRUC model reflects a stronger trend of under-prediction than the two-strut sqrt(2e) alternative  $d_{||_0}$  fibre RRUC model. Both these models are dependent on the accuracy of the experimental value obtained for the porosity in the uncompressed state. Nevertheless, the models are adequate for a first order prediction of permeability if the porosity is accurately determined.

In the analytical model presented by Woudberg (2012a), the inertial effects in the Forchheimer flow regime have been incorporated to highlight the contribution thereof on the prediction efficiency of the three-strut fibre model. This will not be done for the two-strut model when comparing the results to those of Akaydin et al. (2011). Future work may include the adaption of the model to include the effects of developing flow.

Increasing the thickness of a porous medium does not influence the solidity (SVF) of the medium (e.g. Zobel et al. (2007)). The results from Akaydin et al. (2011) confirm the fact that permeability data does not depend on the initial uncompressed sample length of the porous medium. Caution is therefore appropriate in any modelling process, as is evident in the current context: Employing the given original height of the porous medium to determine  $d_{||_0}$  may accidentally lead to dimensions of the two-strut RRUC which provide reasonable permeability predictions whilst a different height could have led to an inappropriate value for  $d_{||_0}$ .

Permeability ( $\mu\text{m}^2$ )				
Two-strut fibre RRUCs (General non-linear $e - \epsilon$ relationship.)				
Exp.	2-strut alt $d_{\parallel 0}$ RRUC	% error	2-strut sqrt(2e) alt $d_{\parallel 0}$ RRUC	% error
9220	15740	71	26406	186
6170	7912	28	16720	171
3720	2695	-28	6724	81
2820	1520	-46	3870	37
2110	799	-62	2023	-4.1
1340	277	-79	684	-49
620	25	-96	69	-89

**Table 6.1:** Relative percentage error in the permeability prediction of the two-strut alternative  $d_{\parallel 0}$ - and the two-strut sqrt(2e) alternative  $d_{\parallel 0}$  fibre RRUC models for a soft porous medium. (General non-linear relationship between  $e$  and  $\epsilon$ .)

## 6.2 Data sets from Jackson & James (1986)

A different scenario could be where available data regarding fibrous porous media only include the fibre diameter and porosities (or solid-volume fractions) corresponding to different levels of compression. No values for the compression fractions or -factors are available and the type of compression is also not described. In this case the two-strut alternative  $d_{\parallel 0}$  fibre RRUC model can also be utilized, but in a different manner. As a result, no relationship between the compression fraction and porosity will be employed. If the porosity in a certain compressed state is known, the corresponding dimensions of the RRUC representing the fibrous porous medium in that state will be calculated by solving the simultaneous equations

$$d_{\parallel} = \frac{(d_{\perp})^2}{2d_{\perp} - d_s} \quad (6.5)$$

and

$$\epsilon = \frac{(d_{\perp})^2 d_{\parallel} - 2(d_s)^2 d_{\perp} + (d_s)^3}{(d_{\perp})^2 d_{\parallel}}, \quad (6.6)$$

referring to Figure 6.3. (Note that the views are not drawn to scale.)

The permeability at each level of compression is then predicted by substituting the values of the dimensions of the two-strut fibre RRUC, representing the porous medium in that state, into equation (4.33). For the sake of clarity, this model will be referred to as the two-strut general alternative  $d_{\parallel 0}$  fibre RRUC model.

Jackson & James (1986) reported data produced by Ingmanson and co-authors on glass fibres with a radius of 0.082 mm and nylon fibres with a radius of 0.0965 mm. The data will be compared to the permeability prediction of the two-strut general alternative  $d_{\parallel 0}$

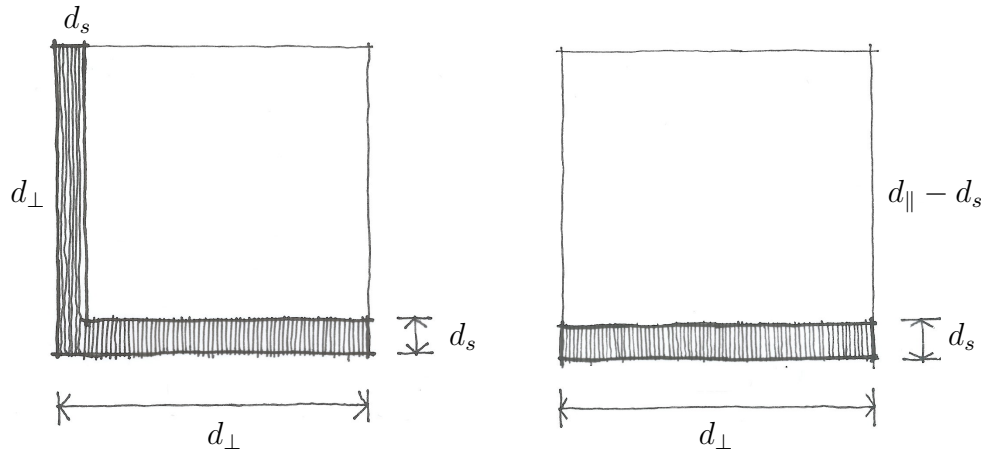


**Figure 6.3:** Top view (left) and side view (right) of the two-strut general alternative  $d_{||0}$  fibre RRUC.

fibre RRUC model. The dimensionless permeability provided by Jackson & James (1986) is multiplied by the square of the given radius to obtain permeability dimensions in  $\text{mm}^2$ . Since the choice was made in the modelling process to equate the length  $d_s$  to the fibre diameter, the corresponding values for  $d_s$  were calculated by multiplying the given radii by 2.

For the sake of completeness and comparison between the two-strut- and three-strut fibre models, the permeability prediction of the three-strut fibre model is also shown in Figures 6.4 and 6.5. For comparison purposes the porosity range on the horizontal axis is the same in both graphs (glass- and nylon fibres).

Predictions within the correct order of magnitude were obtained via the two-strut general alternative  $d_{||0}$  fibre RRUC model. The percentage difference between the experimental values and the values predicted by the analytical model ranges from -8.5% to -52%. For the nylon fibres the percentage difference ranges from -22% to -51%. The permeability prediction of the two-strut general alternative  $d_{||0}$  fibre RRUC model shows a trend of under-prediction.

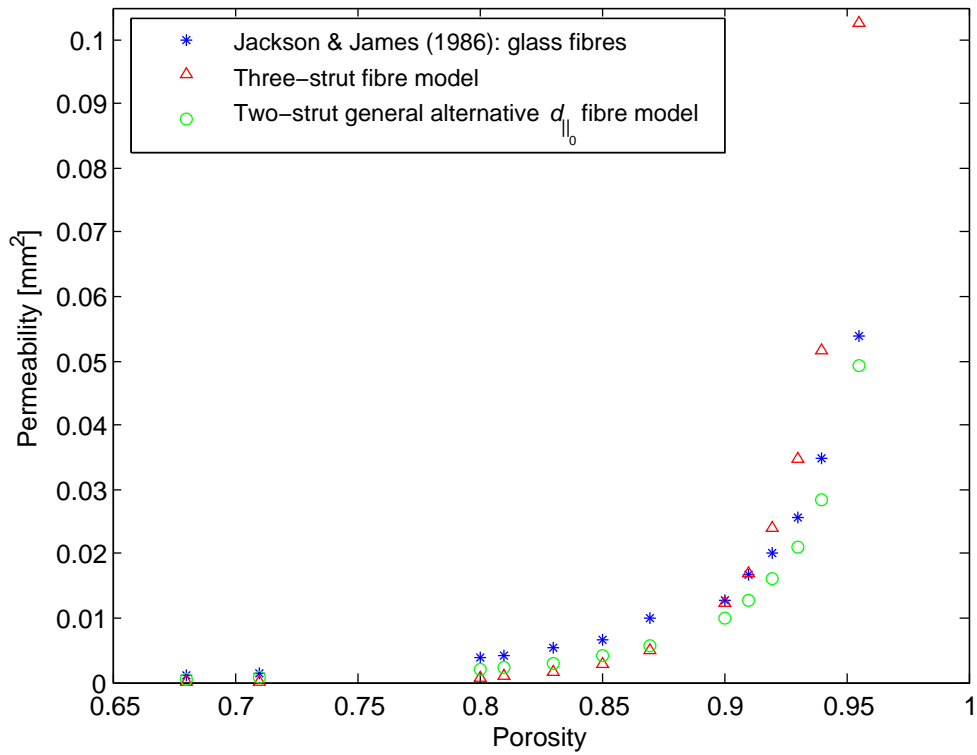


**Figure 6.4:** Permeability predictions of the three-strut- and two-strut general alternative  $d_{||_0}$  fibre RRUC models for glass fibres with radius 0.082 mm.

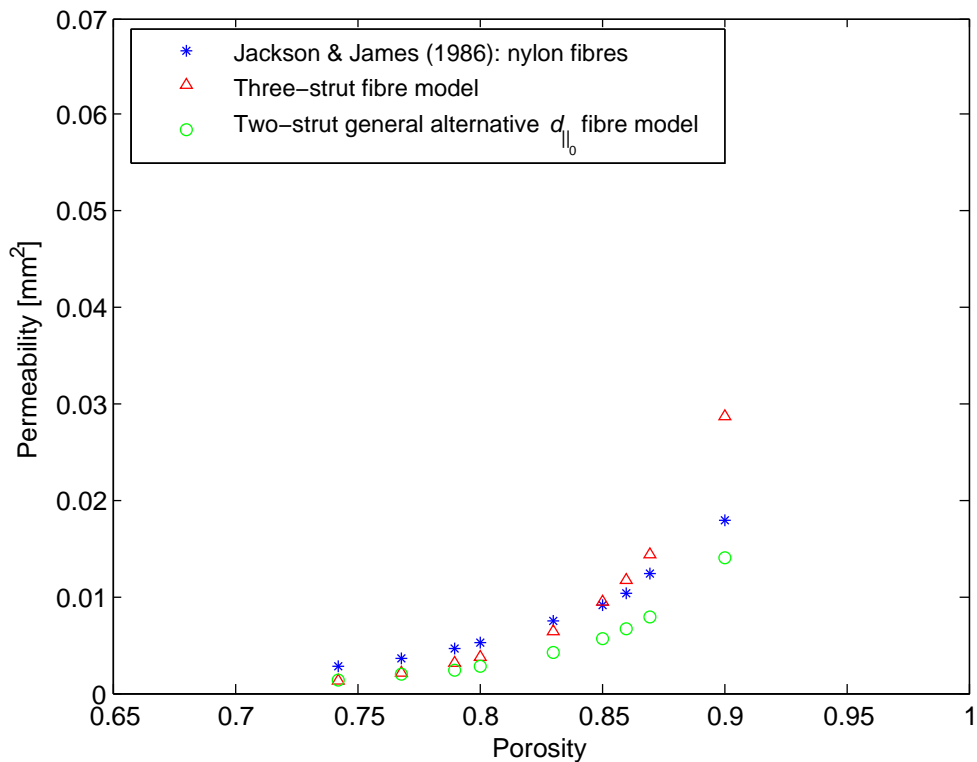


**Figure 6.5:** Permeability predictions of the three-strut- and two-strut general alternative  $d_{||_0}$  fibre RRUC models for nylon fibres with radius 0.0965 mm.

The prediction capability (in terms of relative percentage errors) of the two-strut general alternative  $d_{\parallel_0}$  fibre RRUC model for fibrous porous media of different fibre radii is given in Table 6.2. In this case the fibrous porous media are anisotropic but not compressed. Again the dimensionless permeability provided by Jackson & James (1986) is multiplied by the square of the given radius to obtain permeability dimensions in  $\text{mm}^2$ .

Permeability ( $\text{mm}^2$ )				
Type	Radius (mm)	Exp.	2-strut gen. alt. $d_{\parallel_0}$ RRUC	% error
Nylon	$9.65 \times 10^{-2}$	$1.8 \times 10^{-2}$	$1.4 \times 10^{-2}$	-22
Glass	$8.2 \times 10^{-2}$	$5.4 \times 10^{-2}$	$4.9 \times 10^{-2}$	-9
Glass	$3.9 \times 10^{-5}$	$7.2 \times 10^{-10}$	$2.4 \times 10^{-10}$	-67
Glass	$7.2 \times 10^{-5}$	$2.1 \times 10^{-9}$	$1.1 \times 10^{-9}$	-48
Nylon	$1.2 \times 10^{-3}$	$1.4 \times 10^{-6}$	$7.5 \times 10^{-7}$	-46

**Table 6.2:** Relative percentage errors in the permeability prediction of the two-strut general alternative  $d_{\parallel_0}$  fibre RRUC model for anisotropic fibrous porous media of different radii.

Although the two-strut general alternative  $d_{\parallel_0}$  fibre RRUC model shows a general trend of under-prediction, the percentage errors indicate that over a wide range of radii and permeabilities this model can be employed for first order approximations.

# Chapter 7

## Conclusions and future work

In this chapter conclusions regarding the present study are drawn and a comparative summary is given, followed by future work.

### 7.1 Conclusions

An analytical geometric model for predicting the effect of compression on the permeability of an unconsolidated fibrous porous medium was presented. It serves as a basis for predictions suitable for the exploratory phases of new applications. A first order prediction of the permeability of a fibrous porous medium subject to compression (for flow within the Darcy regime) can be obtained by solely attributing pressure losses to shear stresses and remodelling the geometric micro-structure.

All the models reflect the significant influence of compression on permeability. The model prediction of the existing three-strut fibre model was improved by employing alternative compression-porosity relationships. The prediction capability of the newly proposed initial two-strut model was improved by refining the mathematical relation between the compression fraction and the porosity. Optimal preference could not be given to any of the proposed models since the choice in model depends strongly on the compression fraction - porosity relationship. The compression fraction - porosity relationship in turn depends on which measured parameters are provided (i.e. the porosity-, compression fraction and/or hydraulic diameter values). The type of fibrous porous medium (e.g. glass, nylon, polyester) may influence the solid representation within the two-strut fibre RRUCs since different types of fibres could distribute in different manners when compressed.

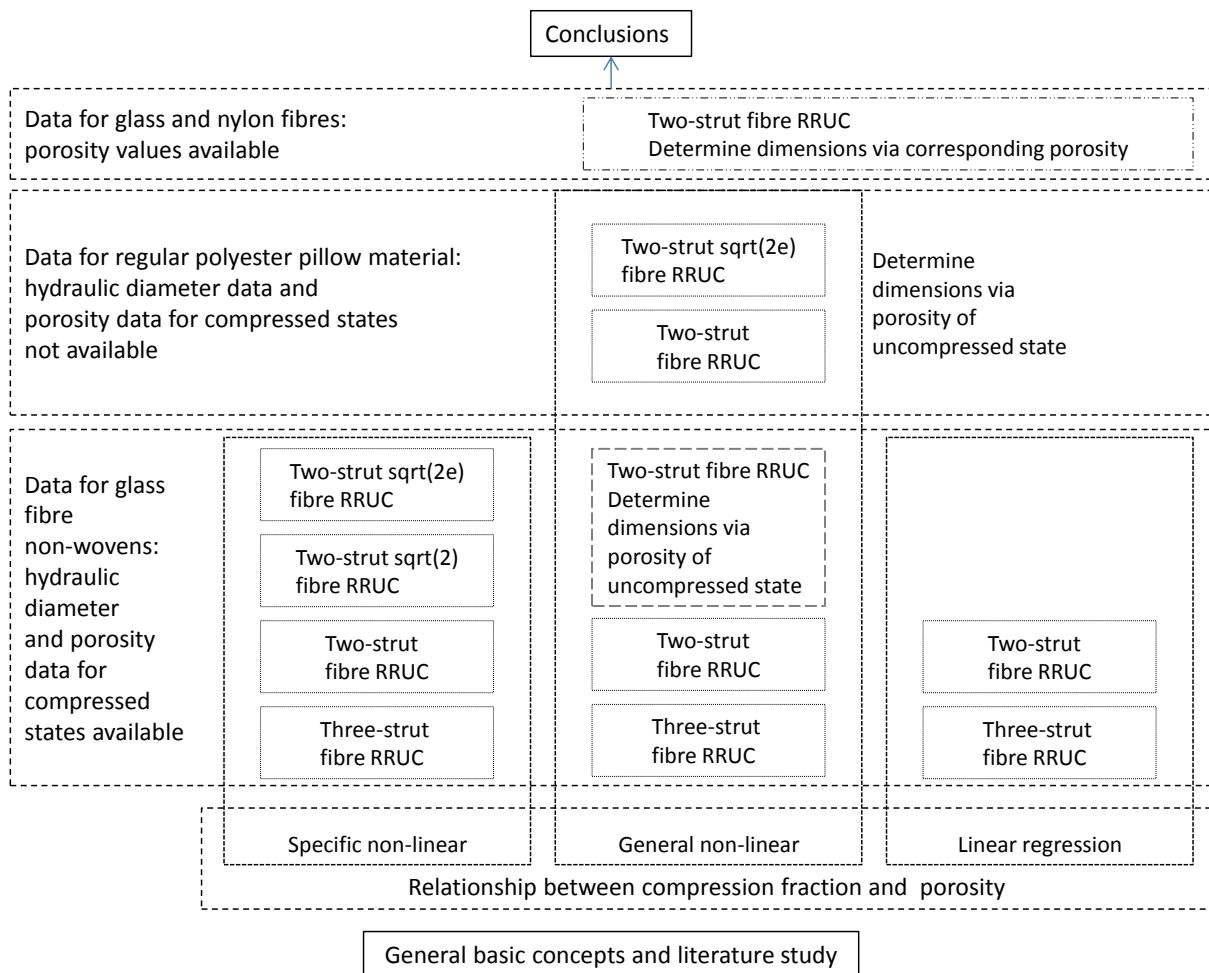
It is evident from the range in relative percentage differences in the permeability prediction of the proposed models that balancing mathematical simplicity with prediction capability is viable. Discrepancies may be attributed to different assumptions made (and consequently different equations) in the different contexts. Examples hereof are: The underlying assumption of mercury porosimetry that the porous medium can be characterized as a set of cylindrical, straight capillaries versus the rectangular geometry of the two-strut fibre RRUC; the equations used by Le Coq (2008) for obtaining the permeability from

the structural data differs from those employed in the analytical models of the present study and, the experimental methods used to determine the porosity versus the values obtained via a chosen relationship (as was done in the present modelling procedure). Critical aspects thus include the method with which the hydraulic diameter is experimentally obtained in combination with the definition there-of in the RRUC context; the mathematical approaches applied in determining the permeability as well as the accuracy of the porosity measurements.

Further discrepancies may be a result of comparing variables that were obtained in different manners and are in a sense not ‘the same’ variable. For instance, to obtain permeability values related to different compression ratios, Akaydin et al. (2011) measured the pressure and velocities at different points in the medium and calculated the permeability with Darcy’s law. The permeability values to be compared with these values must then also be obtained under the assumptions related to Darcy’s law (velocity independent permeability) otherwise two ‘different’ permeability definitions are compared. Le Coq (2008), on the other hand, determined the permeability coefficient from structural parameters.

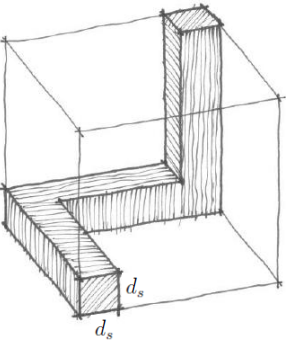
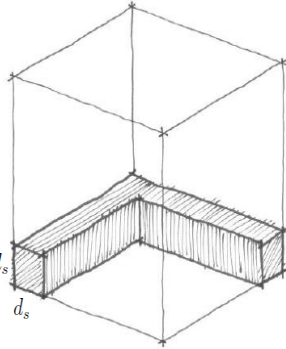
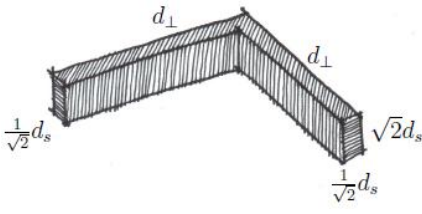
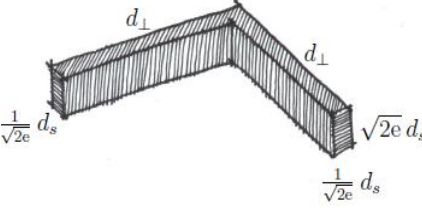
The prediction capability is highly sensitive to the accuracy of the porosity in the uncompressed state, as was also observed by e.g. Akaydin et al. (2011). It is also significantly influenced by the representation of the porosity of the porous material in the uncompressed state through the dimensions of the geometric model (e.g. the value of  $d_{||0}$ ).

Figure 7.1 gives an outline of the structure of the thesis. The effect of parameter change on the prediction capability of the proposed models is summarized in Figure 7.2 through comparison of the percentage difference relative to the experimental values obtained by Le Coq (2008) i.e. a single data set.



**Figure 7.1:** Overview of the investigation into the effect of compression of a fibrous porous medium on the permeability thereof.



Solid Geometry	Relationship between compression fraction and porosity	Method for determining $d_{  0}$	Difference in permeability prediction relative to the experimental values 8.2; 2.0; 1.4; 0.17			
	Linear regression	Hydraulic diameter and porosity data for different levels of compression	-34%	65%	7%	200%
	General non-linear		-32%	0%	-65%	-24%
	Specific non-linear		1.2%	60%	-34%	76%
	Linear regression	Hydraulic diameter and porosity data for different levels of compression	-51%	25%	-29%	88%
	General non-linear		-49%	-35%	-79%	-65%
	Specific non-linear		-19%	20%	-56%	0%
	General non-linear	Ratio of void to total area of the top- and side views	-6.1%	45%	-44%	41%
	Specific non-linear	Hydraulic diameter and porosity data for different levels of compression	0%	35%	-63%	-59%
	Specific non-linear	Hydraulic diameter and porosity data for different levels of compression	-6.1%	30%	-54%	24%

**Figure 7.2:** Overview of the relative percentage difference between the permeability predictions of the proposed models and the experimental values obtained by Le Coq (2008).

Equation (5.16) can be generalized by introducing the coefficient  $\alpha$  which serves as a solid distribution parameter, reflecting the average relative solid distribution of the type of fibrous porous medium in question. The permeability prediction is based on the geometric model in Figure 4.2. The general solid is reflected in Figure 7.3 and the top- and side views (not drawn to scale) are shown in Figure 7.4. The generalized equation for the permeability prediction is given by:

$$k = \frac{e d_{\parallel 0} (e d_{\parallel 0} - \sqrt{\alpha e} d_s)^2 \left(d_{\perp} - \frac{1}{\sqrt{\alpha e}} d_s\right)^4}{24 \sqrt{\alpha e} d_s (d_{\perp})^2 (e d_{\parallel 0} - \sqrt{\alpha e} d_s)^2 + 6 \left(4 \frac{1}{\sqrt{\alpha e}} d_s (d_{\perp})^2 - 2 \frac{1}{\alpha e} (d_s)^2 d_{\perp}\right) \left(d_{\perp} - \frac{1}{\sqrt{\alpha e}} d_s\right)^2} \quad (7.1)$$

with  $\alpha$  the solid distribution parameter and  $e$  the compression fraction.

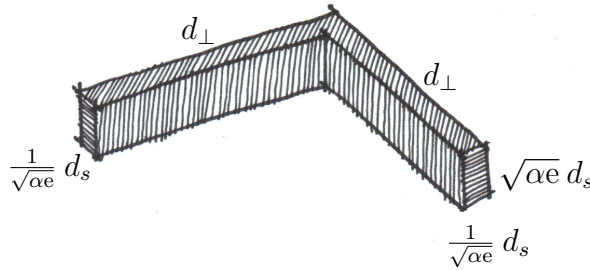


**Figure 7.3:** Solid with dimensions  $d_{\perp}$ ,  $\frac{1}{\sqrt{\alpha e}} d_s$  and  $\sqrt{\alpha e} d_s$  for the general two-strut fibre RRUC model.

The solid distribution parameter (also in combination with  $e$ ) reflect the ratio of the sides producing a cross-sectional area of  $(d_s)^2$  and, in mathematical terms, may be any positive number. In combination with  $e$ , the solid distribution parameter represents the *manner in which fibres, and therefore surface areas, are re-distributed* under uni-axial compression. (Although in the present context there is no fibre deformation, this can also be a cause for surface area redistribution under compression.) For a certain fibrous porous medium the solid distribution parameter is a constant which, in combination with the geometry of the two-strut fibre RRUC and porosity, represent/reflect the ratio of fluid-solid interfaces in the directions perpendicular and parallel to the streamwise direction. If it is assumed that compression of a certain fibrous porous medium does not influence the solid distribution in the same manner as it influences the void volume, the compression fraction,  $e$ , should not be incorporated in the side lengths involving  $d_s$ .

When hydraulic diameter- and porosity data are available for the uncompressed- and one or more compressed states of the porous medium, the best prediction results (for glass fibres) are obtained when the dimensions of the two-strut fibre RRUC in the uncompressed state are calculated through the specific non-linear relationship in combination with solid

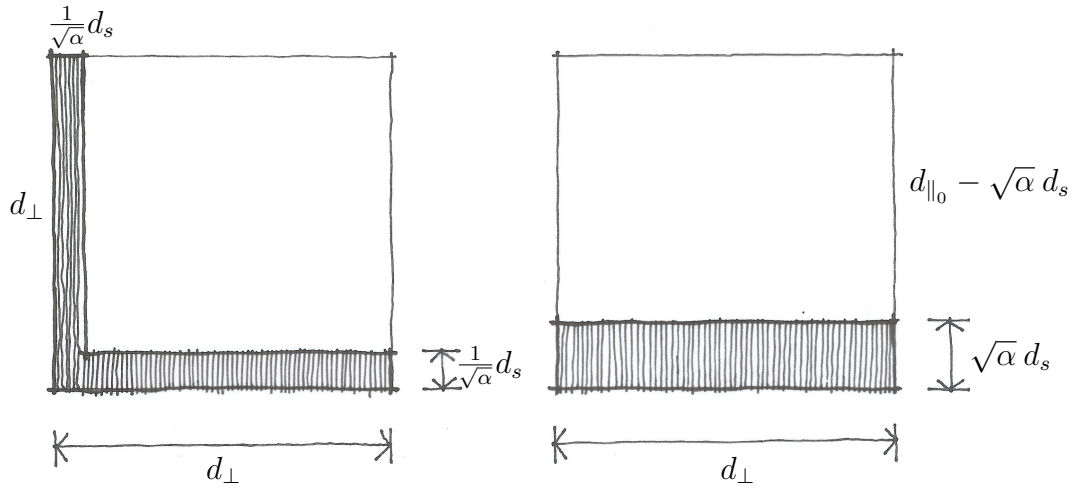


**Figure 7.4:** Top view (left) and side view (right) of the general two-strut fibre RRUC for the uncompressed state ( $e=1$ ).

geometry of side lengths  $d_{\perp}$ ,  $d_s$  and  $d_s$ . When such data is not available, the dimensions of the two-strut fibre RRUC in the uncompressed state should be calculated by employing  $\epsilon_0$  and solving the (general) simultaneous equations (7.2) and (7.3). With  $e = 1$  and referring to Figure 7.4 the equations

$$d_{\parallel 0} = \frac{\alpha (d_{\perp})^2}{2 d_{\perp} - \frac{1}{\sqrt{\alpha}} d_s} \quad (7.2)$$

and

$$\epsilon_0 = \frac{(d_{\perp})^2 d_{\parallel 0} - 2(d_s)^2 d_{\perp} + \frac{1}{\sqrt{\alpha}} (d_s)^3}{(d_{\perp})^2 d_{\parallel 0}}, \quad (7.3)$$

can, combined, be written as

$$(\epsilon_0 - 1)(d_{\perp})^4 + \frac{4}{\alpha} (d_s)^2 (d_{\perp})^2 - \frac{4}{\alpha \sqrt{\alpha}} d_{\perp} (d_s)^3 + \frac{1}{\alpha^2} (d_s)^4 = 0. \quad (7.4)$$

When the dimensions of the two-strut fibre RRUC in the uncompressed state are calculated by employing only  $\epsilon_0$  and solving for  $d_{\perp}$  and  $d_{\parallel 0}$ , equation (7.1) can in principle be employed to predict the permeability of any fibrous porous medium in an uncompressed state ( $e = 1$ ). The dimensions of the two strut fibre RRUC corresponding to the porosity is determined and consequently the permeability can be predicted.

The streamwise side length (representing a compressed state) can be regarded as a function of the compression fraction only if it is known that the compression was uni-axial and static. If information regarding the compression process is not known, the assumption that  $d_{\parallel} = e d_{\parallel 0}$  must be revisited.

As mentioned by Jaganathan et al. (2009), many studies are based on over-simplified (and/or sometimes unrealistic) assumptions. The fact that fibrous porous media is in general not homogeneous and/or isotropic and have different degrees of in-plane and/or

through plane inhomogeneities are often put aside for the sake of simplicity. In line with this, it is evident from the present study that mathematical simplicity has its place in analytical modelling processes if the awareness of the consequences of assumptions is evident.

## 7.2 Future work

It was shown in this study that the proposed models are geometrically as well as mathematically adaptable. The models may thus furthermore be adapted and refined in the following manners:

- Inclusion of the application of the general definition of the hydraulic diameter for porous media in the two-strut fibre RRUC model.
- Incorporation of the effect of developing flow could be investigated by introducing appropriate apparent friction factors in the pressure drop prediction of the proposed analytical model.
- Accounting for anisotropy is an essential new feature of the two-strut fibre RRUC and could be refined. Although the model was developed with the aim of investigating the effect of compression on a fibrous porous medium, it shows a reasonable first order permeability prediction capability for anisotropic fibrous porous media.
- The model was developed for a fibrous porous medium but it could be investigated whether the solid geometry in combination with the idea of a solid distribution variable could not be extended to other unconsolidated porous structures.
- Tortuosity was not explicitly incorporated in the present two-strut fibre RRUC model (and its modifications) and may be investigated in the future.
- Accounting for slip-flow in combination with a stochastic approach may also be a subject for further study.
- Applying the newly developed two-strut model, in combination with the solid distribution parameter, to liquid flow through fibrous porous media.
- Combining the solid distribution parameter with the compression fraction provides a parameter for solid *re*-distribution. This may be extended to contexts of fibre deformation under compression.

# Appendix A

## General fluid flow concepts

The **fundamental governing equations** of fluid dynamics, namely the *continuity*, *momentum* and *energy equations* can be obtained in various different forms. Anderson, Jr (1995) states the importance of the difference between the finite control volume approach which directly leads to fluid-flow equations in integral form and the infinitesimally small element approach which directly leads to fluid-flow equations in partial differential equation form. When describing fluid flow using a control volume or an infinitesimally small element (which is fixed in space with the fluid moving through it), the so-called *conservation* form of the governing equations are obtained. The *non-conservation* form of the governing equations are obtained when the control volume move with the fluid (then often referred to as a material volume), or when the infinitesimal fluid element moves along a streamline with the velocity equal to the local flow velocity at each point. Worster (2009) refers to the conservation form of the governing equations as an Eulerian description of fluid flow and to the non-conservation form as a Lagrangian description of fluid flow.

The **continuity equation**,

$$\frac{\partial \rho}{\partial t} + \nabla \cdot (\rho \underline{v}) = \frac{\partial \rho}{\partial t} + \underline{v} \cdot \nabla \rho + \rho \nabla \cdot \underline{v} = 0, \quad (\text{A.1})$$

expresses the physical principle that mass is conserved.

The **Navier-Stokes (momentum) equations**, expressing the conservation of momentum (representing Newton's second law not for a fixed-mass system, but a fixed finite volume), in terms of the  $x$ -,  $y$ -, and  $z$ -components within a rectangular Cartesian coordinate system (Anderson, Jr (1995)) are respectively given by:

$$\frac{\partial (\rho u)}{\partial t} + \nabla \cdot (\rho u \underline{v}) = \rho f_x - \frac{\partial p}{\partial x} + \frac{\partial \tau_{xx}}{\partial x} + \frac{\partial \tau_{yx}}{\partial y} + \frac{\partial \tau_{zx}}{\partial z}, \quad (\text{A.2})$$

$$\frac{\partial (\rho v)}{\partial t} + \nabla \cdot (\rho v \underline{v}) = \rho f_y - \frac{\partial p}{\partial y} + \frac{\partial \tau_{xy}}{\partial x} + \frac{\partial \tau_{yy}}{\partial y} + \frac{\partial \tau_{zy}}{\partial z}, \quad (\text{A.3})$$

$$\frac{\partial (\rho w)}{\partial t} + \nabla \cdot (\rho w \underline{v}) = \rho f_z - \frac{\partial p}{\partial z} + \frac{\partial \tau_{xz}}{\partial x} + \frac{\partial \tau_{yz}}{\partial y} + \frac{\partial \tau_{zz}}{\partial z}, \quad (\text{A.4})$$

where the velocity field may be expressed as

$$\underline{v} = u(x, y, z, t) \underline{i} + v(x, y, z, t) \underline{j} + w(x, y, z, t) \underline{k},$$

$f_x, f_y, f_z$ , are the components of the total body force per unit mass (examples are gravitational, electric and magnetic forces),

$p$  is the thermodynamic pressure acting on the surface of a fluid element (Bird et al. (2007)), and

$\tau_{yx}, \tau_{zx}, \tau_{xy}, \tau_{zy}, \tau_{xz}, \tau_{yz}, \tau_{zz}, \tau_{xx}, \tau_{yy}$  are the shear and normal viscous stress components acting on the surface of a fluid element. (The following convention is used:  $\tau_{yx}$  indicates the stress in the  $x$ -direction on a unit area with normal vector in the  $y$ -direction.)

In the late seventeenth century, Isaac Newton stated that the shear stress in a fluid is proportional to the time rate of strain, i.e. velocity gradients. In 1845 Stokes found that for these **Newtonian fluids** the following hold:

$$\begin{aligned} \tau_{xx} &= \lambda (\nabla \cdot \underline{v}) + 2\mu \frac{\partial u}{\partial x}, & \tau_{yy} &= \lambda (\nabla \cdot \underline{v}) + 2\mu \frac{\partial v}{\partial y}, & \tau_{zz} &= \lambda (\nabla \cdot \underline{v}) + 2\mu \frac{\partial w}{\partial z}, \\ \tau_{xy} &= \tau_{yx} &= \mu \left[ \frac{\partial v}{\partial x} + \frac{\partial u}{\partial y} \right], \\ \tau_{xz} &= \tau_{zx} &= \mu \left[ \frac{\partial u}{\partial z} + \frac{\partial w}{\partial x} \right], \\ \tau_{zy} &= \tau_{yz} &= \mu \left[ \frac{\partial w}{\partial y} + \frac{\partial v}{\partial z} \right], \end{aligned} \quad (\text{A.5})$$

where  $\mu$  is the molecular (or dynamic) viscosity coefficient and  $\lambda$  is the second viscosity coefficient (dilatational viscosity). Stokes made the hypothesis that  $\lambda = -\frac{2}{3}\mu$ . (Assuming that the *mean* normal stress is independent of the rate of dilation (Fung (1977)).)

The assumption that the volume (bulk) viscosity  $\lambda + \frac{2}{3}\mu$  is zero is frequently used but has still not been definitely confirmed (Anderson, Jr (1995)). It has some basis in theory only in the case of ideal monatomic gases but has been carried over implicitly to both liquids and gases of all degrees of complexity. One might therefore expect some differences between theoretical predictions and experimental results due to this over-simplification. In most viscous flows the normal stresses,  $\tau_{xx}, \tau_{yy}$  and  $\tau_{zz}$ , are significantly less than the shear stresses and are therefore often neglected.

## Viscosity

Being a measure of a fluid's resistance to flow, viscosity is an important parameter in any investigation regarding fluids in motion. Viscosity is a major factor in determining the prevalent forces during liquid flow e.g. in spraying, injection molding, and surface coating. Barnes (2002) also relates the importance of viscosity to the importance of satisfying and even delighting the end consumer in the areas of foods, personal products as well as household commodities ranging from detergent liquids through paints to greases and oils. Technical requirements such as the clean application of ink in printing need careful control of viscosity. Knowledge of the viscosity is also crucial for sizing pumps, choosing the speed of mixers, etc.

As opposed to non-Newtonian fluids where the viscosity is also a function of the shear rate, the viscosity of Newtonian fluids (stress and strain rate tensors are linearly related (Hughes (1979))) is only a function of temperature and pressure.

The viscosity of simple *liquids* such as water and many oils is a function of the average distance between the constituent molecules, and this in turn depends on the temperature via Brownian thermal energy. The higher the temperature, the greater the distance between molecules; it is therefore easier for them to move past one another and hence the viscosity is lower. The rate at which viscosity decreases with increasing temperature usually depends on the actual viscosity level, such that the viscosity of higher-viscosity liquids decreases faster with increase in temperature than that of lower-viscosity liquids. *Large* changes in pressure are required to produce significant changes in viscosity in these simple liquids. Viscosity normally rises exponentially with pressure, but very large pressures are required to produce any sensible changes. The higher the actual viscosity level, the greater the dependence of viscosity on pressure (Barnes (2002)). Important to mention is the anomaly that the viscosity of water initially *decreases* with increasing pressure (at temperatures below 33 degrees Celsius). (The generally accepted explanation is that pressure reduces the hydrogen-bonded network, which, with the size of the voids between molecules, is responsible for the viscosity. This effect more than compensates for the reduced average inter-molecular distance with increase in pressure.) Although water behaves as a “normal” liquid at even higher pressures, no measurable effect of pressure on the viscosity of water is evident up to about 100 bar. The viscosity of water in the shear rate range of about  $0.01 - 20000 \text{ s}^{-1}$  is independent of shear rate (Barnes (2002)).

Considering the ways in which viscosity can be manipulated for optimum flow properties, it is important to realize that it is usually possible to identify a continuous liquid phase of which the viscosity forms the basis of any subsequent overall viscosity. According to Barnes (2002) this continuous-phase viscosity becomes progressively modified as different materials are dispersed or dissolved into it. Sometimes chemical additives can decrease the viscosity of water by interfering with the hydrogen bonding. Adding ethyl alcohol to water (miscible liquids with almost the same viscosity) produces complex mixture properties and consequently a mixture viscosity very different from the original viscosities. Barnes (2002) gives a detailed description of how viscosity can be manipulated and the role that shear rate (or shear stress) plays in different contexts.

The viscosity of *gases* has a different temperature dependence than that of liquids because gases and liquids have different frictional mechanisms at the molecular level. Intermolecular forces in gases are not as important a factor in viscosity as collisions between the molecules. An increase in temperature increases the number of collisions, thus increasing the viscosity. A striking result of the kinetic theory of gases is that the viscosity of a gas is (roughly) independent of the density of a gas (Fung (1977)). The density does, however, influence the type of dependency of viscosity on temperature.

Viscosity is the principal factor resisting motion in laminar flow. However, when the velocity has increased to the point at which the flow becomes turbulent, pressure differences resulting from eddy currents, rather than viscosity, provide the major resistance to motion. Shah & London (1978) state that flow is laminar when the velocities are free of macroscopic fluctuations at any point in the flow field. The terms viscous flow and

laminar flow are often used as synonyms but under certain conditions viscous flow may become turbulent.

## Reynolds number

By a procedure of dimensional analysis (based on Fourier's *principle of dimensional homogeneity*) a phenomenon may be expressed as a relationship amongst a set of variables that forms a *dimensionless group* (Bear (1988)). A system (experimental or analytical) can be scaled up (or down) in such a way that exactly the same flow patterns occur in the original system and the scaled system, by maintaining geometric as well as dynamic similarity between the two systems. Dynamic similarity is maintained if the dimensionless groups in the differential equations and boundary conditions are the same for both systems. Characteristic length, characteristic velocity, etc. are typical 'scaling factors' used to define dimensionless groups for each system (Bird et al. (2007)).

The Reynolds number is an essential non-dimensional (physical) parameter for viscous flows. The same Reynolds number in a model and the (geometrically similar) full-scale prototype, ensures dynamic similarity if only inertial- and frictional forces are assumed to be present (Fung (1977)). The magnitude of the dimensionless group

$$Re \equiv \frac{\rho u_0 l_0}{\mu}, \quad (\text{A.6})$$

with  $u_0$  a characteristic velocity (average system velocity),  $\rho$  the fluid density,  $\mu$  the viscosity of the fluid and  $l_0$  a characteristic length, indicates the relative importance of inertial- and viscous forces in a specific fluid system (Bird et al. (2007)). According to Hughes (1979), for given flow configurations and fluid properties, the Reynolds number depends directly on the magnitude of the fluid velocity.

## Friction factor

In the modelling processes where the influence of developing flow is incorporated, the friction factor - Reynolds number product (**Poiseuille number**) is usually employed. The (dimensionless) **friction factor**,  $f$ , is in general a function of the pipe roughness, pipe diameter, fluid kinematic viscosity, and velocity of flow.

Assuming laminar fully developed flow in a a straight conduit of uniform cross section, with a pressure difference  $\Delta p$  over length  $L$ , a mean velocity of  $u_m$ , a hydraulic radius  $R_h$  and constant fluid density  $\rho$ , the definition of the Fanning friction factor is given by

$$f \equiv \frac{\Delta p}{L} \frac{R_h}{\frac{1}{2}\rho u_m^2}. \quad (\text{A.7})$$

According to Shah & London (1978), the Fanning friction factor for laminar flow in ducts is defined as the ratio of the wall shear stress  $\tau_w$  to the flow kinetic energy per unit volume:

$$f \equiv \frac{\tau_w}{\frac{1}{2}\rho u_m^2}. \quad (\text{A.8})$$

(The  $\equiv$  is used to indicate a choice of definition.)



The value of the Darcy-Weisbach friction factor is 4 times that of the Fanning friction factor since the hydraulic diameter is employed and not the hydraulic radius as in the Fanning friction factor.

When considering developing flow, the pressure drop is related to an *apparent* friction factor which accounts for the pressure drop due to friction as well as the developing region effects. According to Steinke & Kandlikar (2006), the apparent friction factor consists of two components: the friction factor from the theory for fully developed flow and an incremental pressure defect.

# Bibliography

- Akaydin, H., Pierides, A., Weinbaum, S., & Andreopoulos, Y. (2011). Permeability of soft porous media under one-dimensional compaction. *Chemical Engineering science*, *66*, 1–14.
- Anderson, Jr, J. D. (1995). *Computational Fluid Dynamics: The basics with applications*. McGraw-Hill, Inc.
- Bahrami, M., Yovanovich, M., & Culham, J. (2007). A novel solution for pressure drop in singly connected microchannels of arbitrary cross-section. *International Journal of Heat and Mass Transfer*, *50*, 2492–2502.
- Barnes, H. A. (2002). *Viscosity*. The University of Wales Institute of Non-Newtonian Fluid Mechanics.
- Bear, J. (1988). *Dynamics of Fluids in Porous Media*. Dover Publications Inc.
- Bear, J. & Bachmat, Y. (1990). *Introduction to Modelling of Transport Phenomena in Porous Media*. Kluwer Academic Publishers.
- Bird, R. B., Stewart, W. E., & Lightfoot, E. N. (2007). *Transport Phenomena*. John Wiley and Sons, Inc.
- Case, J. (1957). *The Strength of Materials*. Edward Arnold Ltd.
- Du Plessis, J. P. (1991). Saturated crossflow through a two-dimensional porous medium. *Adv. Water Resources*, *14*(3), 131–137.
- Du Plessis, J. P. & Diedericks, G. P. J. (1997). *Advances in Fluid Mechanics: Fluid Transport in Porous Media*, chapter 2, (pp. 61–104). 13. Computational Mechanics Publications.
- Du Plessis, J. P. & Masliyah, J. H. (1988). Mathematical modelling of flow through consolidated isotropic porous media. *Transport in Porous Media*, *3*, 145–161.
- Du Plessis, J. P. & Masliyah, J. H. (1991). Flow through isotropic granular porous media. *Transport in Porous Media*, *6*, 207–221.
- Du Plessis, J. P. & Van der Westhuizen, J. (1993). Laminar Crossflow Through Prismatic Porous Domains. *R&D Journal*, *9*(2), 18–24.
- Dukhan, N. (2006). Correlations for the pressure drop for flow through metal foam. *Experiments in Fluids*, *41*, 665–672.

- Fung, Y. C. (1977). *A First Course in Continuum Mechanics*. Prentice Hall, Inc.
- Giesche, H. (2006). Mercury porosimetry: A general (practical) overview. *Particle and Particle Systems Characterization*, 23, 1–11.
- Hughes, W. F. (1979). *An Introduction to Viscous Flow*. Hemisphere Publishing Corporation.
- Jackson, G. W. & James, D. F. (1986). The permeability of fibrous porous media. *The Canadian Journal of Chemical Engineering*, 64, 364–374.
- Jaganathan, S., Vahedi Tafreshi, H., Shim, E., & Pourdeyhimi, B. (2009). A study on compression-induced morphological changes of non-woven fibrous materials. *Colloids and Surfaces A: Physicochemical and Engineering Aspects*, 337, 173–179.
- Kołodziej, J. A., Dziecielak, R., & Kończak, Z. (1998). Permeability tensor for heterogeneous porous medium of fibre type. *Transport in Porous Media*, 32, 1–19.
- Korteland, S., Bottero, S., & Hassanizadeh, S. M. (2010). What is the correct definition of average pressure? *Transport in Porous Media*, 84, 153–175.
- Le Coq, L. (2008). Influence on permeability of the structural parameters of heterogeneous porous media. *Environmental Technology*, 29, 141–149.
- Lloyd, C. (2003). *Hydrodynamic permeability of staggered and non-staggered regular arrays of squares*. MSc(Eng) thesis, Stellenbosch University, South Africa.
- Lloyd, C. A., Du Plessis, J. P., & Halvorsen, B. M. (2004). On closure modelling of volume averaged equations for flow through two-dimensional arrays of squares. *Proceedings of the Fifth International Conference on Advances in Fluid Mechanics, Advances in Fluid Mechanics V (Editors: Brebbia, C.A., Mendes, A.C., and Rahman, M.)*, 85–93.
- Mansfield, P. & Bencsik, M. (2001). Stochastic effects on single phase fluid flow in porous media. *Magnetic Resonance Imaging*, 19, 333–337.
- Montillet, A. & Le Coq, L. (2003). Image analysis: A useful tool for porous media characterization. *Chemical Engineering and Technology*, 26(12), 1285 – 1289.
- Nabovati, A., Llewellyn, E. W., & Sousa, A. C. M. (2009). A general model for the permeability of fibrous porous media based on fluid flow simulations using the lattice Boltzmann method. *Composites Part A: Applied Science and Manufacturing*, 40, 860–869.
- Pradhan, A. K., Das, D., Chattopadhyay, R., & Singh, S. N. (2012). Effect of 3D fiber orientation distribution on transverse air permeability of fibrous porous media. *Powder Technology*, 221, 101–104.
- Shah, R. K. & London, A. L. (1978). *Laminar Flow Forced Convection in Ducts*. Academic Press.
- Shou, D., Fan, J., & Ding, F. (2011). Hydraulic permeability of fibrous porous media. *International Journal of Heat and Mass Transfer*, 54, 4009–4018.

- Skartsis, L., Kardos, J. L., & Khomami, B. (1992). Resin flow through fibre beds during composite manufacturing processes. Part 1: Review of Newtonian flow through fiber beds. *Polymer Engineering and Science*, *32*, 221–230.
- Smit, G. J. F., Du Plessis, J. P., & Du Plessis Sr., J. P. (2007). Modelling of airflow through a stack in a timber-drying kiln. *Applied Mathematical Modelling*, *31*, 270 – 282.
- Steinke, M. E. & Kandlikar, S. G. (2006). Single-phase liquid friction factors in microchannels. *International Journal of Thermal Sciences*, *45*, 1073–1083.
- Tamayol, A. & Bahrami, M. (2009). Analytical determination of viscous permeability of fibrous porous media. *International Journal of Heat and Mass Transfer*, *52*, 2407–2414.
- Tamayol, A. & Bahrami, M. (2011). Transverse permeability of fibrous porous media. *Physical Review E*, *83*, (046314)1–9.
- Tamayol, A., McGregor, F., & Bahrami, M. (2012). Single phase through-plane permeability of carbon paper gas diffusion layers. *Journal of Power Sources*, *204*, 94–99.
- Thompson, K. E., Gordon, A., & Cain, M. (2002). Pore-Scale Modeling of fluid transport in disordered fibrous materials. *AIChE Journal*, *48*, 1369–1389.
- Whitaker, S. (1986). Flow in Porous Media I: A theoretical derivation of Darcy's law. *Transport in Porous Media*, *1*, 3–25.
- Whitaker, S. (1999). *The Method of Volume Averaging*. Kluwer Academic Publishers.
- Worster, G. (2009). *Understanding fluid flow*. Cambridge University Press.
- Woudberg, S. (2006). *Laminar Flow through Isotropic Granular Porous Media*. MSc(Eng) thesis, Stellenbosch University, South Africa.
- Woudberg, S. (2012a). *Comparative analysis of predictive equations for transfer processes in different porous structures*. PhD thesis, Stellenbosch University, South Africa.
- Woudberg, S. (2012b). A Geometric Pore-Scale Model for Predicting the Permeability of 3D Flow through Fibrous Porous Media. *Proceedings of the Fourth International Conference on Porous media and its applications in Science, Engineering and Industry (Editor: Kambiz Vafai)*, *1453*, 327–332.
- Zade, A. Q., Renksizbulut, M., & Friedman, J. (2011). Heat transfer characteristics of developing gaseous slip-flow in rectangular microchannels with variable physical properties. *International Journal of Heat and Fluid Flow*, *32*, 117–127.
- Zobel, S., Maze, B., Vahedi Tafreshi, H., Wang, Q., & Pourdeyhimi, B. (2007). Simulating permeability of 3-D calendered fibrous structures. *Chemical Engineering Science*, *62*, 6285–6296.